



1 Modelling the influence of biotic plant stress on atmospheric aerosol 2 particle processes throughout a growing season

3 Ditte Taipale^{1,2,3,4}, Veli-Matti Kerminen¹, Mikael Ehn¹, Markku Kulmala¹, Ülo Niinemets²

4 ¹Institute for Atmospheric and Earth System Research / Physics, Faculty of Science, University of Helsinki, P.O. Box 64,
5 00014 Helsinki, Finland

6 ²Institute of Agricultural and Environmental Sciences, Estonian University of Life Sciences, Kreutzwaldi 1, Tartu 51006,
7 Estonia

8 ³Institute for Atmospheric and Earth System Research / Forest Sciences, Faculty of Agriculture and Forestry, University of
9 Helsinki, PO Box 27, 00014 Helsinki, Finland

10 ⁴Hyytiälä Forestry Field Station, Hyytiäläntie 124, 35500 Korkeakoski, Finland

11 Correspondence to: Ditte Taipale (ditte.taipale@helsinki.fi)

12

13 **Abstract.** Most trees emit volatile organic compounds (VOCs) continuously throughout their life, but the rate of emission,
14 and spectrum of emitted VOCs, become substantially altered when the trees experience stress. Still, models to predict the
15 emissions of VOCs do not account for perturbations caused by biotic plant stress. Considering that such stresses have generally
16 been forecast to increase in both frequency and severity in future climate, the neglect of plant stress-induced emissions in
17 models might be one of the key obstacles for realistic climate change predictions, since changes in VOC concentrations are
18 known to greatly influence atmospheric aerosol processes. Thus, we constructed a model to study the impact of biotic plant
19 stresses on new particle formation and growth throughout a full growing season. We simulated the influence on aerosol
20 processes caused by herbivory by European gypsy moth (*Lymantria dispar*) and autumnal moth (*Epirrita autumnata*) feeding
21 on pedunculate oak (*Quercus robur*) and mountain birch (*Betula pubescens* var. *pumila*), respectively, and also fungal
22 infections of pedunculate oak and balsam poplar (*Populus balsamifera* var. *suaveolens*) by oak powdery mildew (*Erysiphe*
23 *alphitoides*) and poplar rust (*Melampsora larici-populina*), respectively. Our modelling results indicate that all the investigated
24 plant stresses are capable of substantially perturbing both the number and size of aerosol particles in atmospherically relevant
25 conditions, with increases in the amount of newly formed particles by up to about one order of magnitude and additional daily
26 growth of up to almost 50 nm. We also showed that it can be more important to account for biotic plant stresses in models than
27 significant variations in e.g. leaf area index, and temperature and light conditions, which are currently the main parameters
28 controlling predictions of VOC emissions. Our study, thus, demonstrates that biotic plant stress can be highly atmospherically
29 relevant and it supports biotic plant stress emissions to be integrated into numerical models for prediction of atmospheric
30 chemistry and physics, including climate change projection models.

31 1 Introduction

32 Formation and subsequent growth of atmospheric aerosol particles is globally a major source of cloud condensation nuclei
33 (CCN) (Spracklen et al., 2008; Merikanto et al., 2009; Dunne et al., 2016). CCN impact various cloud processes, such as cloud
34 formation, albedo and lifetime (Twomey, 1977; Albrecht, 1989; Makkonen et al., 2009; Kerminen et al., 2005), and
35 atmospheric aerosol particles are thereby able to influence our climate indirectly, in addition to interacting directly with
36 incoming solar radiation. Though atmospheric aerosol particles provide the single largest cooling effect on our climate, they
37 are also connected with the greatest uncertainty in climate change projections (IPCC, 2013). Part of this uncertainty is caused
38 by limited knowledge about the aerosol precursor molecules.



39 Oxidation products of certain volatile organic compounds (VOCs) participate in both the formation of new particles
40 (Donahue et al., 2013; Schobesberger et al., 2013; Kulmala et al., 2014; Riccobono et al., 2014; Kirkby et al., 2016; Tröstl
41 et al., 2016) and growth of existing particles via gas-to-particle condensation (Riipinen et al., 2012; Ehn et al., 2014; Bianchi
42 et al., 2019). Globally, and especially in forested regions, the majority of these organic compounds originate from terrestrial
43 vegetation (Kanakidou et al., 2005; Jimenez et al., 2009). Thus, increases in the emissions of certain biogenic VOCs can lead
44 to enhanced formation of atmospheric aerosol particles and subsequently to a rise in CCN concentration (Kerminen et al.,
45 2012; Paasonen et al., 2013).

46 Biotic plant stress (i.e. stress caused to a plant by living species such as e.g. herbivores and pathogens) is known to
47 substantially alter both the rates of emission and spectrum of emitted VOCs (Holopainen and Gershenson, 2010; Niinemets,
48 2010; Niinemets et al., 2013; Faiola and Taipale, 2020). For example, constitutively emitted isoprene, which is thought to
49 suppress the formation of new atmospheric aerosol particles (Kiendler-Scharr et al., 2009, 2012; Lee et al., 2016; McFiggans
50 et al., 2019; Heinritzi et al., 2020), is usually reduced in response to such stress (e.g. Brilli et al., 2009; Copolovici et al., 2014,
51 2017; Jiang et al., 2016), while the emissions of other VOCs are greatly induced. A large fraction of these stress-induced
52 compounds (e.g. monoterpenes, sesquiterpenes, 4,8-dimethyl-1,3,7-nonatriene (DMNT) and methyl salicylate) has a high
53 potential to produce and grow atmospheric aerosol particles (e.g. Mentel et al., 2013; Joutsensaari et al., 2015; Yli-Pirilä et al.,
54 2016; Ylisirniö et al., 2020), while other induced compounds (e.g. methanol and lipoxygenase oxidation products (LOX),
55 which mostly include C₆ aldehydes, alcohols and esters) are anticipated to suppress aerosol processes (e.g. Mentel et al., 2013).

56 While much attention has been given to representing constitutive emissions of VOCs in numerical models, VOC
57 emissions caused by stress, and in particular biotic stress, have been mostly excluded (Grote et al., 2013; Faiola and Taipale,
58 2020), despite the fact that biotic plant stress is largely ubiquitous. This is mainly due to a lack of measurements, combined
59 with the fact that variations in emission responses are highly stressor-specific (e.g. Holopainen and Gershenson, 2010;
60 Niinemets, 2010; Faiola and Taipale, 2020). Thus, no consistent mechanism for the emissions of VOCs from plants under
61 stress has been proposed until now. Though the most extensively used biogenic emissions model, MEGAN (Guenther et al.,
62 2012), considers a stress emission category, the treatment is not quantitative. The emission factor for stress VOCs is, for
63 example, the same for all plant functional types and is supposed to represent a large range of different types of stresses.
64 Recently, Grote et al. (2019) proposed a new modelling framework for estimating emissions of VOCs induced by both biotic
65 and abiotic plant stresses, while Douma et al. (2019) developed a model to predict both the emissions and concentrations of
66 stress-induced VOCs, which was parameterized to simulate a gypsy moth infested black poplar canopy. Both are promising
67 tools, but in their current states, they exclude important storage emissions which are usually released upon wounding (e.g.
68 Blande et al., 2009; Faiola et al., 2018; Kari et al., 2019), and they do not fully (Grote et al., 2019) - or at all (Douma et al.,
69 2019) - consider how the constitutive emissions of isoprene are modulated. This is as such understandable considering that
70 emissions of isoprene might be either reduced (e.g. Brilli et al., 2009; Copolovici et al., 2017) or induced (e.g. Schaub et al.,
71 2010; Ye et al., 2019) in response to biotic plant stress, but nevertheless problematic since isoprene is globally the VOC that
72 is emitted in largest quantities (Guenther et al., 2012) and it is thought to suppress the formation of aerosol particles (see
73 above). Whilst Grote et al. (2019) assumed a linear response to the degree of damage, which has been shown not always to be
74 true, especially at severe stress levels (e.g. Niinemets et al., 2013; Jiang et al., 2016; Yli-Pirilä et al. 2016; Copolovici et al.,
75 2017; Faiola and Taipale, 2020), it is not obvious how the model results by Douma et al. (2019) depend on the degree of
76 damage, as they operate with “number of larvae” rather than a stand level of defoliation. Additionally, Grote et al. (2019) did
77 not account for an explicit dependency of the emissions on temperature, which is usually considered as one of the most
78 important environmental parameters for emissions of VOCs (e.g. Grote et al., 2013). Common for both studies is that they
79 only simulate rather short time scales (i.e. a few days).

80 Since measurements have clearly illustrated that biotic plant stress is able to significantly influence the amount and
81 size of formed atmospheric aerosol particles (Mentel et al., 2013; Joutsensaari et al., 2015; Yli-Pirilä et al., 2016; Faiola et al.,



82 2019, 2018) via perturbations in VOC emissions, there is an urgent need to quantify the atmospheric importance of biotic plant
83 stress. This need is amplified by the fact that insect outbreaks and fungal diseases generally are expected to increase in both
84 frequency and severity in the future (Cannon, 1998; Bale et al., 2002; Harrington et al., 2007; Pautasso et al., 2012; Boyd et
85 al., 2013). Unfortunately, such quantitative estimates are currently very scarce and connected with a large degree of
86 uncertainty. Bergström et al. (2014) used a regional chemical transport model to simulate the impact of *de novo* emissions,
87 induced by aphid infestation, on secondary organic aerosol (SOA) formation, and estimated that these induced emissions
88 currently account for 20-70 % of total biogenic SOA in northern and central European forests. Meanwhile, Joutsensaari et al.
89 (2015) calculated a local increase of up to 480 % in aerosol mass and 45 % in CCN concentration, when it was assumed that
90 10 % of the boreal forest area experienced stress which increased constitutive monoterpenes emission rates by an order of
91 magnitude. Using satellite observations, Joutsensaari et al. (2015) also found a 2-fold increase in aerosol optical depth over
92 Canadian pine forests during a bark beetle outbreak. To our knowledge, no one has previously considered the dynamics of
93 insect herbivory when simulating the emitted VOCs and produced and grown aerosols from stressed plants. Additionally, there
94 has so far been no attempts to measure nor model the impact of pathogenic infections on atmospheric aerosol processes.

95 We constructed a conceptual model to investigate the atmospheric impacts of biotic plant stresses. We used this model
96 to simulate formation and growth of atmospheric aerosol particles throughout a growing season in pure oak, poplar and birch
97 forest stands in stress-free conditions and under herbivory or fungal stress. By considering the dynamics of insect herbivory
98 and pathogenic infections in combination with seasonal changes in environmental parameters, our aim was to contribute to a
99 discussion about whether biotic plant stress perturbs atmospheric aerosol processes sufficiently to warrant their inclusion in
100 larger scale models.

101

102 2 Materials and methods

103 We constructed a model that includes modules for emissions of VOCs from stress-free and biotically stressed tree species (Sec.
104 2.4), boundary layer meteorology (Sec. 2.5), atmospheric chemistry (Sec. 2.6) and aerosol dynamics (Sec. 2.7). The calculated
105 canopy VOC emissions from biotically stressed trees depend on the dynamics of the biotic stressors of interest (Sec. 2.1 and
106 2.2) and changes in the leaf area index (Sec. 2.3).

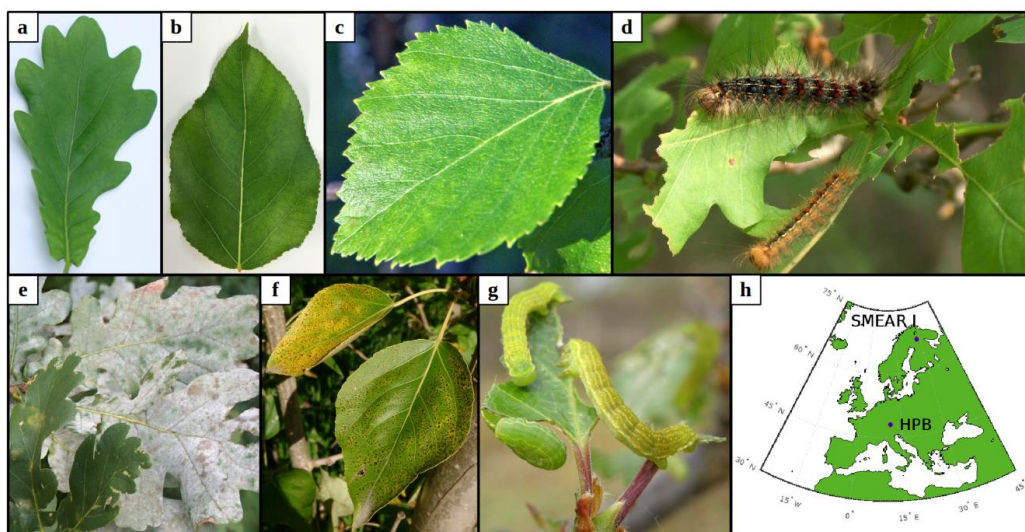
107

108 2.1 Simulations of larval infestation dynamics

109 Whereas mountain birch (*Betula pubescens* var. *pumila*; former spp. *czerepanovii*, Fig. 1c) is the main host for autumnal moths
110 (*Epirrita autumnata*, Fig. 1g), European gypsy moth (*Lymantria dispar*, Fig. 1d) is one of the major defoliating insects feeding
111 on pedunculate oak (*Quercus robur*, Fig. 1a). The larval eggs of both moths hatch in spring synchronously with bud burst
112 (Kaitaniemi et al., 1997; Kaitaniemi and Ruohomäki, 1999; Spear, 2005; McManus et al., 1989). Both sexes have five larval
113 stages, though female gypsy moths have six. These stages are separated by periods of molting where the larvae do not feed. A
114 complete defoliation of vast areas can occur within 4-6 weeks by autumnal moth (Kaitaniemi and Ruohomäki, 1999) and
115 within 6-8 weeks by gypsy moth (McManus et al., 1989). Adults do not feed on leaves (Tammaru et al., 1996; Waring and
116 Townsend, 2009). For simulations of autumnal moth infested mountain birch, our model incorporates atmospheric and
117 ecological conditions observed at the Station for Measuring Ecosystem-Atmosphere Relations (SMEAR I, Fig. 1h), Värriö,
118 Eastern Finnish Lapland (e.g. Hari et al., 1994), due to the high data quality and availability, and since autumnal moth infested
119 mountain birch is common at the site (Hunter et al., 2014). In our simulations, bud burst occurs on 6th of June, the subsequent
120 full leaf state is attained on 10th of June (dates are based on long-term observations from the station), and senescence onsets
121 on 20th of August (Gill et al., 2015). We assumed that the larvae feed for five weeks, starting on 6th of June and they pupate on
122 11th of July (Kaitaniemi and Ruohomäki, 1999). The larvae dynamics (i.e. relative leaf consumption and time spent in each



123 larval stage) that is incorporated in our model is based on Lempa et al. (2004). For simulations of European gypsy moth infested
124 pedunculate oak, our model incorporates mainly atmospheric conditions observed at the Meteorological Observatory
125 Hohenpeißenberg (e.g. Birmili et al., 2003), rural southern Germany (Fig. 1h), since this station has been classified as a
126 representative measurement location for central Europe (Naja et al., 2003), where oak is a very common species. In our
127 simulations, bud burst occurs on 15th of May, the subsequent full leaf state is attained 20 days later on 4th of June, and
128 senescence onsets on 20th of September (Gill et al., 2015). Durations of the various developmental states of the larvae are based
129 on Zúbrik et al. (2007), which is also in agreement with Stoyenoff et al. (1994). Though the length of the larval state of female
130 larvae feeding on pedunculate oak is typically a few days longer than the total duration of the male larval state (e.g. Zúbrik et
131 al., 2007), we did not differentiate between the two genders, but utilised the length of the female larval state due to
132 simplification and since the female is the main consumer (Miller et al., 1991). We assumed that the larvae feed for 41 days
133 (Zúbrik et al., 2007), starting on 15th of May and they pupate on 25th of June. The relative leaf consumption within the different
134 larval stages is based on Kula et al. (2013). The ratio in relative leaf consumption between 4th and 5th instar is also within the
135 range that is reported by Stoyenoff et al. (1994) (where no other ratios were provided). We neglected periods of molting, as
136 those are typically in the order of less than one day (Ayres and MacLean, 1987). We assumed that either 30 % or 80 % of the
137 total leaf area in the forest stand was consumed by the end of the feeding period (Fig. 2a,b).
138



139
140 **Figure 1.** The plant species and biotic stresses we considered together with locations. **a-c**, non-infested leaves; pedunculate
141 oak (*Quercus robur*) (**a**), balsam poplar (*Populus balsamifera* var. *suaveolens*) (**b**) and mountain birch (*Betula pubescens* var.
142 *pumila*; former spp. *czerepanovii*) (**c**). **d-g**, fungal infected or moth infested leaves; pedunculate oak infested by European
143 gypsy moth (*Lymantria dispar*) (**d**) or infected by oak powdery mildew (*Erysiphe alphitoides*) (**e**), poplar infected by rust
144 fungus (*Melampsora larici-populina*) (**f**) and mountain birch infested by autumnal moth (*Epirrita autumnata*) (**g**). **h**, location
145 of the two sites that serve as boundary conditions in our simulations. Photo courtesy: a+c: Juho Aalto, b: Yifan Jiang, d+e:
146 Haruta Ovidiu, University of Oradea, Bugwood.org, f: Ülo Niinemets, g: Tero Klemola.
147

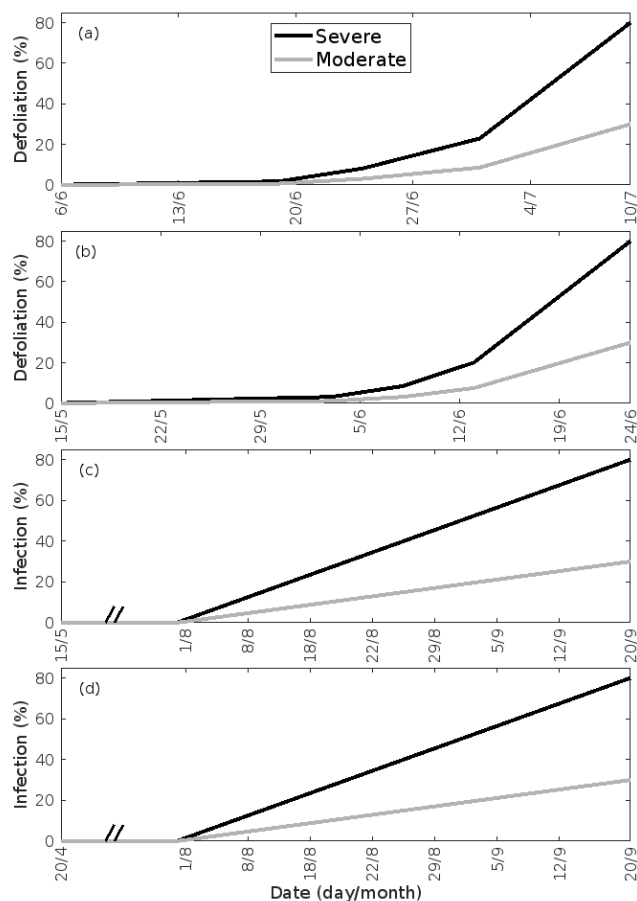
148 2.2 Simulations of fungal infection dynamics

149 Oak powdery mildew (*Erysiphe alphitoides*) is one of the main foliar diseases of pedunculate oak (*Quercus robur*) in Europe
150 (Desprez-Loustau et al., 2011). Among the *Melampsora* species, *Melampsora larici-populina* is the most widespread poplar
151 rust (Vialle et al., 2011). *M. larici-populina* has five morphologically and functionally different spore stages during its life



152 cycle, where the two first stages are retrieved on larch and the last three on poplar (Vialle et al., 2011). The pathogenic fungal
153 infections do not decrease the leaf area of their victim, but as they cover the leaf, they absorb nutrients from the cells of the
154 leaf (Glawe, 2008) and change the physiology of the leaf (e.g. Major et al., 2010; Voegelé and Mendgen, 2003; El-Ghany et
155 al., 2009). The severity and spread of fungal infections depend largely on weather and growth conditions (e.g. Åhman, 1998;
156 Johansson and Alström, 2000; Covarelli et al., 2013), where especially high rainfall in the beginning of the summer greatly
157 enhances both the severity, but also the onset of infection (Covarelli et al., 2013; Pinon et al., 2006). The onset of attack by
158 oak powdery mildew is limited by its morphological development, hence the infection usually starts to appear between the end
159 of June and August (in France; Marçais et al., 2009; Marçais and Desprez-Loustau, 2014; Bert et al., 2016). *M. larici-populina*
160 has been observed to attack young poplar trees as early as June (in Italy, Covarelli et al., 2013), though generally the disease
161 emerges between July and September (in France and Italy, Gérard et al., 2006; Covarelli et al., 2013). In our simulations, we
162 assumed that both fungi started to infect their host on 1st of August. In the case of *M. larici-populina* we only simulated the
163 attack on poplar as the host (and not larch). *Populus balsamifera* var. *suaveolens* was chosen as the poplar species due to the
164 availability of suitable published VOC emissions measurements. Based on Bert et al. (2016), we assumed that the severity of
165 infection increases linearly with time, starting on 1st of August and ending on 20th of September. We assumed that either 30 %
166 or 80 % of the total leaf area in the forest stands was covered by fungi by the end of the growing season (Fig. 2c,d). For these
167 simulations, our model incorporates the same atmospheric conditions as for simulations of gypsy moth infested oak. Poplar
168 bud burst occurs on 20th of April in our model (Tripathi et al., 2016) and we assumed the same timing of senescence as for
169 simulations of oak (Gill et al., 2015; Tripathi et al., 2016).

170



171

172 **Figure 2.** Infection dynamics. (a) birch infested with autumnal moth larvae, (b) oak infested with European gypsy moth larvae,
173 (c) oak infected by oak powdery mildew and (d) poplar infected by rust fungus. The infection dynamics of oak powdery
174 mildew and rust fungus is assumed to be similar, but the duration of growth of the two tree species is different. The dynamics
175 are specific to the locations of Lapland (a) and central Europe (b-d). 30 % (moderate infection scenario) or 80 % (severe
176 infection scenario) of the total leaf area in the forest stands is assumed to be consumed by the end of the feeding period or
177 infected by fungi by the onset of senescence. Note the different time axes.

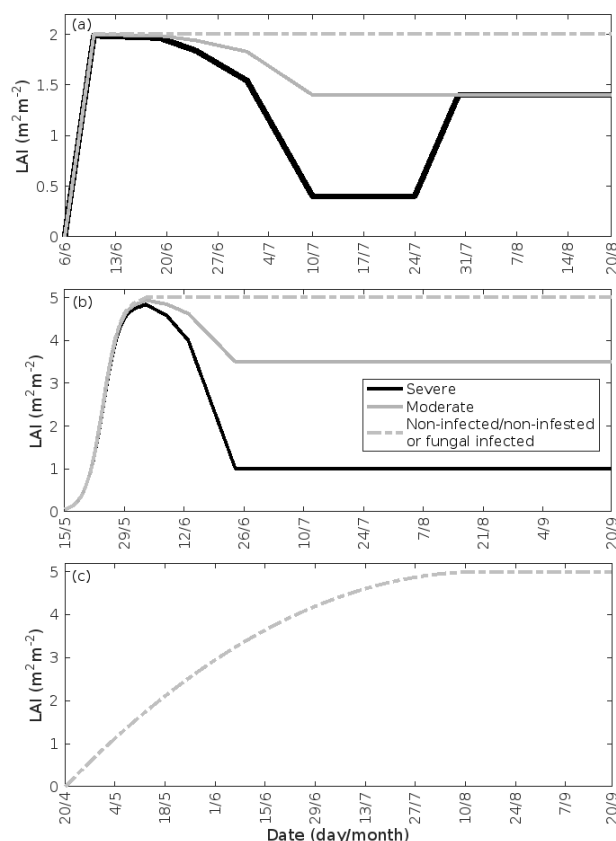
178

179 2.3 Treatment of the leaf area index

180 Low soil temperatures usually prevent growth of a second leaf flush in birch trees (Aphalo et al., 2006). Thus, we assumed
181 that the leaf area index (LAI) of a non-infested mountain birch stand in Lapland increases linearly from 0 – 2.0 m² m⁻²
182 (Dahlberg et al., 2004) in the time period 6th–10th of June (bud burst to full leaf), and stays constant until the onset of senescence
183 (Fig. 3a). The LAI of an infested stand decreases proportionally with the level of defoliation (Fig. 3a). Refoliation only occurs
184 in totally, or near-totally, defoliated mountain birch trees (Kaitaniemi et al., 1997). Hence, we assumed that the LAI of a
185 heavily defoliated stand resumes to 70 % of the original LAI within three weeks of defoliation (personal communication with
186 adj. Prof. Dr. Pekka Kaitaniemi, Fig. 3a). Poplar trees produce leaves throughout the season, and we therefore assumed that
187 the LAI of poplar stands increases quadratically from 20th of April (bud burst) until 15th of August (Fig. 3c, Tripathi et al.,
188 2016). Oak, on the other hand, usually only produces one significant leaf flush, hence we assumed that the LAI of oak stands



189 increases with a sigmoid shape from 15th of May (bud burst) until 4th of June (full leaf state attained) (Fig. 3b, Oláh et al.,
190 2012). In our simulations, the maximum LAI of poplar and oak is 5.0 m² m⁻². The LAI of a gypsy moth infested oak stand
191 decreases proportionally with the level of defoliation (Fig. 3b). The fungal infections do not decrease the leaf area of their host,
192 nor do they prevent the tree from producing multiple flushes of leaves (Marçais and Desprez-Loustau, 2014). The LAI might,
193 however, in reality be less in an infected stand than in a non-infected stand, though this depends highly on the specific
194 genotypes and their individual fungal resistance (Verlinden et al., 2013; Shifflett et al., 2016), but naturally also on the timing
195 of infection. Since most summer leaves already appear before the onset of infection, we did not assume a decrease in LAI.
196 Severe powdery mildew infection (>50 %) has been shown to greatly reduce the infected leaf lifespan (Hajji et al., 2009). The
197 median time before shedding of deformed oak leaves has been estimated to be 10-31 days (Hajji et al., 2009). In our scenario
198 of a heavily infected stand (80 % of the stand leaf area is infected by the end of the season), an infection level of 50 % is
199 reached on 1st of September. Since senescence is assumed to onset on 20th of September, we excluded an earlier shedding of
200 leaves. Hence, in our simulations of fungal infections, we assumed that the LAI is the same as in a non-infected stand (Fig.
201 3b,c).
202



203
204 **Figure 3.** Leaf area index throughout the growing season in infected and non-infected forest stands. (a) mountain birch, (b)
205 oak and (c) poplar. 30 % (moderate infection scenario) or 80 % (severe infection scenario) of the total leaf area in the forest
206 stands is assumed to be consumed by the end of the feeding period in simulations of herbivory, while fungal infections do not
207 decrease the leaf area. Note the different time axes.
208



209 2.4 Plant emissions of volatile organic compounds

210 The plant emissions (F_i) of individual VOCs (i) from various pure stands were computed as:

$$211 F_i = \varepsilon_i \times \text{LAI} \times \gamma_L \times \gamma_T \quad (1)$$

212 where ε_i is the emission rate of i at standard conditions (25 °C, 1000 $\mu\text{mol m}^{-2} \text{s}^{-1}$), LAI is the leaf area index and treated as
213 mentioned in Sec. 2.3, and γ_L and γ_T are the activity factors that account for changes in light and temperature from standard
214 conditions. This expression is adopted from Guenther et al. (2012), Eq. 1-2, when we assume that the soil moisture and ambient
215 CO_2 concentration in our stands are optimal. Generally, we excluded the effect of leaf age on the emissions of VOCs, since
216 we do not know the effect of leaf age on stress-induced emissions. However, we also tested whether the impact of leaf maturity
217 would be able to change the conclusions of our study when making certain assumptions about the leaf age effect. The treatment
218 of the leaf age effects and the results of these tests are presented in Appendix A and discussed in Sec. 3.2.

219 Similarly to e.g. Simpson et al. (1999; 2012) and Bergström et al. (2014), we utilised a simple non-canopy approach,
220 where ambient and leaf temperature are assumed to equal, and where the use of branch-level emission factors accounts for the
221 canopy shading effect (Guenther et al., 1994). We utilised emission rates, reported as a function of the degree of damage, from
222 Copolovici et al. (2017; 2014), Jiang et al. (2016), and Yli-Pirilä et al. (2016). The emission rates reported by Copolovici et al.
223 (2017; 2014) and Jiang et al. (2016) were all retrieved by leaf-level measurements, hence we decreased the reported emission
224 rates by a factor of 0.57, since branch-level emission factors for light sensitive emissions are typically a factor of 1.75 smaller
225 than the corresponding leaf-level values (Simpson et al., 1999; 2012). We did not decrease the emission rates reported by Yli-
226 Pirilä et al. (2016), since these were based on measurements of the whole plant. Instead, the emission rates from mountain
227 birch seedlings (Yli-Pirilä et al., 2016) were upscaled in order to represent the emissions from mature trees, assuming a leaf
228 mass area of 75 g m^{-2} for leaves growing on mature mountain birch trees (Riipi et al., 2005). Since emission response
229 measurements are usually stopped, at a maximum, a few days after the herbivore activity has ceased, we assumed that the
230 effect of stress on the emissions of VOC stops the day that the larvae pupate (e.g. Yli-Pirilä et al., 2016), in order to not
231 overestimate the impact of the stress. The light and temperature dependent emission activity factors are computed using Eq. 2
232 in Guenther (1997), since none of the considered broadleaved species poses storages and birch has specifically been shown to
233 only emit *de novo* (Ghirardo et al., 2010). Similarly to Guenther et al. (2012), we assumed that stress-induced emissions are
234 controlled by light and temperature in a similar way as constitutive emissions, thus the used emission rates from the literature
235 were standardised according to Eq. 1. Copolovici et al. (2014) and Jiang et al. (2016) have also shown that the emissions of
236 isoprene from oak powdery mildew and rust infected oaks and poplars have the same response to light as control plants.
237 Copolovici et al. (2014) additionally demonstrated that the emissions of monoterpenes from oak powdery mildew infected oak
238 depend strongly on light, even though the majority of emitted monoterpenes were not e.g. ocimene and linalool, which are
239 known to be light dependent (Niinemets et al., 2002; Arimura et al., 2008). LOX (lipoxygenase pathway volatile) compounds,
240 on the other hand, are released shortly after damage of leaf tissue, independent of the light conditions (Arimura et al., 2008).
241 LOX compounds do not contribute to the formation and growth processes of atmospheric aerosol particles, but they were
242 included in the model in order to illustrate the changes in the atmospheric concentrations of LOX as a function of stress severity
243 and stress type, and for evaluating the reliability of our modelling results, since LOX, in reality, affect the atmospheric
244 concentration of OH, which was constrained in the model. The equations, which we used in the model for linking the emission
245 factors to the severity of stress, are provided in Table 1 together with the parameters needed for the equations.

246
247 **Table 1.** Equations to calculate the emission factors ($\varepsilon_{i,D}$, in unit $\text{nmol m}^{-2} \text{s}^{-1}$), as a function of the degree of stress (D), together
248 with the parameters needed for the equations. The equations are valid for infection levels ranging from 0 % to 80 % unless
249 otherwise stated. The emission factors, listed for oak and poplar in the table, have not been downscaled (by a factor of 0.57),
250 but the emission factors for mountain birch, listed here, have been upscaled in order to represent the emissions from mature
251 trees. Thus, LMA_f is the fraction of the leaf mass area of leaves growing on mature mountain birch / growing on mountain



252 birch seedlings. ISO = isoprene, MT = monoterpenes, MeSa = methyl salicylate, LOX = lipoxygenase pathway volatile
 253 compounds, DMNT = 4,8-dimethyl-1,3,7-nonatriene, MeOH = methanol, SQT = sesquiterpenes, α -Eud = α -Eudesmol.

Infestation of pedunculate oak (<i>Quercus robur</i>) by European gypsy moth (<i>Lymantria dispar</i>) based on Copolovici et al. (2017).						
VOC	$\varepsilon_{i,D}$ (nmol m ⁻² s ⁻¹)	$\varepsilon_{i,0}$ (nmol m ⁻² s ⁻¹)	A (nmol m ⁻² s ⁻¹)	B	C (nmol m ⁻² s ⁻¹)	
ISO	$\varepsilon_{i,0} + \frac{D \times A}{B + D}, 0 \leq D \leq 60$ $\varepsilon_{i,60} \times 0.5, 60 < D \leq 80$	30.26	-47.40	34.48		
MT	$\varepsilon_{i,0} + \frac{D \times A}{B + D}$	$4.0 \cdot 10^{-2}$	9.22	33.42		
MeSa	$D \times A$		$3.5 \cdot 10^{-3}$			
LOX	$A \times D^2 + C \times D$		$1.1 \cdot 10^{-3}$		$4.7 \cdot 10^{-2}$	
DMNT	$A \times D^2 + C \times D$		$1.0 \cdot 10^{-5}$		$1.3 \cdot 10^{-3}$	
Infection of pedunculate oak (<i>Quercus robur</i>) by oak powdery mildew (<i>Erysiphe alphitoides</i>) based on Copolovici et al. (2014)						
VOC	$\varepsilon_{i,D}$ (nmol m ⁻² s ⁻¹)	$\varepsilon_{i,0}$ (nmol m ⁻² s ⁻¹)	A (nmol m ⁻² s ⁻¹)	B (nmol m ⁻² s ⁻¹)	C (nmol m ⁻² s ⁻¹)	
ISO	$\varepsilon_{i,0} + A \times D + B \times D^2 + C \times D^3$	10.6	-0.244	$3.69 \cdot 10^{-3}$	$-2.05 \cdot 10^{-5}$	
MT	$\varepsilon_{i,0} + A \times D + B \times D^2 + C \times D^3$	$4.0 \cdot 10^{-2}$	$8.7 \cdot 10^{-3}$	$-7.1 \cdot 10^{-5}$	$3.7 \cdot 10^{-7}$	
MeSa	0, $D = 0$ $A \times \frac{\varepsilon_{MT,D}}{\varepsilon_{MT,60}}, 0 < D \leq 80$		0.437			
LOX	$A + B \times D$		$2.13 \cdot 10^{-3}$	$6.24 \cdot 10^{-3}$		
Infection of balsam poplar (<i>Populus balsamifera</i> var. <i>suaveolens</i>) by poplar rust (<i>Melampsora larici-populina</i>) based on Jiang et al. (2016)						
VOC	$\varepsilon_{i,D}$ (nmol m ⁻² s ⁻¹)	$\varepsilon_{i,0}$ (nmol m ⁻² s ⁻¹)	A (nmol m ⁻² s ⁻¹)	B (nmol m ⁻² s ⁻¹)	C	E (nmol m ⁻² s ⁻¹)
ISO	$A + \frac{B}{C + D}$		12.3	366.8	4.98	
MT	0.0625, $D = 0$ $A + B \times D + E \times D^2, 0 < D \leq 80$		0.112	$1.84 \cdot 10^{-3}$		$1.5 \cdot 10^{-4}$
MeSa	$A \times D + B \times D^2 + E \times D^3$		$6.32 \cdot 10^{-3}$	$-8.6 \cdot 10^{-5}$		$5.75 \cdot 10^{-7}$
LOX	0.4814, $D = 0$		2.51	$-2.51 \cdot 10^{-2}$	0.76, $0 < D < 30$	$3.25 \cdot 10^{-3}$



	$(A + B \times D + E \times D^2) \times C, 0 < D \leq 80$				$0.85, 30 \leq D < 60$ $0.93, 60 \leq D \leq 80$	
DMNT	$\varepsilon_{\text{DMNT},60} \times \frac{\varepsilon_{\text{MeSa},D}}{\varepsilon_{\text{MeSa},60}}, 0 \leq D < 60$ $\varepsilon_{\text{MeSa},D} \times C, 60 \leq D \leq 80$				0.36	
MeOH	$\varepsilon_{i,0} + A \times D + B \times D^2$	16.9	-0.338	$1.36 \cdot 10^{-2}$		
SQT	$\varepsilon_{\text{SQT},60} \times \frac{\varepsilon_{\text{MeSa},D}}{\varepsilon_{\text{MeSa},60}}, 0 \leq D < 60$ $\varepsilon_{\text{MeSa},D} \times C, 60 \leq D \leq 80$				2.414	
α -Eud	$\varepsilon_{\alpha\text{-Eud},60} \times \frac{\varepsilon_{\text{MeSa},D}}{\varepsilon_{\text{MeSa},60}}, 0 \leq D < 60$ $\varepsilon_{\text{MeSa},D} \times C, 60 \leq D \leq 80$				0.397	
Infestation of mountain birch (<i>Betula pubescens</i> var. <i>pumila</i>) by autumnal moth (<i>Epirrita autumnata</i>) based on Yli-Pirilä et al. (2016)						
VOC	$\varepsilon_{i,D}$ (nmol m ⁻² s ⁻¹)	A	B	C	E (nmol m ⁻² s ⁻¹)	LMA _f
MT	$\left(A + \frac{D \times B}{\sqrt{1 + \frac{B^2 \times D^2}{C^2}}} \right) \times E \times \text{LMA}_f$	$7.65 \cdot 10^{-2}$	$9.33 \cdot 10^{-3}$	0.2146	0.769	2.23
LOX	$(A \times D + B) \times E \times \text{LMA}_f$	$6.325 \cdot 10^{-3}$	$4.868 \cdot 10^{-2}$		0.8	2.23
DMNT	$\left(A + \frac{D \times B}{\sqrt{1 + \frac{B^2 \times D^2}{C^2}}} \right) \times E \times \text{LMA}_f$	$7.11 \cdot 10^{-4}$	$3.39 \cdot 10^{-4}$	$8.63 \cdot 10^{-3}$	0.769	2.23
SQT	$\frac{\varepsilon_{\text{MT},D}}{3}$					

254

255 2.5 Meteorological conditions

256 The daily maximum radiation during the entire growing season was fixed to 1000 $\mu\text{mol m}^{-2} \text{s}^{-1}$ (Table 2), which corresponds
 257 to the average maximum photosynthetic photon flux density (PPFD) observed at the SMEAR I station during the growing
 258 seasons of 2015-2017 (Aalto et al., 2019). The daily pattern of PPFD then follows the solar zenith angle. For simulations of
 259 mountain birch, we utilised the maximum and minimum mean temperatures on every day in the growing season during 2015-
 260 2017 observed at 9 m at the SMEAR I station (Aalto et al., 2019). The daily maximum and minimum temperatures ranged
 261 from 9.8 to 19.6 °C, and from 2.0 to 11.3 °C, respectively, in the time period of interest (6th of June - 20th of August, Fig. 4a).
 262 For simulations of oak and poplar, we utilised the maximum and minimum temperatures for southern Germany averaged over
 263 the past three decades (data obtained via <https://www.currentresults.com/Weather/Germany/average-annual-temperatures.php>). This was done due to availability and restriction of data obtained at the Hohenpeißenberg Meteorological
 264 Observatory and since our aim was not as such to simulate the atmospheric impact at Hohenpeißenberg, but instead at any
 265 relevant location, i.e. where oaks and poplars, including the biotic stresses of interests, are common. The monthly averaged
 266 daily maximum and minimum temperatures ranged from 15 to 26 °C, and from 6 to 16 °C, respectively, in the time period of
 267 interest (April - September, Fig. 4b). For simplicity, the daily temperature pattern followed that of the solar zenith angle with
 268



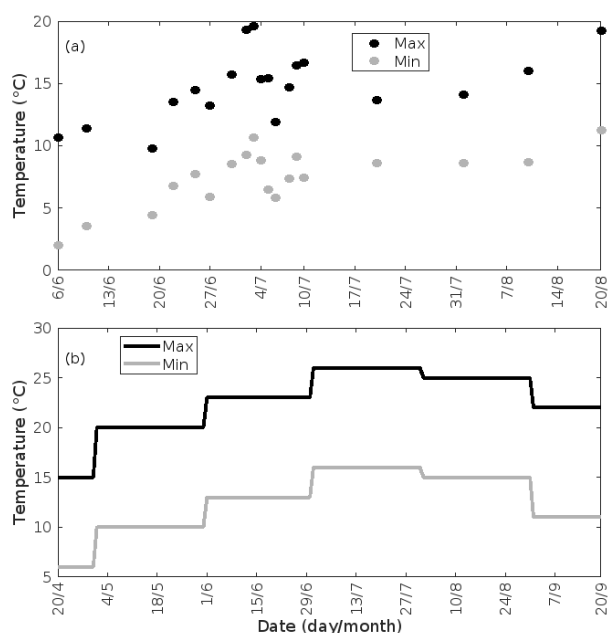
269 a forward shift of 1 h. The default daytime mixing length was kept constant to a value of 700 m (simulations of mountain
270 birch) and 2000 m (simulations of oak and poplar) above ground level (Seidel et al., 2012) (Table 2).

271

272 **Table 2.** Model inputs. Representative summer time conditions in rural central Europe (here indicated by HPB: the
273 Hohenpeißenberg Meteorological Observatory) and Lapland (here indicated by the SMEAR I station), used as default model
274 input. The conditions are chosen such that they are realistic and representative, but they do not inhibit the formation of new
275 particles. The concentrations of OH and sulfuric acid are provided as daily maxima in the table, but their concentrations
276 decrease as a function of the decrease in solar light in the simulations. The concentration of ozone is kept constant throughout
277 the simulations, while the condensation sink (CS) takes into account the relative importance of sulfuric acid and oxidised
278 organic compounds on the CS (Eq. 5; Peräkylä et al., 2020). The condensation sink for sulfuric acid (CS_{SA}) is kept constant
279 throughout the simulations. BHL is the planetary boundary layer height. The photosynthetic photon flux density (PPFD) is
280 provided as the daily maximum in the table, but the daily pattern of PPFD follows the solar zenith angle in the model.

	HPB	SMEAR I
$[O_3]$ (ppb)	45	30
$[OH]_{max}$ (molec cm^{-3})	$6 \cdot 10^6$	$8 \cdot 10^5$
$[H_2SO_4]_{max}$ (molec cm^{-3})	$1 \cdot 10^7$	$2.5 \cdot 10^6$
CS_{SA} (s^{-1})	$2.5 \cdot 10^{-3}$	$7 \cdot 10^{-4}$
BLH (m)	2000	700
$PPFD_{max}$ ($\mu mol m^{-2} s^{-1}$)	1000	

281



282

283 **Figure 4.** Daily maximum and minimum temperatures throughout the growing season at (a) SMEAR I, Lapland, and (b)
284 Southern Germany, used as default model input. Note the different time axes.



285

286 2.6 Atmospheric gas phase chemistry

287 Similarly to previous atmospheric modelling studies of herbivory (Bergström et al., 2014; Douma et al., 2019), we constrained
288 the concentrations of atmospheric oxidants within the model, since it is unreasonable to assume that they can be accurately
289 predicted. Many studies do, for example, report a large (up to at least 89 %) missing sink of OH, especially in forested areas
290 (e.g. Di Carlo et al., 2004; Sinha et al., 2010; Mogensen et al., 2011, 2015; Nölscher et al., 2012, 2016; Zannoni et al., 2016;
291 Praplan et al., 2019) and studies above the Amazonian rainforest, furthermore, indicate that isoprene can recycle OH with a
292 varying efficiency of 40-120 % (Lelieveld et al., 2008; Taraborrelli et al., 2012). In our simulations, the default daily maximum
293 concentration of OH is therefore fixed to $6 \cdot 10^6$ molec cm^{-3} (Petäjä et al., 2009) and $8 \cdot 10^5$ molec cm^{-3} (calculated using observed
294 summertime UVB radiation from the SMEAR I station and the proxy presented by Petäjä et al. (2009)) for simulations of
295 Hohenpeißenberg and Lapland, respectively (Table 2). The daily pattern of the OH concentration then follows the solar zenith
296 angle. The concentration of ozone is kept constant to a value of 45 ppb (Naja et al., 2003) and 30 ppb (Ruuskanen et al., 2003)
297 for simulations of oak and poplar (Hohenpeißenberg conditions) and mountain birch (SMEAR I conditions), respectively
298 (Table 2). In reality, the atmospheric oxidant concentration can, however, decrease or increase depending on changes in the
299 concentrations of individual specific VOCs (Table 3). The impact of changing oxidation concentrations on our simulation
300 results was therefore also tested (Sec. 3.2, Fig. 11a-b,f-g,k-l,p-q).

301 The only source of sulfuric acid (H_2SO_4), in our model, is the reaction between OH and SO_2 , while the only sink is
302 the condensation sink. The concentration of SO_2 is chosen such that the default daytime maximum concentration of H_2SO_4 is
303 $1 \cdot 10^7$ molec cm^{-3} in Hohenpeißenberg (Petäjä et al., 2009; Birmili et al., 2003) and $2.5 \cdot 10^6$ molec cm^{-3} in Lapland (Kyrö et al.,
304 2014) (Table 2). The size distribution of the pre-existing particle population is kept fixed during the simulations, so the number
305 concentration of pre-existing particles is defined by the condensation sink (CS). The overall value of CS is related to that of
306 sulfuric acid (CS_{SA}) via Eq. 5 that takes into account the relative importance of sulfuric acid and oxidised organic compounds
307 on CS (Peräkylä et al., 2020). The condensation sink of sulfuric acid is kept constant to a value of $2.5 \cdot 10^{-3} \text{ s}^{-1}$ (in rural southern
308 Germany) and $7 \cdot 10^{-4} \text{ s}^{-1}$ (in Lapland; Dal Maso et al., 2007; Vana et al., 2016) during our simulations (Table 2).

309 We included reactions for the atmospheric oxidation of SO_2 and the emitted VOCs (Appendix B). Certain VOCs, and
310 especially VOCs with endocyclic double bonds, can form HOM (highly oxygenated organic molecules) upon oxidation by, in
311 particular O_3 , but also OH and NO_3 (e.g. Ehn et al., 2012, 2014; Jokinen et al., 2015; Berndt et al., 2016; Bianchi et al., 2019;
312 Zhao et al., 2020). HOM have been found to be a major component of secondary organic aerosol (e.g. Ehn et al., 2014; Mutzel
313 et al., 2015). HOM yields are specific to individual molecules and isomers and most yields have not been investigated for the
314 exact compounds, which are emitted from the tree species considered in this study. Thus, the yields applied for the production
315 of HOM in the model (Appendix B) are connected with a large degree of uncertainty. The influence of changing HOM yields
316 on our results was therefore also investigated (Sec. 3.2, Fig. 11e,j,o,t). Formation of oxygenated organics from oxidation of
317 sesquiterpenes and methyl salicylate are also included (Appendix B). The sum of all organic compounds, which contribute to
318 aerosol processes, is referred to as “OxOrg”.

319
320
321
322
323
324
325



326 **Table 3.** Common changes in the atmospheric concentrations of volatile organic compounds (VOC) and OH during biotic
 327 plant stress. LOX are lipoxygenase pathway volatile compounds.

	Change in VOC concentration	Change in OH concentration	Reference
Stress↑	[LOX]↑ [methyl salicylate]↑ [methanol]↑ [monoterpenes]↑	[OH]↓	Mentel et al. (2013) Calvert et al. (2000) Atkinson et al. (1992) Hakola et al. (1994)
	[sesquiterpenes]↑	[OH]↑	Atkinson and Arey (2003) Winterhalter et al. (2009)
	[isoprene]↓	[OH]?, but most probably [OH]↑	Lelieveld et al. (2008) Taraborrelli et al. (2012) Wells et al. (2020)

328

329 2.7 Calculation of the formation and growth of secondary organic aerosol particles

330 The clustering and activation of new particles are expressed by a formation rate of neutral 2 nm sized clusters, J_2 ($\text{cm}^{-3} \text{s}^{-1}$),
 331 which is computed by Eq. 20, using coefficients (α_{1-3}) from Table 3, both found in Paasonen et al. (2010):

$$332 J_2 = \alpha_1 \times [\text{H}_2\text{SO}_4]^2 + \alpha_2 \times [\text{H}_2\text{SO}_4][\text{OxOrg}] + \alpha_3 \times [\text{OxOrg}]^2 \quad (2)$$

333 It is here assumed that new particles are formed via heteromolecular homogeneous nucleation between sulfuric acid and
 334 oxidised organic compounds (OxOrg) as well as via homogeneous nucleation of sulfuric acid and OxOrg alone. For
 335 simplification, we only operated with one growing aerosol mode and therefore included a unit-less correction term (KK),
 336 which determines how large a fraction of the activated clusters reaches the growing mode (Kerminen and Kulmala, 2002):

$$337 \text{KK} = \exp\left(\eta \times \left[1/D_p - 1/D_{clus}\right]\right) \quad (3)$$

338 where D_p and D_{clus} are the diameters of the growing mode and clusters, respectively, and $D_{clus} = 2$ nm as stated above. Further,
 339 η (nm) is (Eq. 11-12 and Table 1 in Kerminen and Kulmala, 2002):

$$340 \eta = 1830 \text{ nm}^2 \cdot \text{s} \cdot \text{h}^{-1} \times \text{CS/GR} \quad (4)$$

341 and we account for the the fact that the condensation sink (CS) is compound specific and less for oxidised organic
 342 compounds than for sulfuric acid (CS_{SA}) (Peräkylä et al., 2020):

$$343 \text{CS} = \text{CS}_{\text{SA}} \times \frac{[\text{H}_2\text{SO}_4]}{[\text{H}_2\text{SO}_4] + [\text{OxOrg}]} + \text{CS}_{\text{SA}} \times 0.5 \times \frac{[\text{OxOrg}]}{[\text{H}_2\text{SO}_4] + [\text{OxOrg}]} \quad (5)$$

344 The condensational particle diameter growth rate (GR, nm h^{-1}) of newly formed 2-3 nm particles is calculated according to
 345 Nieminen et al. (2010):

$$346 \text{GR}_{2-3 \text{ nm}} = 0.5 \text{ nm} \cdot \text{h}^{-1} \times \text{CC} \times 10^{-7} \text{ cm}^3 \quad (6)$$

347 where CC is the concentration of condensable vapours which we assumed to be the sum of sulfuric acid and OxOrg. In addition,
 348 we assumed that the molar mass of OxOrg are 3.5 times larger than that of sulfuric acid (Ehn et al., 2014), hence:

$$349 \text{CC} = [\text{H}_2\text{SO}_4] + [\text{OxOrg}] \times 3.5^{1/3} \quad (7)$$

350 It is a complex matter to model nanoparticle growth, especially in forested environments, since thousands of individual
 351 molecules with different vapour pressures contribute to the growth, but particle growth rates have been observed to be strongly
 352 size-dependent in the field (Hirsikko et al., 2005; Yli-Juuti et al., 2011; Häkkinen et al., 2013). Hence, we accounted for this
 353 size-dependency by enhancing the growth rates of particles larger than 3 nm, as according to Hirsikko et al. (2005) and Yli-
 354 Juuti et al. (2011):

$$355 \text{GR}_{3-7 \text{ nm}} = 2 \times \text{GR}_{2-3 \text{ nm}} \quad (8)$$

$$356 \text{GR}_{>7 \text{ nm}} = 2.3 \times \text{GR}_{2-3 \text{ nm}} \quad (9)$$



357 The increase in the diameter of the growing mode (D_p) is defined by the growth rate:

$$358 \Delta D_p / \Delta t = GR / 3600 \text{ s} \cdot \text{h}^{-1} \quad (10)$$

359 while the increase in the number of new particles (N_p , cm^{-3}) is determined by the formation of new particles which reaches
360 the growing mode and the coagulation of particles in the growing mode by:

$$361 \Delta N_p / \Delta t = J_2 \times KK - \text{CoagS} \times N_p \quad (11)$$

362 where the coagulation sink (CoagS , s^{-1}) is calculated according to (Lehtinen et al., 2007):

$$363 \text{CoagS} = \text{CS} \times (0.71 \text{ nm} / D_p)^{1.6} \quad (12)$$

364

365 **3 Results and discussion**

366 **3.1 Simulations of biotically stressed and non-infected forest stands throughout a growing season**

367 Simulation results of one full growing season from various non-infected, and moderately and severely infected forest stands
368 are presented in Figs. 5-9. In the figures, emissions, concentrations, the isoprene-to-monoterpenes carbon concentration ratio
369 ($R = [\text{isoprene C}] / [\text{monoterpenes C}] = 0.5 \cdot [\text{isoprene}] / [\text{monoterpenes}]$), the formation and growth rates and number of newly
370 formed particles are expressed as median values during 10:00-16:00 local time, while the particle diameter of the growing
371 mode is provided as the daily maximum.

372

373 **3.1.1 Canopy emissions of VOCs**

374 The emissions of VOCs (Figs. 5a,c,e,g, 7a,b, 8a,b, 9a-c) change throughout the season due to variations in temperature, light,
375 LAI and infection severity. The impact of leaf maturity development on emission predictions are presented in Appendix A and
376 its atmospheric relevance discussed in Sec. 3.2. Canopy emissions of VOCs are highly different from non-infected and infected
377 forest stands, due to plant stress responses, but also due to a decrease in LAI in case of larval infestations (Figs. 5a,c,e,g, 9a-
378 c). Constitutive isoprene emitters (i.e. oak and poplar) decrease their emissions of isoprene significantly during the episodes
379 of biotic stress, and a stronger reduction is observed as a function of an increase in stress severity (Figs. 5a, 7a, 8a). All
380 investigated stresses cause the plants to induce their emissions of monoterpenes greatly (Figs. 5c, 7b, 8b, 9a). The induction
381 in the emissions of monoterpenes increases as a function of stress severity per unit leaf area, but the LAI simultaneously
382 decreases in case of larval infestations, which result in smaller canopy scale emissions from severely defoliated stands
383 compared to moderately stressed stands (Figs. 5c, 9a). Also the emissions of compounds, and groups of compounds, such as
384 methyl salicylate, LOX, methanol, DMNT, sesquiterpenes and oxygenated sesquiterpenes are significantly induced as a result
385 of biotic plant stress (Figs. 5e,g, 7a,b, 8a,b, 9b,c). These compounds, together with monoterpenes, are in most cases not emitted
386 constitutively at all or only in very small abundances. Though the emissions of all induced VOCs increase as a function of the
387 degree of damage, the responses to the level of stress severity are not necessarily the same for all VOCs and all individual
388 stresses. This difference can, for example, be seen in the emissions of monoterpenes (Fig. 5c) and LOX compounds (Fig. 5e)
389 from gypsy moth infested oak forests, which do not peak at the same time in the season.

390

391 **3.1.2 Ambient concentrations of VOCs and OxOrg**

392 Since the concentrations of OH and O_3 are constrained within the simulations, the VOC emission patterns are reflected in the
393 concentration patterns (Figs. 5b,d,f,h, 7c-e, 8c-e, 9e-g). All VOCs, except LOX and methanol, contribute to the formation of
394 OxOrg (Figs. 6a, 7c, 8c, 9d), but the contributions from oxidation of the individual VOCs, or groups of VOCs, vary between



395 the various stress cases and infection severity levels due to differences in emission rates and OxOrg forming yields (Appendix
396 B). For example, in herbivory infested stands, OxOrg originating from monoterpenes make up by far the largest fraction of
397 total OxOrg. This is mainly due to the fact that the induced emissions of monoterpenes are significantly higher than the
398 emissions of other VOCs which contribute to OxOrg formation (Figs. 5c,g, 9a,c). In case of oak powdery mildew infected oak,
399 HOM from monoterpenes and oxygenated organics from methyl salicylate reactions contribute about evenly to the total OxOrg.
400 The reason for this is that the canopy emissions of these VOCs are roughly similar (Fig. 7a,b), the OxOrg yield of methyl
401 salicylate is significantly higher than that of monoterpenes, but oxidation of methyl salicylate is correspondingly slower
402 (Appendix B). The main contributor to the total OxOrg in poplar rust infected poplar stands is sesquiterpenes. Contributions
403 from methyl salicylate, DMNT and α -Eudesmol to total OxOrg are individually rather small, but together, they are close to
404 matching the contribution from monoterpenes. When emissions of sesquiterpenes are omitted from simulations of a severely
405 rust infected poplar stand, the concentration of OxOrg decreases with ~46 %, while, in comparison, the concentration of OxOrg
406 decreases with ~30 % if the emissions of monoterpenes are instead excluded.

407 In the simulations, the daily median (10:00-16:00) ambient concentration of OxOrg is at maximum $\sim 4.2 \times 10^7 \text{ cm}^{-3}$
408 in a gypsy moth infested oak stand (Fig. 6a), $\sim 1.1 \times 10^7 \text{ cm}^{-3}$ in an oak powdery mildew infected oak stand (Fig. 7c), \sim
409 $4.2 \times 10^7 \text{ cm}^{-3}$ in a rust infected poplar stand (Fig. 8c), and $\sim 3.3 \times 10^7 \text{ cm}^{-3}$ in an autumnal moth infested mountain birch
410 stand (Fig. 9d). The ambient concentration of OxOrg is much higher in gypsy moth infested oak stands, than in a non-infested
411 oak stand, during the period of stress (Fig. 6a). When the period of feeding has been concluded, the concentration of OxOrg is
412 higher in non-infested oak stands than in stands that have been exposed to stress due to a higher LAI. However, the
413 concentration of OxOrg is then only ~15-20 % of the OxOrg concentration during the period of stress and it is almost
414 exclusively composed of HOM originating from isoprene. The concentration of OxOrg increases as a function of fungal
415 infection severity, and in our simulations the concentration of OxOrg is higher in fungally infected stands by a factor of up to
416 ~6.9 (oak powdery mildew infected oak stands, Fig. 7c) and ~3.3 (poplar rust infected poplar stands, Fig. 8c). Since the
417 investigated poplar species is a great constitutive isoprene emitter, relatively high concentrations of OxOrg are predicted for
418 the non-infested poplar stand (Fig. 8c). In mountain birch stands, the concentration of OxOrg is up to 2-2.5 times higher in
419 autumnal moth infested stands during the feeding period than in a non-infested birch stand (Fig. 9d). The difference in OxOrg
420 concentration between moderately and severely infested birch stands is small, due to the combined effects of stress response
421 (which is a function of the degree of damage) and LAI reduction (Fig. 9d), but towards the conclusion of the feeding period,
422 the concentration of OxOrg is significantly higher in the less defoliated stand.

423

424 3.1.3 Formation of new particles

425 New particles are assumed to be formed from OxOrg and sulfuric acid (Sec. 2.7, Eq. 2). Since the concentration of sulfuric
426 acid is constrained within the simulations, the concentration pattern of OxOrg is reflected in the seasonal pattern of the
427 formation rates (Figs. 6c-e, 7f, 8f, 9h,i). Thus, in case of gypsy moth infested oak, the formation rates are much higher (increase
428 by up to a factor of ~5 (J_2), ~7 (J_3), ~11 (J_{10})) in stressed stands than in non-infested stands during the period when the plants
429 are exposed to stress (Figs. 6c-e). The predicted J_2 in gypsy moth infested oak stands is comparable to e.g. observations from
430 Melpitz, Germany ($\sim 9.4 \text{ cm}^{-3} \text{ s}^{-1}$, Paasonen et al., 2010) and San Pietro Capofiume, Italy ($\sim 13 \text{ cm}^{-3} \text{ s}^{-1}$, Paasonen et al.,
431 2010). Both Melpitz and San Pietro Capofiume are rural sites influenced by anthropogenic pollution (Paasonen et al., 2010).
432 The modelled J_2 in a non-infested oak stand is comparable to observations from Hohenpeissenberg ($\sim 2.3 \text{ cm}^{-3} \text{ s}^{-1}$, Paasonen
433 et al., 2010) and similar or even higher than typical formation rates measured in the boreal Scots pine forest in Hyytiälä,
434 Finland ($\sim 1 - 2 \text{ cm}^{-3} \text{ s}^{-1}$, Paasonen et al., 2010; Kulmala et al., 2012, 2013; Vana et al., 2016) and in the hemiboreal forest
435 in Järvseljä, Estonia ($\sim 1.09 \pm 1.06 \text{ cm}^{-3} \text{ s}^{-1}$, Vana et al., 2016). By analysing data from Hyytiälä and Järvseljä, Vana et al.
436 (2016) showed that the values of J_3 were in general about 60-80 % of those of J_2 . Our simulations of a non-infested oak stand



437 follow this threshold, thus, the predicted J_3 in a non-infested oak stand is somewhat higher than observations from Hyytiälä
438 ($\sim 0.6 \text{ cm}^{-3} \text{ s}^{-1}$, Kulmala et al., 2012, 2013; Nieminen et al., 2014; Vana et al., 2016) and Järvelsä ($\sim 0.8 \text{ cm}^{-3} \text{ s}^{-1}$, Vana
439 et al., 2016). J_3 in gypsy moth infested oak stands is high, but similar values have occasionally been observed in Hyytiälä (up
440 to about $10 \text{ cm}^{-3} \text{ s}^{-1}$, Nieminen et al., 2014). Formation rates of 5 nm particles ($J_5 = 1.0 \pm 1.1 \text{ cm}^{-3} \text{ s}^{-1}$, Yu et al., 2014)
441 measured in an oak forest in Missouri, USA, are much less than J_{10} in our simulated infested stands, and so are e.g. also
442 formation rates of 10 nm particles ($J_{10} = 1.2 \text{ cm}^{-3} \text{ s}^{-1}$, Yli-Juuti et al., 2009) measured in a mixed forest in K-pusztá, rural
443 Hungary. Thus, the predicted formation rates in a non-infested oak stand are comparable, and in the case of gypsy moth infested
444 oak stands, often much higher than observations from forests with intense new particle formation events.

445 The formation rates of new particles are always higher in oak powdery mildew infected oak stands than in a non-
446 infested oak stand (Fig. 7f), though the fungus is not able to perturb the formation rates as strongly (increase by up to a factor
447 of ~ 2.3 (J_2), ~ 3.0 (J_3), ~ 5.3 (J_{10})) as herbivory by gypsy moth larvae.

448 Simulations of poplar stands suggest that particles will be formed at high rates in the range $\sim 3.6 - 11.4 \text{ cm}^{-3} \text{ s}^{-1}$
449 (J_2) and $\sim 2.7 - 10.6 \text{ cm}^{-3} \text{ s}^{-1}$ (J_3) during the late summer when the full leaf state has been attained, and our simulations
450 suggest that new particles will be formed the fastest in severely rust infected stands (increase by up to a factor of ~ 3.2 (J_2),
451 ~ 3.9 (J_3)).

452 In our simulations, herbivory by autumnal moth induces the formation rates of new particles in mountain birch stands
453 by up to a factor of ~ 2.5 (J_2) and ~ 2.6 (J_3). The formation rates of 2 and 3 nm particles are predicted to vary between
454 $0.38 \text{ cm}^{-3} \text{ s}^{-1}$ and $2.5 \text{ cm}^{-3} \text{ s}^{-1}$ (J_2), and $0.31 \text{ cm}^{-3} \text{ s}^{-1}$ and $2.5 \text{ cm}^{-3} \text{ s}^{-1}$ (J_3) in stressed stands, and between $0.32 \text{ cm}^{-3} \text{ s}^{-1}$
455 and $1.1 \text{ cm}^{-3} \text{ s}^{-1}$ (J_2), and $0.26 \text{ cm}^{-3} \text{ s}^{-1}$ and $0.99 \text{ cm}^{-3} \text{ s}^{-1}$ (J_3) in non-infested stands. The higher end of these values is
456 comparable to rates observed in Hohenpeissenberg and Hyytiälä (see above). Kyrö et al. (2014) reported that the monthly
457 averaged formation rate of 3 nm particles during 2005 - 2011, at the SMEAR I station in Värriö, varied throughout the year by
458 $0.04 - 0.45 \text{ cm}^{-3} \text{ s}^{-1}$, and by $0.16 - 0.23 \text{ cm}^{-3} \text{ s}^{-1}$ during the summer months. Analysis of year 2013 and 2014, also in
459 Värriö, lead to a median formation rate of $0.14 \pm 0.05 \text{ cm}^{-3} \text{ s}^{-1}$ (J_3) (Vana et al., 2016). Thus, the predicted formation rates
460 in, especially, non-infested mountain birch stands in Lapland are generally within range, but often somewhat higher than
461 observations from the same location. It should, though, be mentioned that these literature values cannot be used to validate our
462 simulation results, since Scots pines, and not mountain birches, dominate the SMEAR I site (Kyrö et al., 2014), and the LAI
463 of mountain birches at the station is significantly less than $2 \text{ m}^2 \text{ m}^{-2}$ (Ylivinkka et al., 2020). The modelled formation rates are
464 not compared to observations from the mountain birch dominated areas in Lapland, since such observations do not, to our
465 knowledge, exist.

466 A very recent investigation of long-term field observations (25 years) from the SMEAR I station (Ylivinkka et al.,
467 2020), where autumnal moth larvae are prominent defoliators of mountain birches, did, however, not find any evidence that
468 herbivory by autumnal moth would enhance the formation, nor growth, of atmospheric aerosol particles during the summer of
469 infestation. Instead there was some evidence of elevated total particle concentrations for a few years after the summer with
470 larval infestation, which was speculated to be caused by delayed defense responses of mountain birches. It is, however, possible
471 that the total foliage mass of mountain birches in the area is too small, or that the level of infestation was too low during the
472 investigated time period, in order to cause detectable changes in aerosol variables (Ylivinkka et al., 2020).

473 The amount of newly formed particles is predicted to be up to about one order of magnitude higher in a gypsy moth
474 infested oak stand than in a non-infested oak stand, with a 10:00-16:00 median of up to $\sim 1.4 \cdot 10^5 \text{ cm}^{-3}$ in an infested stand
475 (Fig. 6f). Such a high production of new particles is comparable to observations from e.g. Melpitz (Größ et al., 2018). The
476 number of produced particles in a non-infested oak stand ($\sim 1.1 \cdot 10^4 \text{ cm}^{-3}$; Fig. 6f) is comparable to e.g. the number of new
477 particles produced during a typical new particle formation event in Hyytiälä ($\sim 1 - 2 \cdot 10^4 \text{ cm}^{-3}$; Dal Maso et al., 2008;
478 Nieminen et al., 2014), but significantly higher than observations from a Missouri oak forest, where sub-5 nm particles were
479 measured to be up to $\sim 2 \cdot 10^4 \text{ cm}^{-3}$, and 5-25 nm particles to $\sim 3000 \text{ cm}^{-3}$, during typical new particle formation events



480 (Yu et al., 2014). After the period of stress, the number of particles in the growing mode is predicted to range between $\sim 7 \cdot$
481 10^3 cm^{-3} and $\sim 17 \cdot 10^3 \text{ cm}^{-3}$ in a non-infested stand, $\sim 6 \cdot 10^3 \text{ cm}^{-3}$ and $\sim 12 \cdot 10^3 \text{ cm}^{-3}$ in a 30 % defoliated stand and
482 between $\sim 3 \cdot 10^3 \text{ cm}^{-3}$ and $\sim 5 \cdot 10^3 \text{ cm}^{-3}$ in a 80 % defoliated oak stand (Fig. 6f). Oak powdery mildew is predicted to
483 enhance the number of particles in the growing mode by up to a factor of ~ 4 compared to the corresponding non-infected
484 stand, resulting in a maximum of $\sim 1.7 \cdot 10^4 \text{ cm}^{-3}$ in an infested stand, under the used border conditions (Fig 7g). Under the
485 same environmental conditions, a severely poplar rust infected poplar stand is predicted to produce up to about five times as
486 many new particles as a non-infected poplar stand, leading to a maximum of about $1.1 \cdot 10^5 \text{ cm}^{-3}$ in a severely infected stand
487 (Fig 8h). Finally, it is predicted that herbivory by autumnal moth enhances the amount of produced particles by up to a factor
488 of ~ 2.7 , with a maximum number of particles in the growing mode of $\sim 3 \cdot 10^4 \text{ cm}^{-3}$ in an infested birch stand (Fig. 9j). The
489 predicted amount of particles in a non-infested mountain birch stand is in the same order as observations from Finnish Lapland
490 (Komppula et al., 2006).

491

492 3.1.4 New particle growth

493 New particles are assumed to grow by sulfuric acid and OxOrg (Sec. 2.7, Eq. 6-9), hence the seasonal patterns of formation
494 rates and OxOrg concentration are reflected in the pattern of the growth rates (Figs. 6g, 7h, 8g, 9k), and therefore also in the
495 season pattern of the number (Figs. 6f, 7g, 8h, 9j) and size (Figs. 6h, 7g, 8g, 9l) of the growing particle mode. We predict that
496 the 10:00-16:00 median growth rate in a gypsy moth infested oak stand is at maximum $\sim 5.9 \text{ nm h}^{-1}$ under the assumed
497 boundary conditions, whereas the corresponding growth rate in a non-infested oak stand is around 1.6 nm h^{-1} , when the full
498 leaf state has been attained (Fig. 6g). For comparison, the growth rate of new particles has been reported to range from 0.5 to
499 12 nm h^{-1} in Hyytiälä (Dal Maso et al., 2007), with median values of 2.1 nm h^{-1} (Vana et al., 2016), 2.5 nm h^{-1} (Dal Maso
500 et al., 2007), and 3.3 nm h^{-1} (Paasonen et al., 2010), depending on which years the data covered. Dal Maso et al. (2007)
501 reported that the growth rate of new small particles in Aspöreten, a rural site in Sweden dominated by deciduous and conifer
502 forests and some farmlands, ranged between 1 and 11 nm h^{-1} , with a median value of 3.4 nm h^{-1} . The growth rate was found
503 to range from 2.1 to 22.9 nm h^{-1} , with a median value of 7.25 nm h^{-1} during spring in a mixed deciduous forest area close
504 to Heidelberg in Germany, under influence of anthropogenic pollution (Fiedler et al., 2005). Growth rates from an oak forest
505 in Missouri, USA, were in the range $1.6 - 11.2 \text{ nm h}^{-1}$ (Yu et al., 2014). Median values for the growth rate have been reported
506 to be 4.2 nm h^{-1} in Melpitz (Paasonen et al., 2010), 4.6 nm h^{-1} in Järveljä (Vana et al., 2016), 4.8 nm h^{-1} in
507 Hohenpeißenberg (Paasonen et al., 2010) and 9.5 nm h^{-1} in San Pietro Capofiume (Paasonen et al., 2010). Thus, we can
508 conclude that our predicted growth rates are comparable to atmospheric observations from several different rural sites. Growth
509 rates obtained from areas influenced by anthropogenic pollution are generally higher than our simulated rates, but this is
510 expected, since our model is constrained by conditions representative for rural sites.

511 Growth rates are predicted to be lower in an oak powdery mildew infected oak forest, than in a gypsy moth infested
512 oak forest. The rates are predicted to, at maximum, be $\sim 2.0 \text{ nm h}^{-1}$ (80 % of leaf area covered by mildew), $\sim 1.6 \text{ nm h}^{-1}$
513 (30 % of leaf area covered by mildew) and $\sim 1.2 \text{ nm h}^{-1}$ (non-infested, in the same environmental conditions as the infected
514 trees) (Fig. 7h). Thus, the growth rates are similar to the lower end of the observed range.

515 The growth of small particles in non-infested and rust infected poplar stands are predicted to range between ~ 2.1
516 and $\sim 5.7 \text{ nm h}^{-1}$, during the late summer when the full leaf state has been attained, with the fastest growth in a heavily rust
517 infected forest stand (Fig. 8g). This range in growth rates is thus similar to simulation results of herbivory infested oak (see
518 above; Fig. 6g).

519 The predicted growth rates are smallest in simulations of non-infested mountain birch stands in Lapland. The 10:00-
520 16:00 median growth rate is at maximum predicted to be $\sim 4.1 \text{ nm h}^{-1}$ in an infested stand and varies between $\sim 0.6 \text{ nm h}^{-1}$
521 and $\sim 2.0 \text{ nm h}^{-1}$ in a non-infested stand (Fig. 9k). These values are in line with observations from Värriö (median: $1.6 \pm$



522 0.9 nm h⁻¹, Vana et al., 2016; monthly summer mean: 3.7 – 4.4 nm h⁻¹, Kyrö et al., 2014; range: 1 – 10 nm h⁻¹, median:
523 2.4 nm h⁻¹, Dal Maso et al., 2007) and from Pallas, Finnish Lapland (median: 2.0 nm h⁻¹, daily range: 0.5 – 11 nm h⁻¹, Dal
524 Maso et al., 2007; monthly range: 1.9 – 4.6 nm h⁻¹, Asmi et al., 2011).

525 According to our predictions, new particles will grow up to about 46 nm larger in an oak gypsy moth infested oak
526 stand compared to a non-infested oak stand within one day (Fig. 6h). Simulation results for the other species/stressors show
527 that new particles will grow up to about 8 nm more in an oak powdery mildew infected stand (Fig. 7g), ~ 28 nm more in a
528 poplar rust infected poplar stand (Fig. 8g), and ~ 26 nm larger in an autumnal moth infested mountain birch stand (Fig. 9l),
529 within one day, compared to their corresponding non-infested stands. In our simulations, the newly formed particles in non-
530 infested oak stands are always mainly formed and grown by sulfuric acid (Figs. 6h, 7g), but in modelling of non-infested
531 poplar, more than half of the formation and growth is due to HOM originating from isoprene (Fig. 8g), while HOM formed
532 from monoterpenes account for a large fraction of the predicted formation and growth in non-infested birch stands (Fig. 9l).

533

534 3.1.5 R: the isoprene-to-monoterpenes carbon concentration ratio

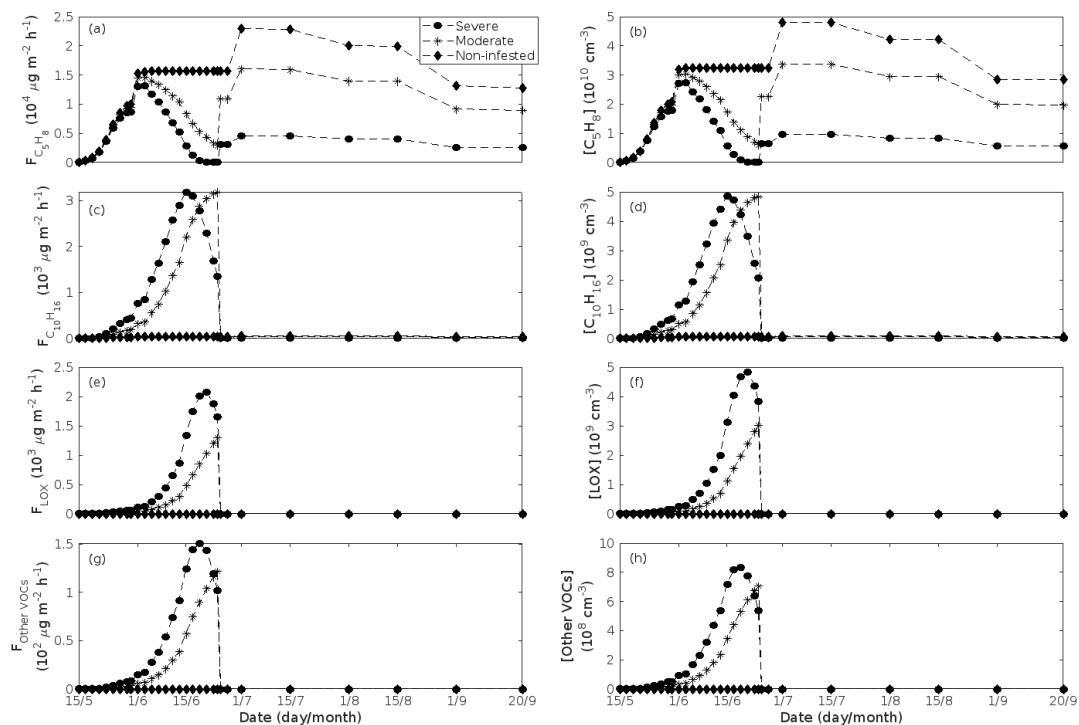
535 Previous chamber studies (Kiendler-Scharr et al., 2009, 2012; McFiggans et al., 2019; Heinritzi et al., 2020) have suggested
536 that isoprene suppresses the formation of new particles from monoterpenes when the isoprene-to-monoterpene carbon
537 concentration ratio (R) becomes too high. New particle formation has rarely been observed in the field when R>1 (e.g.
538 Kanawade et al., 2011; Pöschl et al., 2010; Pöhlker et al., 2012; Lee et al., 2016). For example, Yu et al. (2014) observed
539 formation of sub-5 nm particles during 64 % of the measured days in an oak forest, though R was 15.3 ± 7.2 during the
540 campaign period. However, since the formation of new particles occurs on a regional scale, the authors suggested that the
541 detected particles could have been formed at lower R and advected to their measurement site. Contrarily, it has earlier been
542 proposed that oxidation products of isoprene (e.g. IEPOX) promote the growth of existing new particles ($D_p > 3$ nm, e.g.
543 Surratt et al., 2010; Lin et al., 2013), while Heinritzi et al. (2020) observed the growth of particles above 3.2 nm to be unaffected
544 by the concentration of isoprene. It is thus likely that the zone of R values, inside which the probability for new particle
545 formation to occur changes, is influenced by other environmental factors and is therefore location and/or season dependent.

546 New particle formation has also been observed in the upper troposphere in tropical regions (Andreae et al., 2018;
547 Williamson et al., 2019) where isoprene dominates the emission spectrum greatly. The hypothesis is that isoprene is vertically
548 transported via strong convection and new particles are formed from isoprene oxidation products, which is possible due to
549 lower temperature conditions in the upper troposphere.

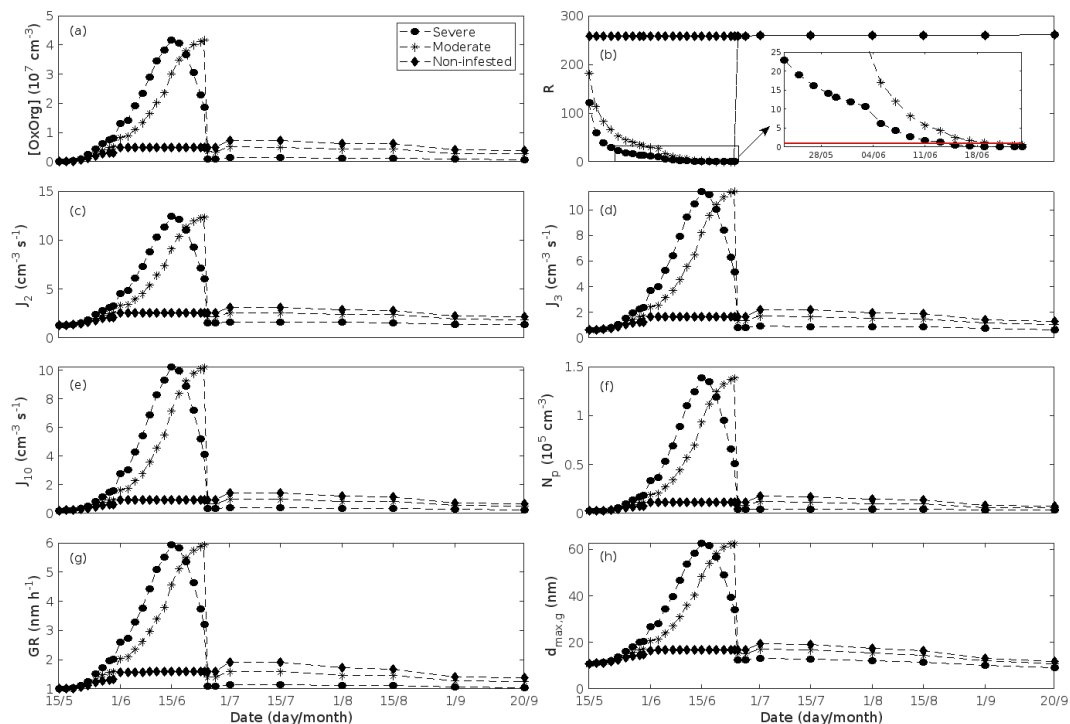
550 The concentration ratio of isoprene-to-monoterpene carbon is very high in non-infested oak and poplar stands and in
551 oak stands which are no longer exposed to herbivory (Figs. 6b, 7d, 8d), and it is therefore questionable whether particles will
552 be formed at all in the atmospheric boundary layer from these stands when they are not experiencing stress. Biotic stress greatly
553 reduces R in all three cases. R is most significantly decreased to a minimum 10:00-16:00 median value of 0.004 in simulations
554 of gypsy moth infested oak stands (Fig. 6b), but the period with low R values is rather short. For example, R < 1 during only
555 11 and 4 days, respectively, while R < 22.5 (probably the highest ratio at which new particles formation has been observed in
556 the field, Yu et al., 2014) during 32 and 21 days, respectively, in our simulations of a severely and moderately European gypsy
557 moth infested oak stand (Fig. 12e). R is predicted to be close to 1, though never below 1, in simulations of both oak powdery
558 mildew infected oak stands and rust infected poplar stands. The duration where R is e.g. less than 22.5 is 39 days in a severely
559 mildew infected oak stand, 31 days in a moderately mildew infected oak stand, and 27 days in a severely rust infected poplar
560 stand (Fig. 12e). For comparison, R is never predicted to be less than 22.5 in a moderately infected poplar stand (Fig. 8d).
561 Even if new particles are not formed from oak powdery mildew or poplar rust infected stands in the boundary layer, then both
562 the potential to form new particles in the upper troposphere (Figs. 7f,g, 8f,h) and the potential to grow already existing particles,
563 which are formed in nearby stands and horizontally transported to the infected stands (Figs. 7g,h, 8g), are still predicted to be



564 greater than in our simulations of the correspondingly non-infested stands. R is not relevant in the case of mountain birch,
565 since this tree species does not emit isoprene constitutively, nor in response to herbivory stress by autumnal moth larvae (Yli-
566 Pirilä et al., 2016; Rieksta et al., 2020).
567



568
569 **Figure 5.** A pure oak stand infested with European gypsy moth larvae in comparison to a non-infested pure oak stand. Canopy
570 emissions of (a) isoprene, (c) monoterpenes, (e) lipoxigenase pathway volatiles (LOX), and (g) the sum of other VOCs which
571 contribute to OxOrg formation (here i.e. methyl salicylate and dimethyl-nonatriene). Atmospheric concentrations of (b)
572 isoprene, (d) monoterpenes, (f) lipoxigenase pathway volatiles, and (h) the sum of other VOCs which contribute to OxOrg
573 formation. “Moderately” and “severely” refer to 30 % and 80 %, respectively, of the leaf area that has been consumed by the
574 end of the feeding period.
575

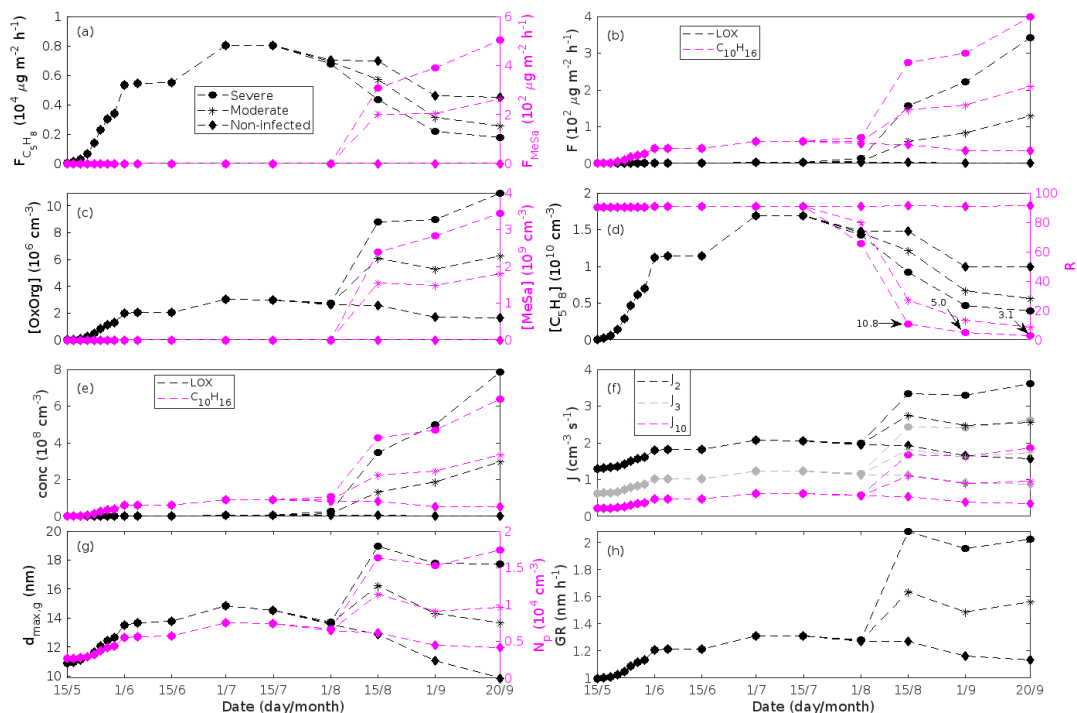


576

577 **Figure 6.** A pure oak stand infested with European gypsy moth larvae in comparison to a non-infested pure oak stand. (a)
 578 atmospheric concentrations of OxOrg. (b) the ratios of isoprene-to-monoterpenes carbon concentrations, where the red line
 579 indicates $R = 1$. Formation rates of (c) 2, (d) 3 and (e) 10 nm particles. (f) number concentrations of formed particles, (g)
 580 growth rates of newly formed particles, and (h) the daily maxima diameter of the growing particle mode. “Moderately” and
 581 “severely” refer to 30 % and 80 %, respectively, of the leaf area that has been consumed by the end of the feeding period.



582

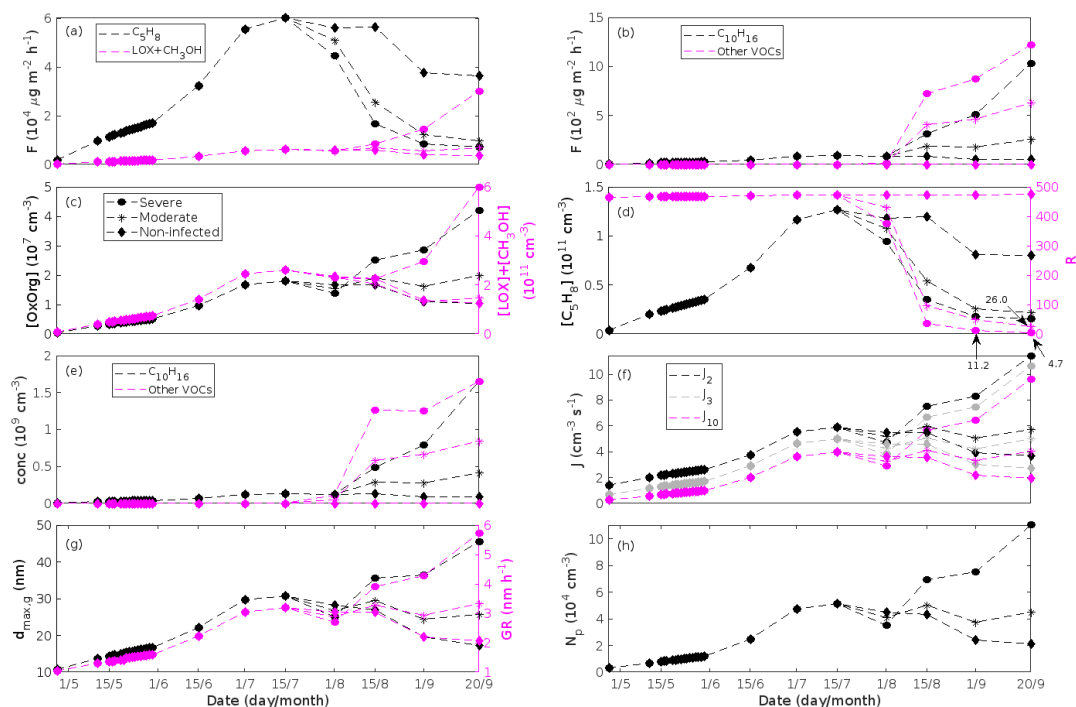


583

584 **Figure 7.** A pure oak stand infected by oak powdery mildew in comparison to a non-infected pure oak stand. Canopy emissions
 585 of (a, left axis) isoprene, (a, right axis) methyl salicylate, (b) lipoxygenase pathway volatiles and monoterpenes. Atmospheric
 586 concentrations of (c, left axis) OxOrg, (c, right axis) methyl salicylate, (d, left axis) isoprene, and (e) lipoxygenase pathway
 587 volatiles and monoterpenes. (d, right axis) the ratios of isoprene-to-monoterpene carbon concentrations. (f) formation rates of
 588 2, 3 and 10 nm particles. (g, left axis) daily maxima diameter of the growing particle mode, and (g, right axis) number
 589 concentrations of formed particles. (h) growth rates of newly formed particles. “Moderately” and “severely” refer to 30 % and
 590 80 %, respectively, of the leaf area that has been infected by fungi by the onset of senescence.



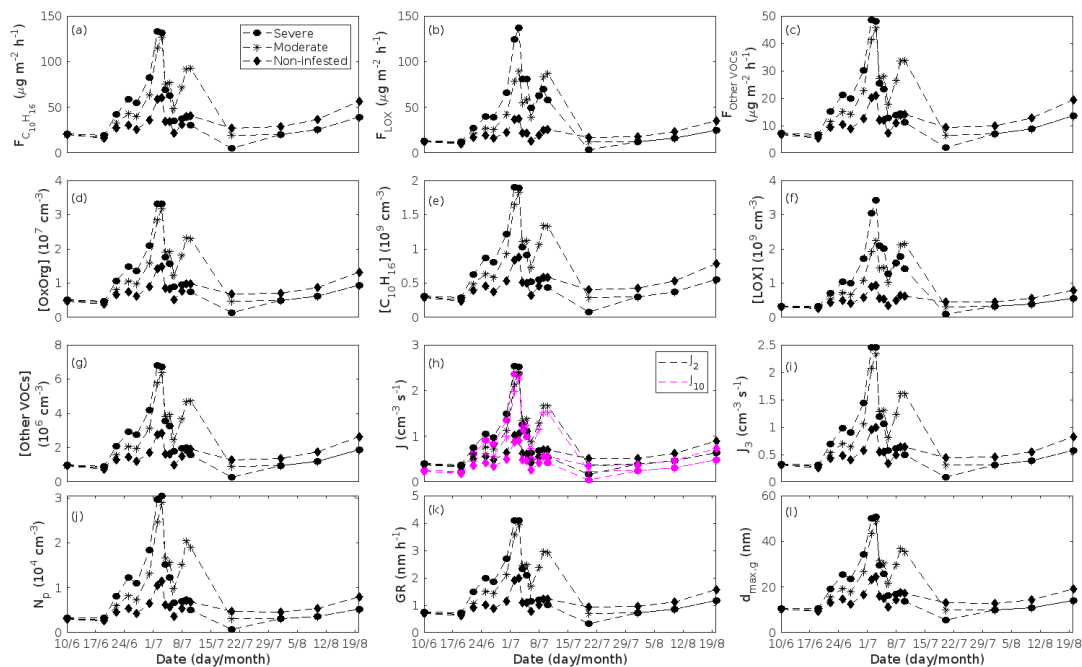
591



592

593 **Figure 8.** A pure poplar stand infected by rust fungi in comparison to a non-infected pure poplar stand. Canopy emissions of
 594 (a) isoprene and the sum of lipoxygenase pathway volatiles and methanol, (b) monoterpenes and the sum of other VOCs which
 595 contribute to OxOrg formation (here i.e. methyl salicylate, dimethyl-nonatriene, α -Eudesmol and sesquiterpenes). Atmospheric
 596 concentrations of (c, left axis) OxOrg, (c, right axis) the sum of lipoxygenase pathway volatiles and methanol, (d, left axis)
 597 isoprene, and (e) monoterpenes and the sum of other VOCs which contribute to OxOrg formation. (d, right axis) the ratios of
 598 isoprene-to-monoterpene carbon concentrations. (f) formation rates of 2, 3 and 10 nm particles. (g, left axis) daily maxima
 599 diameter of the growing particle mode, and (g, right axis) growth rates of newly formed particles. (h) number concentrations
 600 of formed particles. “Moderately” and “severely” refer to 30 % and 80 %, respectively, of the leaf area that has been infected
 601 by fungi by the onset of senescence.

602



603

604 **Figure 9.** A pure mountain birch stand infested with autumnal moth larvae in comparison to a non-infested pure mountain
 605 birch stand. Canopy emissions of (a) monoterpenes, (b) lipoxygenase pathway volatiles, and (c) the sum of other VOCs which
 606 contribute to OxOrg formation (here i.e. dimethyl-nonatriene and sesquiterpenes). Atmospheric concentrations of (d) OxOrg,
 607 (e) monoterpenes, (f) lipoxygenase pathway volatiles, and (g) the sum of other VOCs which contribute to OxOrg formation.
 608 Formation rates of (h) 2, 10 and (i) 3 nm particles. (j) number concentrations of formed particles. (k) growth rates of newly
 609 formed particles. (l) daily maxima diameter of the growing particle mode. “Moderately” and “severely” refer to 30 % and 80
 610 %, respectively, of the leaf area that has been consumed by the end of the feeding period.

611

612 3.2 Estimating the reliability of our results

613 Since aerosol processes are very sensitive to changes in environmental conditions - conditions which can vary greatly, both
 614 interannually, but also from day to day, we investigated the influence of a wide range of realistic and relevant environmental
 615 conditions (Table C1 in Appendix C) on our model predictions (Figs. 10-11, C1-2 in Appendix C). Nine different sensitivity
 616 tests (ST1-9) were conducted for all plant species and infections, where only one parameter was changed at a time (Table C1).
 617 For these simulations, the default values listed in Table 2 were used, while the default maximum daily temperature at
 618 Hohenpeissenberg and SMEAR I were assigned to 25 °C and 20 °C, respectively, and the default LAI for oak/poplar and birch
 619 was assumed to be 5 m² m⁻² and 2 m² m⁻², respectively. All aerosol parameters (formation and growth rates, diameter, number
 620 of particles) show a similar response to changes in the considered environmental parameters, thus only the impact on the
 621 number of newly formed particles (Figs. 10-11) and the rate at which new small particles grow (Figs. C1-2) is displayed.

622 As is also observed in nature, certain conditions suppress or prevent the formation of new particles, such as for
 623 example a high condensation sink (Fig. 11d,i,n,s; e.g. Hyvönen et al., 2005; Nieminen et al., 2015; Vana et al., 2016) and low
 624 sulfuric acid concentration (Fig. 11c,h,m,r; e.g. Boy et al., 2005; Nieminen et al., 2014), making the atmospheric relevance of
 625 the forest stands minor. Since we have assumed realistic conditions, but at the same time conditions which do not prevent the
 626 formation of new particles, in our simulations, the number of predicted days with occurring new particle formation is the



627 theoretical maximum for clean environments, which our aerosol theory is based on (Sec. 2.7). Though the absolute number of
628 predicted new particles depend highly on the assumed environmental conditions (Figs. 10-11), the relative difference between
629 non-infected and stressed stands of the same tree species is not impacted: e.g. the number of new particles is always
630 significantly higher in gypsy moth infested, and oak powdery mildew infected, oak stands, than in non-infected oak stands,
631 when the environmental conditions are assumed to be the same in all stands (Figs. 10a-h, 11a-j). Likewise, more particles are
632 always formed in moderately, than severely, moth infested oak and birch stands, since the decrease in LAI is stronger than the
633 increase in the stress-induced emission response per unit leaf area (Figs. 10a-d,m-p, 11a-e,p-t). This is emphasised in very
634 severely infested mountain birch stands (e.g. 80 % defoliation), where the number of produced particles is always less than in
635 its corresponding non-infested stand (Figs. 10m-p, 11p-t).

636 Sensitivity tests were also carried out in order to assess whether the simplifications made in the model are valid: (1)
637 As mentioned earlier (Sec. 2.4), we did not incorporate a full canopy environment in the model - an approach which has also
638 been taken by other investigators (e.g. Simpson et al., 1999, 2012; Bergström et al., 2014). In ST2 (Table C1, Figs. 10b,f,j,n,
639 C1b,f,j,n) changes in light conditions exclusively impact the predicted emissions of VOCs. From Figs. 10b,f,j,n, C1b,f,j,n it is
640 clear that even assuming extremely different light environments would not change our conclusions about the atmospheric
641 importance of biotic plant stresses, since our results show that stressed forest with a maximum light availability down to 200
642 $\mu\text{mol m}^{-2} \text{s}^{-1}$ would still produce more new particles than its correspondingly non-infested stand at theoretically clear sky
643 conditions (Fig. 10b,f,j,n). A highly autumnal moth stressed mountain birch stand (80 % defoliation) would possibly produce
644 slightly more particles than a non-infested stand, if a full canopy environment would be considered. For example, the number
645 of produced particles is slightly higher in a birch stand experiencing a stress level of 80 % under $1000 \mu\text{mol m}^{-2} \text{s}^{-1}$ than a non-
646 infested stand under $400 \mu\text{mol m}^{-2} \text{s}^{-1}$ (Fig. 10n). However, the LAI of mountain birch stands is usually rather low (Heiskanen,
647 2006), making the difference in light environment between a non-infested and a highly defoliated stand small. Since mildew
648 and rust do not decrease the leaf area of their host, a different treatment of the light environment would not influence the
649 relative atmospheric importance of fungally infected oak and poplar vs their correspondingly non-infested stands (Fig. 10f,j).

650 (2) In ST3 (Table C1, Figs. 10c,g,k,o, C1c,g,k,o) and in our seasonal simulations (Figs. 5-9), the change of
651 temperature only impacts the emission rates of VOCs. In reality, the vapour pressures of oxidised compounds increase non-
652 linearly with an increase in temperature (e.g. Bilde et al., 2015), and less HOM, and other oxidised organic compounds, will
653 therefore condense at higher temperatures, whereby the formation and subsequent growth of particles will decrease
654 (Stolzenburg et al., 2018; Simon et al., 2020). Gas phase chemistry, including the formation of HOM, is also in reality
655 temperature dependent (e.g. Quéléver et al., 2019). These effects have not been included in the model. Since the range of daily
656 maximum temperatures throughout the growing season is assumed to be rather narrow (Fig. 4), this effect does not greatly
657 impact our results (Sec. 3.1), but it means that the number of particles produced at high temperatures (Fig. 10c,g,k,o), and the
658 growth rate at which they are produced (Fig. C1c,g,k,o), are overestimated for both non-infested and stressed forests.

659 (3) The concentrations of ozone and OH were unaltered between simulations of non-infested forests and forests under
660 varying degrees of infection (Sec. 2.6), though in reality, the atmospheric oxidation capacity is controlled by changes in the
661 concentration of atmospheric trace gases, including VOCs. The total emission of VOCs from oak and poplar stands is greatly
662 dominated by isoprene, but the emission of isoprene decreases as a function of biotic stress severity (Figs. 5a, 7a, 8a). In
663 contrast, the emission of LOX, methyl salicylate, methanol, monoterpenes and sesquiterpenes increases as the level of stress
664 increases (Figs. 5c,e,g, 7a,b, 8a,b). The oxidation of isoprene, LOX, methyl salicylate and methanol is primarily driven by
665 reactions with OH, and also monoterpenes react with OH, which all leads to reductions in the concentration of OH (Table 3),
666 though e.g. ozonolysis of monoterpenes also produce OH, which thus counters part of the reduction. When considering the
667 reaction rates and emission rates of the considered VOCs in simulations of oak and poplar stands, the concentration of OH is
668 mainly controlled by changes in the emission of isoprene. Thus, we expect that the concentration of OH will increase as the
669 degree of stress increases, but even a strong shift in the concentration of OH, will not change the conclusion about the relative



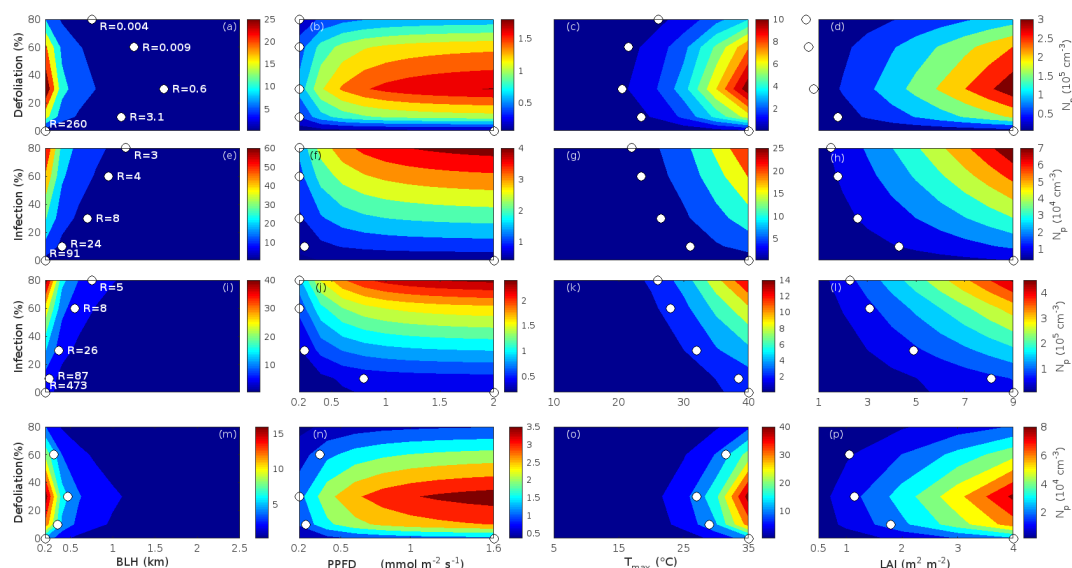
670 atmospheric importance of stressed vs stress-free oak and poplar forests (Figs. 11b,g,l,q, C2b,g,l,q). The absolute number of
671 predicted new particles in herbivory stressed oak stands will, however, be predicted to be smaller at higher levels of OH (Fig.
672 11b), because the oxidation of monoterpenes is then more strongly controlled by OH, which leads to a smaller production of
673 HOM, as monoterpenes typically form HOM at a considerably lower yield from reactions with OH than ozone (Appendix B).
674 A similar shift in the oxidation of monoterpenes is happening in case of oak powdery mildew infected oak, but the effect is
675 counted by an increase in the formation of oxidised organic compounds from oxidation of methyl salicylate at high levels of
676 OH, leading totally to higher predicted particle number concentrations (Fig. 11g). Considering the emissions from biotically
677 stressed and non-infested mountain birch, we estimate that the concentration of OH should stay largely the same, or potentially
678 decrease slightly at higher levels of infestation, which will enhance the oxidation of monoterpenes by ozone, which will lead
679 to a larger production of HOM and thereby a slightly higher predicted number of new particles (Fig. 11q). In the atmosphere,
680 the production of sulfuric acid is limited by the availability of OH, and it is therefore possible that the effects of changes in the
681 concentration of OH (Fig. 11b,q) and sulfuric acid (Fig. 11c,r), in herbivory stressed stands, on the absolute number of
682 predicted new particles, will cancel out or even lead to a stronger particle production than predicted. In case of oak powdery
683 mildew infected oak, the two effects will enhance each other and result in an even higher number of predicted particles. In
684 clean, low NO_x environments, which we aimed to simulate, the concentration of ozone is largely unaffected by the ambient
685 concentration of isoprene (e.g. Jenkin et al., 2015). However, isoprene forms ozone progressively with an increased availability
686 of NO_x (e.g. Jenkin and Clemitshaw, 2000). Higher ozone levels support enhanced formation of HOM, and thus aerosol
687 processes, but the production of HOM is also known to decrease as a function of increased NO_x concentration (e.g. Ehn et al.,
688 2014), whereby the formation and growth of new particles becomes suppressed (e.g. Yan et al., 2020; Pullinen et al., 2020).

689 (4) As mentioned earlier (Sec. 2.6), many HOM yields have not been investigated for the exact compounds which are
690 emitted from the tree species, which are the focus of this study. From Fig. 11e,j,o,t it is obvious, that even if all the OxOrg
691 yields used for simulations of only biotically stressed forests were to be decreased significantly - in case of moderately
692 herbivory infested oak (30 % of leaf area defoliated) by down to about 95 % - biotically stressed oak, poplar and mountain
693 birch forests would still, in most cases, produce more particles than non-infested forests of the same tree species. The yields,
694 at which HOM are formed, have been treated as fixed values (Appendix B) in the seasonal simulations (Sec. 3.1), but the yields
695 actually depend on several factors, such as e.g. the concentration of NO_x (point 3 above; Ehn et al., 2014), temperature (point
696 3 above; Quéléver et al., 2019; Simon et al., 2020) and the ambient blend of VOCs (Sec. 3.1.5; McFiggans et al., 2019). Exactly
697 how the formation and growth of new particles depend on the VOC blend is still uncertain, but it has recently been
698 demonstrated that a linear addition of the yields from the individual yields of components in the VOC mixture will result in an
699 overestimation of both the number and size of particles (McFiggans et al., 2019). As we have followed a similar procedure,
700 this effect might cause our predicted aerosol processes (Sec. 3.1) to be overestimated, but since the ratio of isoprene-to-
701 monoterpenes carbon concentration is much higher in non-infested oak and poplar stands than in the correspondingly stressed
702 stands (Figs. 6b, 7d, 8d), the overestimation is expected to be more pronounced in the non-infested stands (McFiggans et al.,
703 2019). The difference in the atmospheric importance of non-infested and biotically stressed oak and poplar stands thereby
704 widens (Fig. 11e,j,o).

705 It is well known that the potential for foliage to emit VOCs depends on the age of the foliage: emerging and growing
706 foliage usually emits isoprene at reduced rates (e.g. Guenther et al., 1991, 2012; Goldstein et al., 1998; Petron et al., 2001) and
707 monoterpenes at enhanced rates (e.g. Guenther et al., 1991, 2012; Aalto et al., 2014; Taipale et al., 2020) compared to that of
708 its corresponding mature foliage. Old leaves do usually additionally emit isoprene at decreased rates (Monson et al., 1994;
709 Schnitzler et al., 1997; Sun et al., 2012). These effects were not considered in our simulations (Sec. 3.1), since the effect of
710 leaf age on biotic plant stress emissions is unexplored. Considering a similar treatment of the impact of leaf maturity on the
711 emissions of VOCs as Gunther et al. (2012) (see Appendix A) would only influence the predicted number and size of particles
712 in herbivory stressed and non-infested oak forests insignificantly (Fig. A2). However, it would decrease the ratio of isoprene-



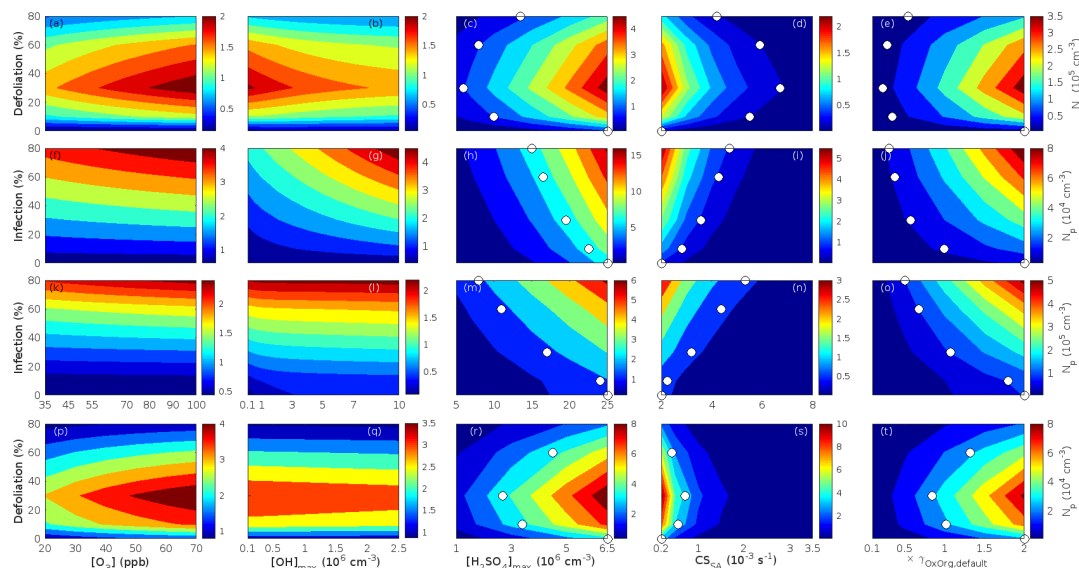
713 to-monoterpenes carbon so significantly in gypsy moth infested oak stands, that the possible suppression of aerosol processes
 714 by isoprene would disappear during most, or even the entire, duration of stress (Fig. A2b). Applying a similar leaf age effect
 715 as described in Gunther et al. (2012) on simulations of fungally infected oak and poplar forests would not decrease the ratio of
 716 isoprene-to-monoterpenes carbon sufficiently in order to avoid the possible suppression effect of isoprene, since Guenther et
 717 al. (2012) only assume a reduction of 10 % on the emissions of isoprene from old leaves. We investigated that the emission of
 718 isoprene from mildew infected oak would need to decrease by ~68-96 % (severity of stress ranging from 80 to 9 %), in
 719 comparison to simulations where the leaf age effect is not considered, in order to reach $R \leq 1$, whereas the emission of isoprene
 720 from non-infected oak would need to decrease by ~99 % (Fig. A3a). In comparison, the emission of isoprene from a non-
 721 infected poplar stand would need to decline by 99.8 %, and from a rust infected poplar stand by at least 79 %, in order to attain
 722 $R \leq 1$ (Fig. A4a). In order to reach $R \leq 22.5$, the upper limit at which new particle formation has been observed in the atmosphere
 723 (Yu et al., 2014), the emission of isoprene from a non-infected poplar stand would need to decrease by ~95 %, whereas heavily
 724 rust infected poplar forest would already be below this limit without considering an age dependent reduction of the emission
 725 potential (Fig A4a). Simulations were not done for mountain birch forest stands, since no emissions are suppressed upon
 726 herbivory stress of mountain birch (Yli-Pirilä et al., 2016) and since Yli-Pirilä et al. (2016) did not provide age information on
 727 the leaves they measured.
 728



729
 730 **Figure 10.** Impact of changed boundary conditions on the number concentrations of newly formed particles in non-infected
 731 and biotically stressed forest stands. The number concentration of newly formed particles is expressed as a function of changes
 732 in the boundary layer height (a, e, i, m), light (b, f, j, n), temperature (c, g, k, o) and leaf area index (d, h, l, p) for non-infected
 733 and infected oak (a-d, gypsy moth, e-h, powdery mildew), poplar (i-l) and birch (m-p) stands. Light (b, f, j, n) and temperature
 734 (c, g, k, o) are given as the daily maxima, but in the simulations the parameters follow a daily cycle. The displayed LAI (d, h,
 735 l, p) is that of a non-infected stand, hence e.g. at LAI = 7 m² m⁻², the simulation for a larval infestation level of 80 % has been
 736 conducted with LAI = 1.4 m² m⁻², which is 20 % of the non-infected stand LAI value. Optimal conditions (i.e. leading to
 737 highest number concentrations) for non-infected stands are indicated with white markers at an infection level of 0 %. White
 738 markers located at various infection levels mark the conditions at which an identical or slightly higher number concentration,
 739 as produced by a non-infected forest stand at optimal conditions, is reached. No markers are used for 80 % defoliated mountain
 740 birch (m-p), since the corresponding number concentrations are always lower than in a non-infested birch stand at optimal



741 conditions. Be aware that white markers in **d** and **p** are not located at the LAI of a non-infected stand, but instead at the values
 742 used for the simulations. R values (**a**, **e**, **i**) indicate the ratio of isoprene carbon / monoterpene carbon at the locations of the
 743 write markers. Be aware that the x-axes are different for simulations in Hohenpeißenberg (**a-l**) and SMEAR I conditions (**m-**
 744 **p**) except in the case of changing boundary layer height (**a**, **e**, **i**, **m**).
 745



746
 747 **Figure 11.** Impact of changed boundary conditions on the number concentrations of newly formed particles in non-infected
 748 and biotically stressed forest stands. The number concentration of newly formed particles is expressed as a function of changes
 749 in the concentration of ozone (**a**, **f**, **k**, **p**), OH (**b**, **g**, **l**, **q**) and sulfuric acid (**c**, **h**, **m**, **r**), the condensation sink (**d**, **i**, **n**, **s**)
 750 and OxOrg yields (**e**, **j**, **o**, **t**) for non-infected and infected oak (**a-e**, gypsy moth, **f-j**, powdery mildew), poplar (**k-o**) and birch (**p-**
 751 **t**) stands. The concentrations of OH (**b**, **g**, **l**, **q**) and sulfuric acid (**c**, **h**, **m**, **r**) are given as the daily maxima, but in the simulations
 752 the parameters follow a daily cycle. The displayed condensation sink (CS_{SA} : **d**, **i**, **n**, **s**) is that of sulfuric acid, while the
 753 condensation sink of OxOrg, in the respective simulations, is half of CS_{SA} . White markers are used in a similar way as in Fig.
 754 10. Be aware that the x-axes are different for simulations in Hohenpeißenberg (**a-o**) and SMEAR I conditions (**p-t**) except in
 755 the case of changing Oxorg yields (**e**, **j**, **o**, **t**).
 756

757 3.3 Implications and remaining issues to be explored

758 Our simulation results (Figs. 5-9) illustrate that biotic plant stresses are capable of substantially perturbing both the number
 759 and size of atmospheric aerosol particles throughout a significant fraction of the year (summarised in Fig. 12). Considering
 760 that we calculated *daily* new particle growth, our results point to the direction that induced plant emissions will subsequently
 761 lead to more efficient CCN production in the atmosphere (Fig. 12), which will moreover affect cloud properties, such as cloud
 762 albedo and lifetime (Twomey, 1977; Albrecht, 1989; Grypsperdt et al., 2014; Rosenfeld et al., 2014). The amplitude of the
 763 enhancement, however, depends strongly on the specific stressor and tree species which is attacked.

764 Naturally, both the duration of stress (Fig. 12e) and the predicted number (Fig. 12d)) and size (Fig. 12c) of new
 765 particles depend highly on our assumptions about e.g. when the fungi start to attack their host, how fast the fungi spread,
 766 whether the larval eggs hatch simultaneously with budburst, how fast larval development occurs, and when senescence onsets
 767 - all which depend strongly on environmental conditions. It is furthermore probable that emissions are also induced from



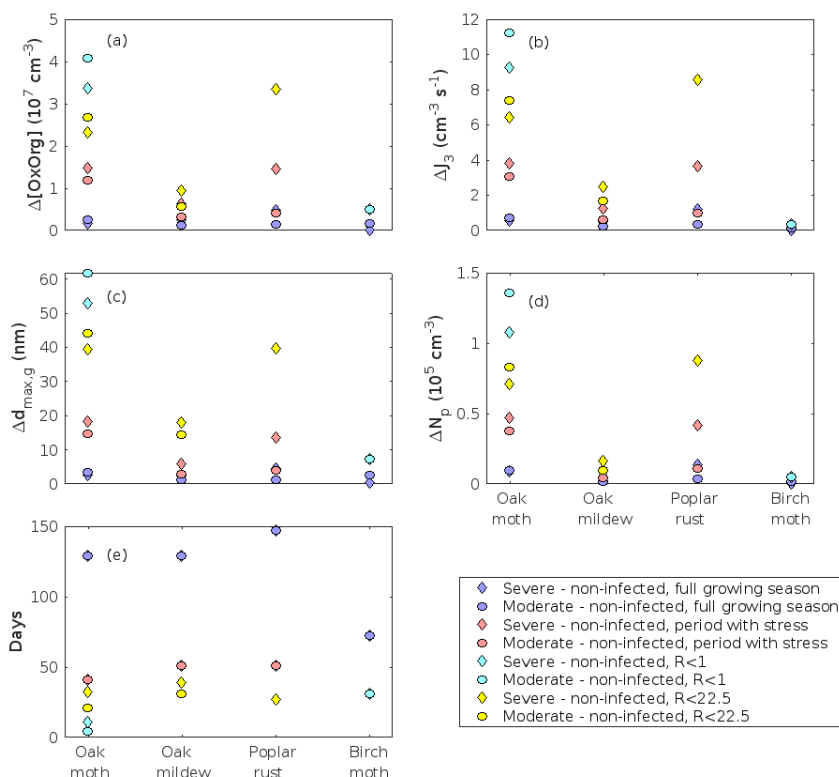
768 fungally infected leaves during senescence, which was not simulated here. The duration of stress can, thus, be significantly
769 longer than what is summarised in Fig. 12e, whereby also the post-defoliation period, in case of herbivory infestations, will be
770 shorter, and the atmospheric importance of the stresses stronger.

771 Vegetation is often subject to more than one type of stress simultaneously, which generally enhances the already
772 induced emission response due to biotic plant stress (e.g. Blande et al., 2007; Vapaavuori et al., 2009; Holopainen and
773 Gershenson, 2010; Kivimäenpää et al., 2016; Ghimire et al., 2017). It has, for example, recently been shown that warming
774 significantly amplifies the emission response due to autumnal moth feeding (Li et al., 2019). Trees which have been subject
775 to herbivory also have a tendency to more often be severely attacked by fungi later during the summer, than trees which have
776 not experienced defoliation (e.g. Marçais and Desprez-Loustau, 2014).

777 Finally, we have shown that it could be more important to account for biotic plant stresses in models than significant
778 variations in those environmental parameters which predictions of VOC emissions are currently controlled by, e.g. light
779 conditions (Fig. 10b,f,j,n), temperature (Fig. 10c,g,k,o) and LAI (Fig. 10d,h,l,p). Considering changes in the emissions of
780 VOCs caused by stress also seems to be more crucial than accounting for large changes in the concentrations of O₃ (Fig.
781 11a,f,k,p) and OH (Fig. 11b,g,l,q).

782 Together with the facts that insect outbreaks and fungal diseases generally are expected to increase in both frequency
783 and severity in the future (Cannon, 1998; Bale et al., 2002; Harrington et al., 2007; Pautasso et al., 2012; Boyd et al., 2013),
784 our findings underline the urgency of accounting for biotic plant stress emissions in numerical models.

785



786

787 **Figure 12.** Differences in atmospheric response from various non-infected and biotically stressed plant species. (a)
788 atmospheric concentrations of OxOrg, (b) formation rates of 3 nm particles, (c) daily maximum diameter of the growing



789 particle mode, **(d)** number concentration of formed particles, and **(e)** amount of days considered. **a-d** are provided as the
790 differences between the averaged parameter in a stressed and stress-free forest stand of the same plant species type. Differences
791 and averages are considered based on the complete growing season, the period with stress, when the ratio of isoprene-to-
792 monoterpenes carbon concentration is less than 1 or less than 22.5. Be aware that R is always zero in simulations of birch. In
793 cases where R does not reach less than 1 or less than 22.5 in the atmosphere surrounding a non-infected forest stand, but it
794 does in the case of the corresponding stressed stand, it is assumed that the atmospheric parameter in the non-infected stand is
795 zero and hence the difference is given as the value of the stressed stand. The concentration differences of OxOrg, formation
796 rates and number concentrations are calculated based on an average, for the period of interest, of the median values during
797 10:00-16:00 local time. “Severe” and “moderate” refer to that 80 % or 30 % of the total leaf area has been consumed or infected
798 by the end of the feeding/infection period, respectively. Southern Germany has been used as border conditions for simulations
799 of oak and poplar, while SMEAR I, Finnish Lapland, has been used for modelling of birch.
800

801 **4 Conclusions**

802 We constructed a conceptual model to simulate new particle formation and growth in various broadleaved forest stands, in
803 clean low NO_x environments, under biotically stressed and stress-free conditions, throughout a full growing season.
804 Unsurprisingly, we found that the predicted atmospheric importance of biotic plant stress highly depends on the specific
805 individual stressor and tree species which is attacked. Thus, the amount of newly formed particles was predicted to be up to
806 about one order of magnitude higher in a gypsy moth infested oak stand than in a non-infested oak stand. In comparison, the
807 number of new particles was simulated to be up to about a factor of 3, 4 and 5 higher in autumnal moth, oak powdery mildew
808 and poplar rust infected mountain birch, pedunculate oak and balsam poplar stands, respectively. We, furthermore, predicted
809 that the new particles will grow up to about 46, 28, 26 and 8 nm larger in an oak gypsy moth, poplar rust, autumnal moth and
810 oak powdery mildew infected stand, respectively, compared to their corresponding non-infested stands within one day. To our
811 knowledge, this study is the first to investigate the atmospheric impact of biotic plant stresses throughout a full growing season.
812 Our modelling results generally indicate that all the investigated plant stresses are capable of substantially perturbing
813 both the number and size of atmospheric aerosol particles, and it is thus likely that the induced emissions will subsequently
814 lead to more efficient CCN production in the atmosphere. We also showed that it can be more important to account for biotic
815 plant stresses in models than significant variations in e.g. LAI, and temperature and light conditions, which are currently the
816 main parameters controlling predictions of VOC emissions. Since insect outbreaks and fungal diseases are generally expected
817 to increase in both frequency and severity in the future, our findings underline the urgency of accounting for biotic plant stress
818 emissions in numerical models.

819

820 *Data availability.* The model code is available upon reasonable request by contacting ditte.taipale[at]helsinki.fi. SMEAR I
821 mountain birch leafing data can be obtained by contacting vesa.haataja[at]helsinki.fi. All other data used to constrain the model
822 is publicly available following the provided references.

823

824 *Author contributions.* Idea and concept by ÜN. ÜN standardised the published emission rates. VM, MK and ME developed
825 the theory for the aerosol module. DT developed the model code, conducted the simulations, and wrote the manuscript, with
826 inputs from all authors. All authors discussed the results, and commented and edited the manuscript.

827

828 *Competing interests.* The authors declare that they have no conflict of interest.

829



830 Acknowledgements. This work was supported by the European Regional Development Fund (Centre of Excellence
831 EcolChange), the European Research Council (advanced grant 322603, SIP-VOL+), the Academy of Finland Center of
832 Excellence project (no. 307331), and the Academy of Finland Flagship funding (grant no. 337549). DT was also supported by
833 the Academy of Finland (no. 307957). DT thanks Pekka Kaitaniemi for valuable discussions related to autumnal moth
834 simulation set-up and Juho Aalto, Yifan Jiang and Tero Klemola for use of photos.
835

836 **References**

837 Aalto, J., Kolari, P., Hari, P., Kerminen, V.-M., Schiestl-Aalto, P., Aaltonen, H., Levula, J., Siivola, E., Kulmala, M., and
838 Bäck, J.: New foliage growth is a significant, unaccounted source for volatiles in boreal evergreen forests, *Biogeosciences*, 11,
839 1331–1344, <https://doi.org/10.5194/bg-11-1331-2014>, 2014.

840

841 Aalto, P., Aalto, T., and Keronen, P. SMEAR I Väriö forest meteorology, air quality and soil, Institute for Atmospheric and
842 Earth System Research, urn:nbn:fi:att:2a9c28bd-ca13-4a17-8b76-922bafa067a7, 2019.

843

844 Åhman, I: Rust scorings in a plantation of *Salix viminalis* clones during ten consecutive years, *Eur. J. For. Path.*, 28, 251-258,
845 <https://doi.org/10.1111/j.1439-0329.1998.tb01180.x>, 1998.

846

847 Albrecht, B. A.: Aerosols, cloud microphysics, and fractional cloudiness, *Science*, 245, 1227-1230, DOI:
848 10.1126/science.245.4923.1227, 1989.

849

850 Andreae, M. O., Afchine, A., Albrecht, R., Holanda, B. A., Artaxo, P., Barbosa, H. M. J., Borrmann, S., Cecchini, M. A.,
851 Costa, A., Dollner, M., Fütterer, D., Järvinen, E., Jurkat, T., Klimach, T., Konemann, T., Knote, C., Krämer, M., Krisna, T.,
852 Machado, L. A. T., Mertes, S., Minikin, A., Pöhlker, C., Pöhlker, M. L., Pöschl, U., Rosenfeld, D., Sauer, D., Schlager, H.,
853 Schnaiter, M., Schneider, J., Schulz, C., Spanu, A., Sperling, V. B., Voigt, C., Walser, A., Wang, J., Weinzierl, B., Wendisch,
854 M., and Ziereis, H.: Aerosol characteristics and particle production in the upper troposphere over the Amazon Basin, *Atmos.*
855 *Chem. Phys.*, 18, 921–961, <https://doi.org/10.5194/acp-18-921-2018>, 2018.

856

857 Aphalo, P. J., Lahti, M., Lehto, T., Repo, T., Rummukainen, A., Mannerkoski, H., and Finér, L.: Responses of silver birch
858 saplings to low soil temperature, *Silva Fenn.*, 40, 429-444, <https://doi.org/10.14214/sf.328>, 2006.

859

860 Arimura, G.-I., Köpke, S., Kunert, M., Volpe, V., David, A., Brand, P., Dabrowska, P., Maffei, M. E., and Boland, W.: Effects
861 of feeding *Spodoptera littoralis* on lima bean leaves. IV. Diurnal and nocturnal damage differentially initiate plant volatile
862 emission, *Plant Physiol.*, 146, 965-973, <https://doi.org/10.1104/pp.107.111088>, 2008.

863

864 Asmi, E., Kivekäs, N., Kerminen, V.-M., Komppula, M., Hyvärinen, A.-P., Hatakka, J., Viisanen, Y., and Lihavainen, H.:
865 Secondary new particle formation in Northern Finland Pallas site between the years 2000 and 2010, *Atmos. Chem. Phys.*, 11,
866 12959–12972, <https://doi.org/10.5194/acp-11-12959-2011>, 2011.

867

868 Atkinson, R., and Arey, J.: Atmospheric degradation of volatile organic compounds, *Chem. Rev.*, 103, 4605-4638,
869 <https://doi.org/10.1021/cr0206420>, 2003.

870



- 871 Atkinson, R., Aschmann, S. M., Arey, J., and Shorees, B.: Formation of OH radicals in the gas phase reactions of O₃ with a
872 series of terpenes, *J. Geophys. Res. A*, 97, 6065-6073, <https://doi.org/10.1029/92JD00062>, 1992.
873
- 874 Ayres, M. P., and MacLean, Jr. S. F.: Molt as a component of insect development: *Galerucella sagittariae* (Chrysomelidae)
875 and *Epirrita autumnata* (Geometridae), *Oikos* 48, 273-279, doi:10.2307/3565514, 1987.
876
- 877 Bale, J. S., Masters, G. J., Hodkinson, I. D., Awmack, C., Bezemer, T. M., Brown, V. K., Butterfield, J., Buse, A., Coulson, J.
878 C., Farrar, J., Good, J. E. G., Harrington, R., Hartley, S., Jones, T. H., Lindroth, R. L., Press, M. C., Symrnioudis, I., Watt, A.
879 D., and Whittaker, J. B.: Herbivory in global climate change research: direct effects of rising temperature on insect herbivores,
880 *Glob. Change Biol.*, 8, 1-16, <https://doi.org/10.1046/j.1365-2486.2002.00451.x>, 2002.
881
- 882 Bergström, R., Hallquist, M., Simpson, D., Wildt, J., and Mentel, T. F.: Biotic stress: a significant contributor to organic
883 aerosol in Europe?, *Atmos. Chem. Phys.*, 14, 13643-13660, <https://doi.org/10.5194/acp-14-13643-2014>, 2014.
884
- 885 Berndt, T., Richters, S., Jokinen, T., Hyttinen, N., Kurtén, T., Otkjær, R. V., Kjaergaard, H. G., Stratmann, F., Herrmann, H.,
886 Sipilä, M., Kulmala, M., and Ehn, M.: Hydroxyl radical-induced formation of highly oxidized organic compounds, *Nat.*
887 *Commun.*, 7 13677, <https://doi.org/10.1038/ncomms13677>, 2016.
888
- 889 Berresheim, H., Elste, T., Plass-Dülmer, C., Eisele, F. L., and Tanner, D. J.: Chemical ionization mass spectrometer for long-
890 term measurements of atmospheric OH and H₂SO₄, *Int. J. Mass. Spectrom.*, 202, 91-109, [https://doi.org/10.1016/S1387-3806\(00\)00233-5](https://doi.org/10.1016/S1387-3806(00)00233-5), 2000.
891
892
- 893 Bert, D., Lasnier, J.-B., Capdevielle, X., Dugravot, A., and Desprez-Loustau, M.-L.: Powdery mildew decreases the radial
894 growth of oak trees with cumulative and delayed effects over years, *PLoS ONE*, 11, e0155344, doi:10.1371/journal.
895 pone.0155344, 2016.
896
- 897 Bianchi, F., Kurtén, T., Riva, M., Mohr, C., Rissanen, M. P., Roldin, P., Berndt, T., Crouse, J. D., Wennberg, P. O., Mentel,
898 T. F., Wildt, J., Junninen, H., Jokinen, T., Kulmala, M., Worsnop, D. R., Thornton, J. A., Donahue, N., Kjaergaard, H. G., and
899 Ehn, M.: Highly oxygenated organic molecules (HOM) from gas-phase autoxidation involving peroxy radicals: A key
900 contributor to atmospheric aerosol, *Chem. Rev.*, 119, 3472-3509, <https://doi.org/10.1021/acs.chemrev.8b00395>, 2019.
901
- 902 Bilde, M., Barsanti, K., Booth, M. D., Cappa, C. D., Donahue, N. M., McFiggans, G., Krieger, U. K., Marcolli, C., Topping,
903 D., Ziemann, P., Barley, M., Clegg, S., Dennis-Smith, B., Emanuelsson, E. U., Hallquist, M., Hallquist, Å. M., Khlystov,
904 A., Kulmala, M., Mogensen, D., Percival, C. P., Pope, F., Reid, J. R., Ribeiro da Silva, M. A. V., Rosenoern, T., Salo, K.,
905 Soonsin, V. P., Yli-Juuti, T., Prisle, N. L., Pagels, J., Rarey, J., Zardini, A. A., and Riipinen, I.: Saturation vapor pressures and
906 transition enthalpies of low-volatility organic molecules of atmospheric relevance: from dicarboxylic acids to complex
907 mixtures, *Chem. Rev.*, 115, 3679-4570, <https://doi.org/10.1021/cr5005502>, 2015.
908
- 909 Birmili, W., Berresheim, H., Plass-Dülmer, C., Elste, T., Gilge, S., Wiedensohler, A., and Uhrner, U.: The Hohenpeissenberg
910 aerosol formation experiment (HAFEX): a long-term study including size-resolved aerosol, H₂SO₄, OH, and monoterpenes
911 measurements, *Atmos. Chem. Phys.*, 3, 361-376, <https://doi.org/10.5194/acp-3-361-2003>, 2003.
912



- 913 Blande, J. D., Tiiva, P., Oksanen, E., and Holopainen, J. K.: Emission of herbivore-induced volatile terpenoids from two hybrid
914 aspen (*Populus tremula* × *tremuloides*) clones under ambient and elevated ozone concentrations in the field, *Glob. Chang. Biol.*,
915 13, 2538-2550, 10.1111/j.1365-2486.2007.01453.x, 2007.
- 916
- 917 Blande, J. D., Turunen, K., and Holopainen, J. K.: Pine weevil feeding on Norway spruce bark has a stronger impact on needle
918 VOC emissions than enhanced ultraviolet-B radiation, *Environ. Pollut.*, 157, 174-180, 10.1016/j.envpol.2008.07.007, 2009.
- 919
- 920 Boy, M., Kulmala, M., Ruuskanen, T. M., Pihlatie, M., Reissell, A., Aalto, P. P., Keronen, P., Dal Maso, M., Hellen, H.,
921 Hakola, H., Jansson, R., Hanke, M., and Arnold, F.: Sulphuric acid closure and contribution to nucleation mode particle growth,
922 *Atmos. Chem. Phys.*, 5, 863-878, <https://doi.org/10.5194/acp-5-863-2005>, 2005.
- 923
- 924 Boyd, I. L., Freer-Smith, P. H., Gilligan, C. A., and Godfray, H. C. J: The consequence of tree pests and diseases for ecosystem
925 services, *Science*, 342, 1235773, doi: 10.1126/science.1235773, 2013.
- 926
- 927 Brilli, F., Ciccioli, P., Frattoni, M., Prestinanzi, M., Spanedda, A. F., and Loreto, F.: Constitutive and herbivore-induced
928 monoterpenes emitted by *Populus* × *euroamericana* leaves are key volatiles that orient *Chrysomela populi* beetles, *Plant Cell*
929 *Environ.*, 32, 542-552, 10.1111/j.1365-3040.2009.01948.x, 2009.
- 930
- 931 Cannon, R. J. C.: The implications of predicted climate change for insect pests in the UK, with emphasis on non-indigenous
932 species, *Glob. Chang. Biol.*, 4, 785-796, 10.1046/j.1365-2486.1998.00190.x, 1998.
- 933
- 934 Calvert, J., Atkinson, R., Kerr, J. A., Madronich, S., Moortgat, G. K., Wallington, T. J., and Yarwood, G.: The Mechanisms
935 of Atmospheric Oxidation of the Alkenes, Oxford University Press, Oxford, UK, 2000.
- 936
- 937 Copolovici, L., Väärtnõu, F., Portillo Estrada, M., and Niinemets, Ü.: Oak powdery mildew (*Erysiphe alphitoides*)-induced
938 volatile emissions scale with the degree of infection in *Quercus robur*, *Tree Physiol.*, 34, 1399-1410,
939 <https://doi.org/10.1093/treephys/tpu091>, 2014.
- 940
- 941 Copolovici, L., Pag, A., Kännaste, A., Bodescu, A., Tomescu, D., Copolovici, D., Soran, M.-L., and Niinemets, Ü.:
942 Disproportionate photosynthetic decline and inverse relationship between constitutive and induced volatile emissions upon
943 feeding of *Quercus robur* leaves by large larvae of gypsy moth (*Lymantria dispar*), *Environ. Exp. Bot.* 138 184-192,
944 <https://doi.org/10.1016/j.envexpbot.2017.03.014>, 2017.
- 945
- 946 Covarelli, L., Beccari, G., Tosi, L., Fabre, B., and Frey, P.: Three-year investigations on leaf rust of poplar cultivated for
947 biomass production in Umbria, Central Italy, *Biomass Bioenerg.*, 49, 315-322,
948 <https://doi.org/10.1016/j.biombioe.2012.12.032>, 2013.
- 949
- 950 Dahlberg, U., Berge, T. W., Petersson, H., and Vencatasawmy, C. P.: Modelling biomass and leaf area index in a sub-arctic
951 Scandinavian mountain area, *Scand. J. Forest Res.*, 19, 60-71, <https://doi.org/10.1080/02827580310019266>, 2004.
- 952
- 953 Dal Maso, M., Sogacheva, L., Aalto, P. P., Riipinen, I., Komppula, M., Tunved, P., Korhonen, L., Suur-Uski, V., Hirsikko,
954 A., Kurtén, T., Kerminen, V.-M., Lihavainen, H., Viisanen, Y., Hansson, H.-C., and Kulmala, M.: Aerosol size distribution



- 955 measurements at four Nordic field stations: identification, analysis and trajectory analysis of new particle formation bursts,
956 *Tellus B*, 59, 350-361, doi: 10.1111/j.1600-0889.2007.00267.x, 2007.
- 957
- 958 Dal Maso, M., Hyvärinen, A., Komppula, M., Tunved, P., Kerminen, V.-M., Lihavainen, H., Viisanen, Y., Hansson, H.-C.,
959 and Kulmala, M.: Annual and interannual variation in boreal forest aerosol particle number and volume concentration and their
960 connection to particle formation, *Tellus* 60B, 495-508, <https://doi.org/10.1111/j.1600-0889.2008.00366.x>, 2008.
- 961
- 962 Desprez-Loustau, M. L., Feau, N., Mougou-Hamdane, A., and Dutech, C.: Interspecific and intraspecific diversity in oak
963 powdery mildews in Europe: coevolution history and adaptation to their hosts, *Mycoscience*, 52, 165-173,
964 <https://doi.org/10.1007/s10267-010-0100-5>, 2011.
- 965
- 966 Di Carlo, P., Brune, W. H., Martinez, M., Harder, H., Leshner, R., Ren, X., Thornberry, T., Carroll, M. A., Young, V., Shepson,
967 P. B., Riemer, D., Apel, E., and Campbell, C.: Missing OH reactivity in a forest: Evidence for unknown reactive biogenic
968 VOCs, *Science*, 304, 722-725, doi: 10.1126/science.1094392, 2004.
- 969
- 970 Donahue, N. M., Ortega, I. K., Chuang, W., Riipinen, I., Riccobono, F., Schobesberger, S., Dommen, J., Baltensperger, U.,
971 Kulmala, M., Worsnop, D. R., Vehkamäki, H.: How do organic vapors contribute to new-particle formation?, *Faraday Discuss.*,
972 165, 91-104, 10.1039/C3FD00046J, 2013.
- 973
- 974 Douma, J. C., Ganzeveld, L. N., Unsicker, S. B., Boeckler, A., and Dicke, M.: What makes a volatile organic compound a
975 reliable indicator of insect herbivory?, *Plant Cell Environ.*, 42, 3308-3325, <https://doi.org/10.1111/pce.13624>, 2019.
- 976
- 977 Dunne, E. M., Gordon, H., Kürten, A., Almeida, J., Duplissy, J., Williamson, C., Ortega, I. K., Pringle, K. J., Adamov, A.,
978 Baltensperger, U., Barmet, P., Benduhn, F., Bianchi, F., Breitenlechner, M., Clarke, A., Curtius, J., Dommen, J., Donahue, N.
979 M., Ehrhart, S., Flagan, R. C., Franchin, A., Guida, R., Hakala, J., Hansel, A., Heinritzi, M., Jokinen, T., Kangasluoma, J.,
980 Kirkby, J., Kulmala, M., Kupic, A., Lawler, M. J., Lehtipalo, K., Makhmutov, V., Mann, G., Mathot, S., Merikanto, J.,
981 Miettinen, P., Nenes, A., Onnela, A., Rap, A., Reddington, C. L. S., Riccobono, F., Richards, N. A. D., Rissanen, M. P., Rondo,
982 L., Sarnela, N., Schobesberger, S., Sengupta, K., Simon, M., Sipilä, M., Smith, J. N., Stozkhov, Y., Tomé, A., Tröstl, J.,
983 Wagner, P. E., Wimmer, D., Winkler, P. M., Worsnop, D. R., and Carslaw, K. S.: Global atmospheric particle formation from
984 CERN CLOUD measurements, *Science*, 354, 1119-1124, DOI: 10.1126/science.aaf2649, 2016.
- 985
- 986 Ehn, M., Kleist, E., Junninen, H., Petäjä, T., Lönn, G., Schobesberger, S., Dal Maso, M., Trimborn, A., Kulmala, M., Worsnop,
987 D. R., Wahner, A., Wildt, J., and Mentel, Th. F.: Gas phase formation of extremely oxidized pinene reaction products in
988 chamber and ambient air, *Atmos. Chem. Phys.*, 12, 5113-5127, <https://doi.org/10.5194/acp-12-5113-2012>, 2012.
- 989
- 990 Ehn, M., Thornton, J. A., Kleist, E., Sipilä, M., Junninen, H., Pullinen, I., Springer, M., Rubach, F., Tillmann, R., Lee, B.,
991 Lopez-Hilfiker, F., Andres, S., Acir, I-H., Rissanen, M., Jokinen, T., Schobesberger, S., Kangasluoma, J., Kontkanen, J.,
992 Nieminen, T., Kurtén, T., Nielsen, L. B., Jørgensen, S., Kjaergaard, H. G., Canagaratna, M., Maso, M. D., Berndt, T., Petäjä,
993 T., Wahner, A., Kerminen, V.-M., Kulmala, M., Worsnop, D. R., Wildt, J., and Mentel, T. F.: A large source of low-volatility
994 secondary organic aerosol, *Nature* 506, 476-479, <https://doi.org/10.1038/nature13032>, 2014.
- 995
- 996 El-Ghany, T. M. A., Eman, M. E., and El-Sheikh, H. H.: Efficacy of fungal rust disease on willow plant in Egypt, *Aust. J.*
997 *Basic Appl. Sci.*, 3, 1527-1539, 2009.



- 998
- 999 Faiola, C. and Taipale, D.: Impact of insect herbivory on plant stress volatile emissions from trees: A synthesis of quantitative
1000 measurements and recommendations for future research, *Atmos. Environ.* X, 5, 100060,
1001 <https://doi.org/10.1016/j.aeaoa.2019.100060>, 2020.
- 1002
- 1003 Faiola, C. L., Buchholz, A., Kari, E., Yli-Pirilä, P., Holopainen, J. K., Kivimäenpää, M., Miettinen, P., Worsnop, D. R.,
1004 Lehtinen, K. E. J., Guenther, A. B., and Virtanen, A.: Terpene composition complexity controls secondary organic aerosol
1005 yields from Scots pine volatile emissions, *Sci. Rep.*, 8, 3053, [10.1038/s41598-018-21045-1](https://doi.org/10.1038/s41598-018-21045-1), 2018.
- 1006
- 1007 Faiola, C. L., Pullinen, I., Buchholz, A., Khalaj, F., Ylisirniö, A., Kari, E., Miettinen, P., Holopainen, J. K., Kivimäenpää, M.,
1008 Schobesberger, S., Yli-Juuti, T., and Virtanen, A.: Secondary Organic aerosol formation from healthy and aphid-stressed Scots
1009 pine emissions, *ACS Earth Space Chem.*, 3, 1756-1772, <https://doi.org/10.1021/acsearthspacechem.9b00118>, 2019.
- 1010
- 1011 Fiedler, V., Dal Maso, M., Boy, M., Aufmhoff, H., Hoffmann, J., Schuck, T., Birmili, W., Hanke, M., Uecker, J., Arnold, F.,
1012 and Kulmala, M.: The contribution of sulphuric acid to atmospheric particle formation and growth: a comparison between
1013 boundary layers in Northern and Central Europe, *Atmos. Chem. Phys.*, 5, 1773–1785, [https://doi.org/10.5194/acp-5-1773-](https://doi.org/10.5194/acp-5-1773-2005)
1014 2005, 2005.
- 1015
- 1016 Gérard, P. R., Husson, C., Pinon, J., and Frey, P.: Comparison of genetic and virulence diversity of *Melampsora larici-populina*
1017 populations on wild and cultivated poplar and influence of the alternate host, *Phytopathology*, 96, 1027-1036, doi:
1018 10.1094/PHYTO-96-1027, 2006.
- 1019
- 1020 Ghimire, R. P., Kivimäenpää, M., Kasurinen, A., Häikiö, E., Holopainen, T., and Holopainen, J. K.: Herbivore-induced BVOC
1021 emissions of Scots pine under warming, elevated ozone and increased nitrogen availability in an open-field exposure, *Agric.*
1022 *For. Meteorol.*, 242, 21-32, [10.1016/j.agrformet.2017.04.008](https://doi.org/10.1016/j.agrformet.2017.04.008), 2017.
- 1023
- 1024 Ghirardo, A., Koch, K., Taipale, R., Zimmer, I., Schnitzler, J.-P., and Rinne, J.: Determination of de novo and pool emissions
1025 of terpenes from four common boreal/alpine trees by ¹³CO₂ labelling and PTR-MS analysis, *Plant Cell Environ.*, 33, 781-792,
1026 <https://doi.org/10.1111/j.1365-3040.2009.02104.x>, 2010.
- 1027
- 1028 Gill, A. L., Gallinat, A. S., Sanders-DeMott, R., Rigden, A. J., Short Gianotti, D. J., Mantooth, J. A., and Templer, P. H.:
1029 Changes in autumn senescence in northern hemisphere deciduous trees: a meta-analysis of autumn phenology studies. *Ann.*
1030 *Bot.* 116, 875-888, doi: 10.1093/aob/mcv055, 2015.
- 1031
- 1032 Glawe, D. A.: The powdery mildews: a review of the world's most familiar (yet poorly known) plant pathogens, *Annu. Rev.*
1033 *Phytopathol.*, 46, 27-51, doi: 10.1146/annurev.phyto.46.081407.104740, 2008.
- 1034
- 1035 Goldstein, A., Goulden, M., Munger, J. W., Wofsy, S., and Geron, C.: Seasonal course of isoprene emissions from a midlatitude
1036 forest, *J. Geophys. Res.*, 103, 31 045–31 056, <https://doi.org/10.1029/98JD02708>, 1998.
- 1037
- 1038 Größ, J., Hamed, A., Sonntag, A., Spindler, G., Manninen, H. E., Nieminen, T., Kulmala, M., Hörrak, U., Plass-Dülmer, C.,
1039 Wiedensohler, A., and Birmili, W.: Atmospheric new particle formation at the research station Melpitz, Germany: connection



- 1040 with gaseous precursors and meteorological parameters, *Atmos. Chem. Phys.*, 18, 1835–1861, [https://doi.org/10.5194/acp-18-](https://doi.org/10.5194/acp-18-1835-2018)
1041 1835-2018, 2018.
- 1042
- 1043 Grote, R., Monson, R. K., Niinemets, Ü.: Leaf-level models of constitutive and stress-driven volatile organic compound
1044 emissions, *Biology, Controls and Models of Tree Volatile Organic Compound Emissions*, Tree Physiology, Springer,
1045 Dordrecht, 315-355, 10.1007/978-94-007-6606-8_12, 2013.
- 1046
- 1047 Grote, R., Sharma, M., Ghirardo, A., Schnitzler, J.-P.: A new modeling approach for estimating abiotic and biotic stress-
1048 induced de novo emissions of biogenic volatile organic compounds from plants, *Front. For. Glob. Change*, 2, 26, doi:
1049 10.3389/ffgc.2019.00026, 2019.
- 1050
- 1051 Gryspeerdt, E., Stier, P., and Partridge, D. G.: Satellite observations of cloud regime development: the role of aerosol processes,
1052 *Atmos. Chem. Phys.*, 14, 1141–1158, <https://doi.org/10.5194/acp-14-1141-2014>, 2014.
- 1053
- 1054 Guenther, A.: Seasonal and spatial variations in natural volatile organic compound emissions, *Ecol. Appl.*, 7, 34–45,
1055 [https://doi.org/10.1890/1051-0761\(1997\)007\[0034:SASVIN\]2.0.CO;2](https://doi.org/10.1890/1051-0761(1997)007[0034:SASVIN]2.0.CO;2), 1997.
- 1056
- 1057 Guenther, A. B., Monson, R. K., and Fall, R.: Isoprene and monoterpene emission rate variability: Observations with
1058 eucalyptus and emission rate algorithm development, *J. Geophys. Res.*, 96, 10799-10808, <https://doi.org/10.1029/91JD00960>,
1059 1991.
- 1060
- 1061 Guenther, A., Zimmerman, P., and Wildermuth, M.: Natural volatile organic compound emission rate estimates for U.S.
1062 woodland landscapes, *Atmos. Environ.*, 28, 1197-1210, [https://doi.org/10.1016/1352-2310\(94\)90297-6](https://doi.org/10.1016/1352-2310(94)90297-6), 1994.
- 1063
- 1064 Guenther, A., Karl, T., Harley, P., Wiedinmyer, C., Palmer, P. I., and Geron, C.: Estimates of global terrestrial isoprene
1065 emissions using MEGAN (Model of Emissions of Gases and Aerosols from Nature), *Atmos. Chem. Phys.*, 6, 3181–3210,
1066 <https://doi.org/10.5194/acp-6-3181-2006>, 2006.
- 1067
- 1068 Guenther, A. B., Jiang, X., Heald, C. L., Sakulyanontvittaya, T., Duhl, T., Emmons, L. K., and Wang, X.: The Model of
1069 Emissions of Gases and Aerosols from Nature version 2.1 (MEGAN2.1): an extended and updated framework for modeling
1070 biogenic emissions, *Geosci. Model Dev.*, 5, 1471–1492, <https://doi.org/10.5194/gmd-5-1471-2012>, 2012.
- 1071
- 1072 Hajji, M., Dreyer, M., and Marçais, B.: Impact of *Erysiphe alphitoides* on transpiration and photosynthesis in *Quercus robur*
1073 leaves, *Eur. J. Plant. Pathol.*, 125, 63-72, <https://doi.org/10.1007/s10658-009-9458-7>, 2009.
- 1074
- 1075 Häkkinen, S. A. K., Manninen, H. E., Yli-Juuti, T., Merikanto, J., Kajos, M. K., Nieminen, T., D'Andrea, S. D., Asmi, A.,
1076 Pierce, J. R., Kulmala, M., and Riipinen, I.: Semi-empirical parameterization of size-dependent atmospheric nanoparticle
1077 growth in continental environments, *Atmos. Chem. Phys.*, 13, 7665–7682, <https://doi.org/10.5194/acp-13-7665-2013>, 2013.
- 1078
- 1079 Hakola, H., Arey, J., Aschmann, S. M., and Atkinson, R.: Product formation from the gas phase reactions of OH radicals and
1080 O₃ with a series of monoterpenes, *J. Atmos. Chem.*, 18, 75-102, <https://doi.org/10.1007/BF00694375>, 1994.
- 1081



- 1082 Hari, P., Kulmala, M., Pohja, T., Lahti, T., Siivola, R., Palva, L., Aalto, P., Hämeri, K., Vesala, T., Luoma, S., and Pulliainen,
1083 E.: Air pollution in eastern Lapland: challenge for an environmental measurement station, *Silva Fenn.*, 28, 29-39,
1084 <https://doi.org/10.14214/sf.a9160>, 1994.
1085
- 1086 Harrington, R., Clark, S. J., Welham, S. J., Verrier, P. J., Denholm, C. H., Hullé, M., Maurice, D., Rounsevell, M. D., and
1087 Cocu, N.: Environmental change and the phenology of European aphids, *Glob. Chang. Biol.*, 13, 1550-1564, 10.1111/j.1365-
1088 2486.2007.01394.x, 2007.
1089
- 1090 Heinritzi, M., Dada, L., Simon, M., Stolzenburg, D., Wagner, A. C., Fischer, L., Ahonen, L. R., Amanatidis, S., Baalbaki, R.,
1091 Baccarini, A., Bauer, P. S., Baumgartner, B., Bianchi, F., Brilke, S., Chen, D., Chiu, R., Dias, A., Dommen, J., Duplissy, J.,
1092 Finkenzeller, H., Frege, C., Fuchs, C., Garmash, O., Gordon, H., Granzin, M., El Haddad, I., He, X., Helm, J., Hofbauer, V.,
1093 Hoyle, C. R., Kangasluoma, J., Keber, T., Kim, C., Kürten, A., Lamkaddam, H., Laurila, T. M., Lampilahti, J., Lee, C. P.,
1094 Lehtipalo, K., Leiminger, M., Mai, H., Makhmutov, V., Manninen, H. E., Marten, R., Mathot, S., Mauldin, R. L., Mentler, B.,
1095 Molteni, U., Müller, T., Nie, W., Nieminen, T., Onnela, A., Partoll, E., Passananti, M., Petäjä, T., Pfeifer, J., Pospisilova, V.,
1096 Quéléver, L. L. J., Rissanen, M. P., Rose, C., Schobesberger, S., Scholz, W., Scholze, K., Sipilä, M., Steiner, G., Stozhkov,
1097 Y., Tauber, C., Tham, Y. J., Vazquez-Pufleau, M., Virtanen, A., Vogel, A. L., Volkamer, R., Wagner, R., Wang, M., Weitz,
1098 L., Wimmer, D., Xiao, M., Yan, C., Ye, P., Zha, Q., Zhou, X., Amorim, A., Baltensperger, U., Hansel, A., Kulmala, M., Tomé,
1099 A., Winkler, P. M., Worsnop, D. R., Donahue, N. M., Kirkby, J., and Curtius, J.: Molecular understanding of the suppression
1100 of new-particle formation by isoprene, *Atmos. Chem. Phys.*, 20, 11809–11821, <https://doi.org/10.5194/acp-20-11809-2020>,
1101 2020.
1102
- 1103 Heiskanen, J.: Estimating aboveground tree biomass and leaf area index in a mountain birch forest using ASTER satellite data,
1104 *Int. J. Remote Sens.*, 6, 1135-1158, <https://doi.org/10.1080/01431160500353858>, 2006.
1105
- 1106 Hirsikko, A., Laakso, L., Hörrak, U., Aalto, P. P., Kerminen, V.-M., and Kulmala, M.: Annual and size dependent variation of
1107 growth rates and ion concentrations in boreal forest, *Boreal Environ. Res.*, 10, 357-369, 2005.
1108
- 1109 Holopainen, J. K. and Gershenson, J.: Multiple stress factors and the emission of plant VOCs, *Trends Plant Sci. Special Issue:*
1110 *Induc. Biog. Volatile Org. Compd. Plant*, 15, 176-184, 10.1016/j.tplants.2010.01.006, 2010.
1111
- 1112 Hunter, M. D., Kozlov, M. V., Itämies, J., Pulliainen, E., Bäck, J., Kyrö, E. M., and Niemelä, P.: Current temporal trends in
1113 moth abundance are counter to predicted effects of climate change in an assemblage of subarctic forest moths, *Glob. Change*
1114 *Biol.*, 20, 1723-1737, doi: 10.1111/gcb.12529, 2014.
1115
- 1116 Hyvönen, S., Junninen, H., Laakso, L., Dal Maso, M., Grönholm, T., Bonn, B., Keronen, P., Aalto, P., Hiltunen, V., Pohja, T.,
1117 Launiainen, S., Hari, P., Mannila, H., and Kulmala, M.: A look at aerosol formation using data mining techniques, *Atmos.*
1118 *Chem. Phys.*, 5, 3345–3356, <https://doi.org/10.5194/acp-5-3345-2005>, 2005.
1119
- 1120 IPCC (2013). “Climate Change 2013: the physical science basis,” in Contribution of Working Group I to the Fifth Assessment
1121 Report of the Intergovernmental Panel on Climate Change, eds F. T. Stocker et al. (Cambridge: Cambridge University Press),
1122 1535.
1123



- 1124 Jenkin, M. E. and Clemitshaw, K. C.: Ozone and other secondary photochemical pollutants: chemical processes governing
1125 their formation in the planetary boundary layer, *Atmos. Environ.*, 34, 2499-2527, 2000.
1126
- 1127 Jenkin, M. E., Young, J. C., and Rickard, A. R.: The MCM v3.3.1 degradation scheme for isoprene, *Atmos. Chem. Phys.*, 15,
1128 11433–11459, <https://doi.org/10.5194/acp-15-11433-2015>, 2015.
1129
- 1130 Jiang, Y., Ye, J., Veromann, L.-L., and Niinemets, Ü.: Scaling of photosynthesis and constitutive and induced volatile
1131 emissions with severity of leaf infection by rust fungus (*Melampsora larici-populina*) in *Populus balsamifera* var. *suaveolens*,
1132 *Tree Physiol.*, 36, 856-872, doi: 10.1093/treephys/tpw035, 2016.
1133
- 1134 Jimenez, J. L., Canagaratna, M. R., Donahue, N. M., Prevot, A. S., Zhang, Q., Kroll, J. H., DeCarlo, P. F., Allan, J. D., Coe,
1135 H., Ng, N. L., Aiken, A. C., Docherty, K. S., Ulbrich, I. M., Grieshop, A. P., Robinson, A. L., Duplissy, J., Smith, J. D., Wilson,
1136 K. R., Lanz, V. A., Hueglin, C., Sun, Y. L., Tian, J., Laaksonen, A., Raatikainen, T., Rautiainen, J., Vaattovaara, P., Ehn, M.,
1137 Kulmala, M., Tomlinson, J. M., Collins, D. R., Cubison, M. J., Dunlea, E. J., Huffman, J. A., Onasch, T. B., Alfarra, M. R.,
1138 Williams, P. I., Bower, K., Kondo, Y., Schneider, J., Drewnick, F., Borrmann, S., Weimer, S., Demerjian, K., Salcedo, D.,
1139 Cottrell, L., Griffin, R., Takami, A., Miyoshi, T., Hatakeyama, S., Shimono, A., Sun, J. Y., Zhang, Y. M., Dzepina, K., Kimmel,
1140 J. R., Sueper, D., Jayne, J. T., Herndon, S. C., Trimborn, A. M., Williams, L. R., Wood, E. C., Middlebrook, A. M., Kolb, C.
1141 E., Baltensperger, U., Worsnop, D. R.: Evolution of organic aerosols in the atmosphere, *Science*, 326, 1525-1529, doi:
1142 10.1126/science.1180353, 2009.
1143
- 1144 Johansson, L. K.-H. and Alström, S.: Field resistance to willow leaf rust *Melampsora epitea* in inter- and intraspecific hybrids
1145 of *Salix viminalis* and *S. dasyclados*, *Eur. J. Plant Pathol.*, 106, 763-769, <https://doi.org/10.1023/A:1026573219481>, 2000.
1146
- 1147 Jokinen, T., Berndt, T., Makkonen, R., Kerminen, V.-M., Junninen, H., Paasonen, P., Stratmann, F., Herrmann, H., Guenther,
1148 A. B., Worsnop, D. R., Kulmala, M., Ehn, M., and Sipilä, M.: Production of extremely low volatile organic compounds from
1149 biogenic emissions: Measured yields and atmospheric implications, *Proc. Natl. Acad. Sci. U. S. A.*, 112, 7123-7128,
1150 <https://doi.org/10.1073/pnas.1423977112>, 2015.
1151
- 1152 Joutsensaari, J., Yli-Pirilä, P., Korhonen, H., Arola, A., Blande, J. D., Hejjari, J., Kivimäenpää, M., Mikkonen, S., Hao, L.,
1153 Miettinen, P., Lyytikäinen-Saarenmaa, P., Faiola, C. L., Laaksonen, A., and Holopainen, J. K.: Biotic stress accelerates
1154 formation of climate-relevant aerosols in boreal forests, *Atmos. Chem. Phys.*, 15, 12139–12157, <https://doi.org/10.5194/acp-15-12139-2015>, 2015.
1155
1156
- 1157 Kaitaniemi, P., Ruohomäki, K., and Haukioja, E.: Consequences of defoliation on phenological interaction between *Epirrita*
1158 *autumnata* and its host plant, mountain birch, *Funct. Ecol.*, 11, 199-208, <https://doi.org/10.1046/j.1365-2435.1997.00063.x>,
1159 1997.
1160
- 1161 Kaitaniemi, P. and Ruohomäki, K.: Effects of autumn temperature and oviposition date on timing of larval development and
1162 risk of parasitism in a spring folivore, *Oikos*, 84, 435-442, doi: 10.2307/3546422, 1999.
1163
- 1164 Kanakidou, M., Seinfeld, J. H., Pandis, S. N., Barnes, I., Dentener, F. J., Facchini, M. C., Van Dingenen, R., Ervens, B., Nenes,
1165 A., Nielsen, C. J., Swietlicki, E., Putaud, J. P., Balkanski, Y., Fuzzi, S., Horth, J., Moortgat, G. K., Winterhalter, R., Myhre,



- 1166 C. E. L., Tsigaridis, K., Vignati, E., Stephanou, E. G., and Wilson, J.: Organic aerosol and global climate modelling: a review,
1167 *Atmos. Chem. Phys.*, 5, 1053–1123, <https://doi.org/10.5194/acp-5-1053-2005>, 2005.
1168
- 1169 Kanawade, V. P., Jobson, B. T., Guenther, A. B., Erupe, M. E., Pressley, S. N., Tripathi, S. N., and Lee, S.-H.: Isoprene
1170 suppression of new particle formation in a mixed deciduous forest, *Atmos. Chem. Phys.*, 11, 6013–6027,
1171 <https://doi.org/10.5194/acp-11-6013-2011>, 2011.
1172
- 1173 Kari, E., Faiola, C. L., Isokääntä, S., Miettinen, P., Yli-Pirilä, P., Buchholz, A., Kivimäenpää, M., Mikkonen, S., Holopainen,
1174 J. K., and Virtanen, A.: Time-resolved characterization of biotic stress emissions from Scots pines being fed upon by pine
1175 weevil by means of PTR-ToF-MS, *Boreal Environ. Res.*, 24, 25–49, 2019.
1176
- 1177 Kerminen, V.-M. and Kulmala, M.: Analytical formulae connecting the “real” and the “apparent” nucleation rate and the nuclei
1178 number concentration for atmospheric nucleation events, *J. Aerosol Sci.*, 33, 609–622, doi: 10.1016/S0021-8502(01)00194-X,
1179 2002.
1180
- 1181 Kerminen, V.-M., Lihavainen, H., Komppula, M., Viisanen, Y., and Kulmala, M.: Direct observational evidence linking
1182 atmospheric aerosol formation and cloud droplet activation, *Geophys. Res. Lett.*, 32, 10.1029/2005GL023130, 2005.
1183
- 1184 Kerminen, V.-M., Paramonov, M., Anttila, T., Riipinen, I., Fountoukis, C., Korhonen, H., Asmi, E., Laakso, L., Lihavainen,
1185 H., Swietlicki, E., Svenningsson, B., Asmi, A., Pandis, S. N., Kulmala, M., and Petäjä, T.: Cloud condensation nuclei
1186 production associated with atmospheric nucleation: a synthesis based on existing literature and new results, *Atmos. Chem.*
1187 *Phys.*, 12, 12037–12059, <https://doi.org/10.5194/acp-12-12037-2012>, 2012.
1188
- 1189 Kiendler-Scharr, A., Wildt, J., Dal Maso, M., Hohaus, T., Kleist, E., Mentel, T. F., Tillmann, R., Uerlings, R., Schurr, U., and
1190 Wahner, A.: New particle formation in forests inhibited by isoprene emissions, *Nature*, 461, 381–384, DOI:
1191 10.1038/nature08292, 2009.
1192
- 1193 Kiendler-Scharr, A., Andres, S., Bachner, M., Behnke, K., Broch, S., Hofzumahaus, A., Holland, F., Kleist, E., Mentel, T. F.,
1194 Rubach, F., Springer, M., Steitz, B., Tillmann, R., Wahner, A., Schnitzler, J.-P., and Wildt, J.: Isoprene in poplar emissions:
1195 effects on new particle formation and OH concentrations, *Atmos. Chem. Phys.*, 12, 1021–1030, [https://doi.org/10.5194/acp-](https://doi.org/10.5194/acp-12-1021-2012)
1196 [12-1021-2012](https://doi.org/10.5194/acp-12-1021-2012), 2012.
1197
- 1198 Kirkby, J., Duplissy, J., Sengupta, K., Frege, C., Gordon, H., Williamson, C., Heinritzi, M., Simon, M., Yan, C., Almeida, J.,
1199 Tröstl, J., Nieminen, T., Ortega, I. K., Wagner, R., Adamov, A., Amorim, A., Bernhammer, A.-K., Bianchi, F., Breitenlechner,
1200 M., Brilke, S., Chen, X., Craven, J., Dias, A., Ehrhart, S., Flagan, R. C., Franchin, A., Fuchs, C., Guida, R., Hakal, J., Hoyle,
1201 C. R., Jokinen, T., Junninen, H., Kangasluoma, J., Him, J., Krapf, M., Kürten, A., Laaksonen, A., Lehtipalo, K., Makhmutov,
1202 V., Mathot, S., Molteni, U., Onnela, A., Peräkylä, O., Piel, F., Petäjä, T., Praplan, A. P., Pringle, K., Rap, A., Richards, N. A.
1203 D., Riipinen, I., Rissanen, M. P., Rondo, L., Sarnela, N., Schobesberger, S., Scott, C. E., Seinfeld, J. H., Sipilä, M., Steiner,
1204 G., Stozhkov, Y., Stratmann, F., Tomé, A., Virtanen, A., Vogel, A. L., Wagner, A. C., Wagner, P. E., Weingartner, E.,
1205 Wimmer, D., Winkler, P. M., Ye, P., Zhang, X., Hansel, A., Dommen, J., Donahue, N. M., Worsnop, D. R., Baltensperger, U.,
1206 Kulmala, M., Carslaw, K. S., and Curtius, J.: Ion-induced nucleation of pure biogenic particles, *Nature*, 533, 521–526,
1207 <https://doi.org/10.1038/nature17953>, 2016.
1208



- 1209 Kivimäenpää, M., Ghimire, R. P., Sutinen, S., Häikiö, E., Kasurinen, A., Holopainen, T., and Holopainen, J. K.: Increases in
1210 volatile organic compound emissions of Scots pine in response to elevated ozone and warming are modified by herbivory and
1211 soil nitrogen availability, *Eur. J. For. Res.*, 135, 343–360, [10.1007/s10342-016-0939-x](https://doi.org/10.1007/s10342-016-0939-x), 2016.
1212
- 1213 Komppula, M., Sihto, S.-L., Korhonen, H., Lihavainen, H., Kerminen, V.-M., Kulmala, M., and Viisanen, Y.: New particle
1214 formation in air mass transported between two measurement sites in Northern Finland, *Atmos. Chem. Phys.*, 6, 2811–2824,
1215 <https://doi.org/10.5194/acp-6-2811-2006>, 2006.
1216
- 1217 Kula, E., Pešlová, A., Martinek, P., and Mazal, P.: The development of caterpillars of gypsy moth (*Lymantria dispar* L.) feeding
1218 on food affected by nitrogen, *Sumar. List*, 137, 51–60, 2013.
1219
- 1220 Kulmala, M., Petäjä, T., Nieminen, T., Sipilä, M., Manninen, H. E., Lehtipalo, K., Dal Maso, M., Aalto, P. P., Junninen, H.,
1221 Paasonen, P., Riipinen, I., Lehtinen, K. E. J., Laaksonen, A., and Kerminen, V.-M.: Measurement of the nucleation of
1222 atmospheric aerosol particles, *Nat. Protoc.*, 7, 1651–1667, <https://doi.org/10.1038/nprot.2012.091>, 2012.
1223
- 1224 Kulmala, M., Kontkanen, J., Junninen, H., Lehtipalo, K., Manninen, H. E., Nieminen, T., Petäjä, T., Sipilä, M., Schobesberger,
1225 S., Rantala, P., Franchin, A., Jokinen, T., Järvinen, E., Äijälä, M., Kangasluoma, J., Hakala, J., Aalto, P. P., Paasonen, P.,
1226 Mikkilä, J., Vanhanen, J., Aalto, J., Hakola, H., Makkonen, U., Ruuskanen, T., Mauldin, R. L. III, Duplissy, J., Vehkamäki,
1227 H., Bäck, J., Kortelainen, A., Riipinen, I., Kurtén, T., Johnston, M. V., Smith, J. N., Ehn, M., Mentel, T. F., Lehtinen, K. E. J.,
1228 Laaksonen, A., Kerminen, V.-M., and Worsnop, D. R.: Direct observations of atmospheric aerosol nucleation, *Science*, 339,
1229 943–946, DOI: 10.1126/science.1227385, 2013.
1230
- 1231 Kulmala, M., Petäjä, T., Ehn, M., Thornton, J., Sipilä, M., Worsnop, D. R., Kerminen, V.-M.: Chemistry of atmospheric
1232 nucleation: on the recent advances on precursor characterization and atmospheric cluster composition in connection with
1233 atmospheric new particle formation, *Annu. Rev. Phys. Chem.*, 65, 21–37, <https://doi.org/10.1146/annurev-physchem-040412-110014>, 2014.
1234
1235
- 1236 Kyrö, E.-M., Väänänen, R., Kerminen, V.-M., Virkkula, A., Petäjä, T., Asmi, A., Dal Maso, M., Nieminen, T., Juhola, S.,
1237 Shcherbinin, A., Riipinen, I., Lehtipalo, K., Keronen, P., Aalto, P. P., Hari, P., and Kulmala, M.: Trends in new particle
1238 formation in eastern Lapland, Finland: effect of decreasing sulfur emissions from Kola Peninsula, *Atmos. Chem. Phys.*, 14,
1239 4383–4396, <https://doi.org/10.5194/acp-14-4383-2014>, 2014.
1240
- 1241 Lee, S.-H., Uin, J., Guenther, A. B., de Gouw, J. A., Yu, F., Nadykto, A. B., Herb, J., Ng, N. L., Koss, A., Brune, W. B.,
1242 Baumann, K., Kanawade, V. P., Keutsch, F. N., Nenes, A., Olsen, K., Goldstein, A., and Ouyang, Q.: Isoprene suppression of
1243 new particle formation: Potential mechanisms and implications, *J. Geophys. Res.*, 121, 14621–14635,
1244 <https://doi.org/10.1002/2016JD024844>, 2016.
1245
- 1246 Lehtinen, K. E. J., Dal Maso, M., Kulmala, M., and Kerminen, V. M.: Estimating nucleation rates from apparent particle
1247 formation rates and vice versa: Revised formulation of the Kerminen-Kulmala equation, *J. Aerosol Sci.*, 38, 988–994,
1248 <https://doi.org/10.1016/j.jaerosci.2007.06.009>, 2007.
1249



- 1250 Lelieveld, J., Butler, T. M., Crowley, J. N., Dillon, T. J., Fischer, H., Ganzeveld, L., Harder, H., Lawrence, M. G., Martinez,
1251 M., Taraborrelli, D., and Williams, J.: Atmospheric oxidation capacity sustained by a tropical forest, *Nature*, 452, 737–740,
1252 <https://doi.org/10.1038/nature06870>, 2008.
- 1253
- 1254 Lempa, K., Agrawal, A. A., Salminen, J.P., Turunen, T., Ossipov, V., Ossipova, S., Haukioja, E., and Pihlaja, K.: Rapid
1255 herbivore-induced changes in mountain birch phenolics and nutritive compounds and their effects on performance of the major
1256 defoliator, *Epirrita autumnata*, *J. Chem. Ecol.*, 30, 303–321, <https://doi.org/10.1023/B:JOEC.0000017979.94420.78>, 2004.
- 1257
- 1258 Li, T., Holst, T., Michelsen, A., and Rinnan, R.: Amplification of plant volatile defence against insect herbivory in a warming
1259 Arctic tundra, *Nat. Plants*, 5, 568–574, doi:10.1038/s41477-019-0439-3, 2019.
- 1260
- 1261 Lin, Y. H., Zhang, H., Pye, H. O. T., Zhang, Z., Marth, W. J., Park, S., Arashiro, M., Cui, T., Budisulistiorini, S. H., Sexton,
1262 K. G., Vizuete, W., Xie, Y., Luecken, D. J., Piletic, I. R., Edney, E. O., Bartolotti, L. J., Gold, A., and Surratt, J. D.: Epoxide
1263 as a precursor to secondary organic aerosol formation from isoprene photooxidation in the presence of nitrogen oxides, *Proc.*
1264 *Natl. Acad. Sci. U.S.A.*, 110, 6718–6723, <https://doi.org/10.1073/pnas.1221150110>, 2013.
- 1265
- 1266 Major, I. T., Nicole, M.-C., Duplessis, S., and Seguin, A.: Photosynthetic and respiratory changes in leaves of poplar elicited
1267 by rust infection, *Photosynth. Res.*, 104, 41–48, doi: 10.1007/s11120-009-9507-2, 2010.
- 1268
- 1269 Makkonen, R., Asmi, A., Korhonen, H., Kokkola, H., Järvenoja, S., Räisänen, P., Lehtinen, K. E. J., Laaksonen, A., Kerminen,
1270 V.-M., Järvinen, H., Lohmann, U., Bennartz, R., Feichter, J., Kulmala, M.: Sensitivity of aerosol concentrations and cloud
1271 properties to nucleation and secondary organic distribution in ECHAM5-HAM global circulation model, *Atmos. Chem. Phys.*,
1272 9, 1747–1766, 10.5194/acp-9-1747-2009, 2009.
- 1273
- 1274 Marçais, B. and Desprez-Loustau, M.-L.: European oak powdery mildew: impact on trees, effects of environmental factors,
1275 and potential effects of climate change, *Ann. For. Sci.*, 71, 633–642, <https://doi.org/10.1007/s13595-012-0252-x>, 2014.
- 1276
- 1277 Marçais, B., Kavkova, M., and Desprez-Loustau, M.-L.: Phenotypic variation in the phenology of ascospore production
1278 between European populations of oak powdery mildew, *Ann. For. Sci.*, 66, 814–822, <https://doi.org/10.1051/forest/2009077>,
1279 2009.
- 1280
- 1281 McFiggans, G., Mentel, T. F., Wildt, J., Pullinen, I., Kang, S., Kleist, E., Schmitt, S., Springer, M., Tillmann, R., Wu, C., Zhao,
1282 D., Hallquist, M., Faxon, C., Le Breton, M., Hallquist, Å. M., Simpson, D., Bergström, R., Jenkin, M. E., Ehn, M., Thornton,
1283 J. A., Alfarra, M. R., Bannan, T. J., Percival, C. J., Priestley, M., Topping, D., and Kiendler-Scharr, A.: Secondary organic
1284 aerosol reduced by mixture of atmospheric vapours, *Nature*, 565, 587–593, 10.1038/s41586-018-0871-y, 2019.
- 1285
- 1286 McManus, M., Schneeberger, N., Reardon, R., and Mason, G.: Forest insect and disease (No 162): Gypsy Moth, Washington,
1287 D.C.: United States Department of Agriculture Forest Service, 1989.
- 1288
- 1289 Mentel, Th. F., Kleist, E., Andres, S., Dal Maso, M., Hohaus, T., Kiendler-Scharr, A., Rudich, Y., Springer, M., Tillmann, R.,
1290 Uerlings, R., Wahner, A., and Wildt, J.: Secondary aerosol formation from stress-induced biogenic emissions and possible
1291 climate feedbacks, *Atmos. Chem. Phys.*, 13, 8755–8770, <https://doi.org/10.5194/acp-13-8755-2013>, 2013.
- 1292



- 1293 Merikanto, J., Spracklen, D. V., Mann, G. W., Pickering, S. J., and Carslaw, K. S.: Impact of nucleation on global CCN,
1294 *Atmos. Chem. Phys.*, 9, 8601–8616, 10.5194/acp-9-8601-2009, 2009.
1295
- 1296 Miller, J. C., Hanson, P. E., and Kimberling, D. N.: Development of the gypsy moth (Lepidoptera: Lymantriidae) on garry oak
1297 and red alder in Western North America, *Environ. Entomol.*, 20, 1097–1101, <https://doi.org/10.1093/ee/20.4.1097>, 1991.
1298
- 1299 Mogensen, D., Smolander, S., Sogachev, A., Zhou, L., Sinha, V., Guenther, A., Williams, J., Nieminen, T., Kajos, M. K.,
1300 Rinne, J., Kulmala, M., and Boy, M.: Modelling atmospheric OH-reactivity in a boreal forest ecosystem, *Atmos. Chem. Phys.*,
1301 11, 9709–9719, <https://doi.org/10.5194/acp-11-9709-2011>, 2011.
1302
- 1303 Mogensen, D., Gierens, R., Crowley, J. N., Keronen, P., Smolander, S., Sogachev, A., Nölscher, A. C., Zhou, L., Kulmala,
1304 M., Tang, M. J., Williams, J., and Boy, M.: Simulations of atmospheric OH, O₃ and NO₃ reactivities within and above the
1305 boreal forest, *Atmos. Chem. Phys.*, 15, 3909–3932, <https://doi.org/10.5194/acp-15-3909-2015>, 2015.
1306
- 1307 Monson, R. K., Harley, P. C., Litvak, M. E., Wildermuth, M., Guenther, A. B., Zimmerman, P. R., and Fall, R.: Environmental
1308 and developmental controls over the seasonal pattern of isoprene emission from aspen leaves, *Oecologia*, 99, 260–270,
1309 <https://doi.org/10.1007/BF00627738>, 1994.
1310
- 1311 Mutzel, A., Poulain, L., Berndt, T., Iinuma, Y., Rodigast, M., Böge, O., Richters, S., Spindler, G., Sipilä, M., Jokinen, T.,
1312 Kulmala, M., and Herrmann, H.: Highly oxidized multifunctional organic compounds observed in tropospheric particles: a
1313 field and laboratory study, *Environ. Sci. Technol.*, 49, 7754–7761, <https://doi.org/10.1021/acs.est.5b00885>, 2015.
1314
- 1315 Naja, M., Akimoto, H., and Staehelin, J.: Ozone in background and photochemically aged air over central Europe: analysis of
1316 long-term ozonesonde data from Hohenpeissenberg and Payerne, *J. Geophys. Res.*, 108, 4063, doi:10.1029/2002JD002477
1317 2003.
1318
- 1319 Nieminen, T., Lehtinen, K. E. J., and Kulmala, M.: Sub-10 nm particle growth by vapor condensation – effects of vapor
1320 molecule size and particle thermal speed, *Atmos. Chem. Phys.*, 10, 9773–9779, <https://doi.org/10.5194/acp-10-9773-2010>,
1321 2010.
1322
- 1323 Nieminen, T., Asmi, A., Dal Maso, M., Aalto, P. P., Keronen, P., Petäjä, T., Kulmala, M., and Kerminen, V.-M.: Trends in
1324 atmospheric new-particle formation: 16 years of observations in a boreal-forest environment, *Boreal Environ. Res.*, 19, suppl.
1325 B, 191–214, 2014.
1326
- 1327 Nieminen, T., Yli-Juuti, T., Manninen, H., Petäjä, T., Kerminen, V.-M., and Kulmala, M.: Technical note: New particle
1328 formation event forecasts during PEGASOS–Zeppelin Northern mission 2013 in Hyytiälä, Finland, *Atmos. Chem. Phys.*, 15,
1329 12385–12396, doi:10.5194/acp-15-12385-2015, 2015.
1330
- 1331 Niinemets, Ü.: Mild versus severe stress and BVOCs: thresholds, priming and consequences, *Trends Plant Sci.*, 15, 145–153,
1332 <https://doi.org/10.1016/j.tplants.2009.11.008>, 2010
1333



- 1334 Niinemets, Ü., Reichstein, M., Staudt, M., Seufert, G., and Tenhunen, J. D.: Stomatal constraints may affect emission of
1335 oxygenated monoterpenoids from the foliage of *Pinus pinea*, *Plant Physiol.*, 130, 1371–1385,
1336 <https://doi.org/10.1104/pp.009670>, 2002.
1337
- 1338 Niinemets Ü., Kännaste, A., and Copolovici, L.: Quantitative patterns between plant volatile emissions induced by biotic
1339 stresses and the degree of damage, *Front. Plant Sci.*, 4, 262, <https://doi.org/10.3389/fpls.2013.00262>, 2013.
1340
- 1341 Nölscher, A. C., Williams, J., Sinha, V., Custer, T., Song, W., Johnson, A. M., Axinte, R., Bozem, H., Fischer, H., Pouvesle,
1342 N., Phillips, G., Crowley, J. N., Rantala, P., Rinne, J., Kulmala, M., Gonzales, D., Valverde-Canossa, J., Vogel, A., Hoffmann,
1343 T., Ouwersloot, H. G., Vilà-Guerau de Arellano, J., and Lelieveld, J.: Summertime total OH reactivity measurements from
1344 boreal forest during HUMPPA-COPEC 2010, *Atmos. Chem. Phys.*, 12, 8257–8270, [https://doi.org/10.5194/acp-12-8257-](https://doi.org/10.5194/acp-12-8257-2012)
1345 2012, 2012.
1346
- 1347 Nölscher, A. C., Yañez-Serrano, A. M., Wolff, S., Carioca de Araujo, A., Lavrič, J. V., Kesselmeier, J., and Williams, J.:
1348 Unexpected seasonality in quantity and composition of Amazon rainforest air reactivity, *Nat. Commun.*, 7, 10383,
1349 <https://doi.org/10.1038/ncomms10383>, 2016.
1350
- 1351 Oláh, V., Szöllösi, E., Lakatos, Á., Kanalas, P., Nyitrai, B., and Mészáros, I.: Springtime leaf development of mature sessile
1352 oak trees as based on multi-seasonal monitoring data, *Acta Silv. Lign. Hung.*, 8, 21–30, [https://doi.org/10.2478/v10303-012-](https://doi.org/10.2478/v10303-012-0002-7)
1353 0002-7, 2012.
1354
- 1355 Paasonen, P., Nieminen, T., Asmi, E., Manninen, H. E., Petäjä, T., Plass-Dülmer, C., Flentje, H., Birmili, W., Wiedensohler,
1356 A., Hörrak, U., Metzger, A., Hamed, A., Laaksonen, A., Facchini, M. C., Kerminen, V.-M., and Kulmala, M.: On the roles of
1357 sulphuric acid and low-volatility organic vapours in the initial steps of atmospheric new particle formation, *Atmos. Chem.*
1358 *Phys.*, 10, 11223–11242, <https://doi.org/10.5194/acp-10-11223-2010>, 2010.
1359
- 1360 Paasonen, P., Asmi, A., Petäjä, T., Kajos, M. K., Äijälä, M., Junninen, H., Holst, T., Abbatt, J. P. D., Arneth, A., Birmili, W.,
1361 van der Gon, H. D., Hamed, A., Höffer, A., Laakso, L., Laaksonen, A., Leaitch, W. R., Plass-Dülmer, C., Pryor, S. C.,
1362 Räisänen, P., Swietlicki, E., Wiedensohler, A., Worsnop, D. R., Kerminen, V.-M., and Kulmala, M.: Warming-induced
1363 increase in aerosol number concentration likely to moderate climate change, *Nat. Geosci.*, 6, 438–442,
1364 <https://doi.org/10.1038/ngeo1800>, 2013.
1365
- 1366 Pacifico, F., Folberth, G. A., Sitch, S., Haywood, J. M., Rizzo, L. V., Malavelle, F. F., and Artaxo, P.: Biomass burning related
1367 ozone damage on vegetation over the Amazon forest: a model sensitivity study, *Atmos. Chem. Phys.*, 15, 2791–2804,
1368 <https://doi.org/10.5194/acp-15-2791-2015>, 2015.
1369
- 1370 Pautasso, M., Döring, T. F., Garbelotto, M., Pellis, L., and Jeger, M. J.: Impacts of climate change on plant diseases - opinions
1371 and trends, *Eur. J. Plant Pathol.*, 133, 295–313, <https://doi.org/10.1007/s10658-012-9936-1>, 2012.
1372
- 1373 Peräkylä, O., Riva, M., Heikkinen, L., Quéléver, L., Roldin, P., and Ehn, M.: Experimental investigation into the volatilities
1374 of highly oxygenated organic molecules (HOMs), *Atmos. Chem. Phys.*, 20, 649–669, [https://doi.org/10.5194/acp-20-649-](https://doi.org/10.5194/acp-20-649-2020)
1375 2020, 2020.
1376



- 1377 Perez-Rial, D., Penuelas, J., Lopez-Mahia, P., and Llusia, J.: Terpenoid emissions from *Quercus robur*. A case study of Galicia
1378 (NW Spain), *J. Environ. Monitor.*, 11, 1268-1275, doi: 10.1039/b819960d, 2009.
1379
- 1380 Petäjä, T., Mauldin, III, R. L., Kosciuch, E., McGrath, J., Nieminen, T., Paasonen, P., Boy, M., Adamov, A., Kotiaho, T., and
1381 Kulmala, M.: Sulfuric acid and OH concentrations in a boreal forest site, *Atmos. Chem. Phys.*, 9, 7435–7448,
1382 <https://doi.org/10.5194/acp-9-7435-2009>, 2009.
1383
- 1384 Petron, G., Harley, P., Greenberg, J., and Guenther, A.: Seasonal temperature variations influence isoprene emission, *Geophys.*
1385 *Res. Lett.*, 28 (9), 1707–1710, <https://doi.org/10.1029/2000GL011583>, 2001.
1386
- 1387 Pinon, J., Frey, P., and Husson, C.: Wettability of poplar leaves influences dew formation and infection by *Melampsora*
1388 *laricipopulina*, *Plant Dis.*, 90, 177-184, doi: 10.1094/PD-90-0177, 2006.
1389
- 1390 Pöhlker, C., Wiedemann, K. T., Sinha, B., Shiraiwa, M., Gunthe, S. S., Smith, M., Su, H., Artaxo, P., Chen, Q., Cheng, Y.,
1391 Elbert, W., Gilles, M. K., Kilcoyne, A. L. D., Moffet, R. C., Weigand, M., Martin, S. T., Pöschl, U., and Andreae, M. O.:
1392 Biogenic potassium salt particles as seeds for secondary organic aerosol in the Amazon, *Science*, 337, 1075-1078, DOI:
1393 10.1126/science.1223264, 2012.
1394
- 1395 Pöschl, U., Martin, S. T., Sinha, B., Chen, Q., Gunthe, S. S., Huffman, J. A., Borrmann, S., Farmer, D. K., Garland, R. M.,
1396 Helas, G., Jimenez, J. L., King, S. M., Manzi, A., Mikhailov, E., Pauliquevis, T., Petters, M. D., Prenni, A. J., Roldin, P., Rose,
1397 D., Schneider, J., Su, H., Zorn, S. R., Artaxo, P., and O., A. M.: Rainforest aerosols as biogenic nuclei of clouds and
1398 precipitation in the Amazon, *Science*, 329, 1513–1516, DOI: 10.1126/science.1191056, 2010.
1399
- 1400 Praplan, A. P., Tykkä, T., Chen, D., Boy, M., Taipale, D., Vakkari, V., Zhou, P., Petäjä, T., and Hellén, H.: Long-term total
1401 OH reactivity measurements in a boreal forest, *Atmos. Chem. Phys.*, 19, 14431–14453, [https://doi.org/10.5194/acp-19-14431-](https://doi.org/10.5194/acp-19-14431-2019)
1402 2019, 2019.
1403
- 1404 Pullinen, I., Schmitt, S., Kang, S., Sarrafzadeh, M., Schlag, P., Andres, S., Kleist, E., Mentel, T. F., Rohrer, F., Springer, M.,
1405 Tillmann, R., Wildt, J., Wu, C., Zhao, D., Wahner, A., and Kiendler-Scharr, A.: Impact of NO_x on secondary organic aerosol
1406 (SOA) formation from α -pinene and β -pinene photooxidation: the role of highly oxygenated organic nitrates, *Atmos. Chem.*
1407 *Phys.*, 20, 10125–10147, <https://doi.org/10.5194/acp-20-10125-2020>, 2020.
1408
- 1409 Quéféver, L. L. J., Kristensen, K., Normann Jensen, L., Rosati, B., Teiwes, R., Daellenbach, K. R., Peräkylä, O., Roldin, P.,
1410 Bossi, R., Pedersen, H. B., Glasius, M., Bilde, M., and Ehn, M.: Effect of temperature on the formation of highly oxygenated
1411 organic molecules (HOMs) from alpha-pinene ozonolysis, *Atmos. Chem. Phys.*, 19, 7609–7625, [https://doi.org/10.5194/acp-](https://doi.org/10.5194/acp-19-7609-2019)
1412 19-7609-2019, 2019.
1413
- 1414 Riccobono, F., Schobesberger, S., Scott, C. E., Dommen, J., Ortega, I. K., Rondo, L., Almeida, J., Amorim, A., Bianchi, F.,
1415 Breitenlechner, M., David, A., Downard, A., Dunne, E. M., Duplissy, J., Ehrhart, S., Flagan, R. C., Franchin, A., Hansel, A.,
1416 Junninen, H., Kajos, M., Keskinen, H., Kupc, A., Kürten, A., Kvashin, A. N., Laaksonen, A., Lehtipalo, K., Makhmutov, V.,
1417 Mathot, S., Nieminen, T., Onnela, A., Petäjä, T., Praplan, A. P., Santos, F. D., Schallhart, S., Seinfeld, J. H., Sipilä, M.,
1418 Spracklen, D. V., Stozhkov, Y., Stratmann, F., Tomé, A., Tsagkogeorgas, G., Vaattovaara, P., Viisanen, Y., Vrtala, A., Wagner,
1419 P. E., Weingartner, E., Wex, H., Wimmer, D., Carslaw, K. S., Curtius, J., Donahue, N. M., Kirkby, J., Kulmala, M., Worsnop,



- 1420 D. R., and Baltensperger, U.: Oxidation products of biogenic emissions contribute to nucleation of atmospheric particles,
1421 Science, 344, 717-721, DOI: 10.1126/science.1243527, 2014.
1422
- 1423 Rieksta, J., Li, T., Junker, R. R., Jepsen, J. U., Ryde, I., and Rinnan, R.: Insect herbivory strongly modifies mountain birch
1424 volatile emissions, Front. Plant Sci., 11: 558979, <https://doi.org/10.3389/fpls.2020.558979>, 2020.
1425
- 1426 Riipi, M., Lempa, K., Haukioja, E., Ossipov, V., and Pihlaja, K.: Effects of simulated winter browsing on mountain birch foliar
1427 chemistry and on the performance of insect herbivores, Oikos, 111, 221-234, <https://doi.org/10.1111/j.0030-1299.2005.13781.x>, 2005.
1428
1429
- 1430 Riipinen, I., Yli-Juuti, T., Pierce, J. R., Petäjä, T., Worsnop, D. R., Kulmala, M., and Donahue, N. M.: The contribution of
1431 organics to atmospheric nanoparticle growth, Nat. Geosci., 5, 453-458, <https://doi.org/10.1038/ngeo1499>, 2012.
1432
- 1433 Rohrer, F. and Berresheim, H.: Strong correlation between levels of tropospheric hydroxyl radicals and solar ultraviolet
1434 radiation, Nature, 442, 184-187, <https://doi.org/10.1038/nature04924>, 2006.
1435
- 1436 Rosenfeld, D., Andreae, M. O., Asmi, A., Chin, M., de Leeuw, G., Donovan, D. P., Kahn, R., Kinne, S., Kivekäs, N., Kulmala,
1437 M., Lau, W., Schmidt, S., Suni, T., Wagner, T., Wildt, M., and Quass, J.: Global observations of aerosol-cloud-precipitation-
1438 climate interactions, Rev. Geophys., 52, 750-808, <https://doi.org/10.1002/2013RG000441>, 2014.
1439
- 1440 Ruuskanen, T. M., Reissell, A., Keronen, P., Aalto, P. P., Laakso, L., Grönholm, T., Hari, P., and Kulmala, M.: Atmospheric
1441 trace gas and aerosol particle concentration measurements in Eastern Lapland, Finland 1992-2001, Boreal Environ. Res., 8,
1442 335-349, 2003.
1443
- 1444 Schaub, A., Blande, J. D., Graus, M., Oksanen, E., Holopainen, J. K., and Hansel, A.: Real-time monitoring of herbivore
1445 induced volatile emissions in the field, Physiol. Plant., 138, 123-133, [10.1111/j.1399-3054.2009.01322.x](https://doi.org/10.1111/j.1399-3054.2009.01322.x), 2010.
1446
- 1447 Schnitzler, J.-P., Lehning, A., and Steinbrecher, R.: Seasonal pattern of isoprene synthase activity in *Quercus robur* leaves and
1448 its significance for modeling isoprene emission rates, Bot. Acta, 110, 240-243, <https://doi.org/10.1111/j.1438-8677.1997.tb00635.x>, 1997.
1449
1450
- 1451 Schobesberger, S., Junninen, H., Bianchi, F., Lönn, G., Ehn, M., Lehtipalo, K., Dommen, J., Ehrhart, S., Ortega, I. K., Franchin,
1452 A., Nieminen, T., Riccobono, F., Hutterli, M., Duplissy, J., Almeida, J., Amorim, A., Breitenlechner, M., Downard, A. J.,
1453 Dunne, E. M., Flagan, R. C., Kajos, M., Keskinen, H., Kirkby, J., Kupc, A., Kürten, A., Kurtén, T., Laaksonen, A., Mathot,
1454 S., Onnela, A., Praplan, A. P., Rondo, L., Santos, F. D., Schallhart, S., Schnitzhofer, R., Sipilä, M., Tomé, A., Tsagkogeorgas,
1455 G., Vehkamäki, H., Wimmer, D., Baltensperger, U., Carslaw, K. S., Curtius, J., Hansel, A., Petäjä, T., Kulmala, M., Donahue,
1456 N. M., and Worsnop, D. R.: Molecular understanding of atmospheric particle formation from sulfuric acid and large oxidized
1457 organic molecules, PNAS 110, 17223-17228, <https://doi.org/10.1073/pnas.1306973110>, 2013.
1458
- 1459 Seidel, D. J., Zhang, Y., Beljaars, A., Golaz, J.-C., Jacobson, A. R., and Medeiros, B.: Climatology of the planetary boundary
1460 layer over the continental United States and Europe, J. Geophys. Res. A, 117, D17106, doi:10.1029/2012JD018143, 2012.
1461



- 1462 Shifflett, S. D., Hazel, D. W., and Guthrie Nichols, E.: Sub-soiling and genotype selection improves *Populus* productivity
1463 grown on a North Carolina sandy soil, *Forests*, 7, 74-84, doi: 10.3390/f7040074, 2016.
- 1464
- 1465 Simon, M., Dada, L., Heinritzi, M., Scholz, W., Stolzenburg, D., Fischer, L., Wagner, A. C., Kürten, A., Rörup, B., He, X.-C.,
1466 Almeida, J., Baalbaki, R., Baccarini, A., Bauer, P. S., Beck, L., Bergen, A., Bianchi, F., Bräkling, S., Brilke, S., Caudillo, L.,
1467 Chen, D., Chu, B., Dias, A., Draper, D. C., Duplissy, J., El-Haddad, I., Finkenzeller, H., Frege, C., Gonzalez-Carracedo, L.,
1468 Gordon, H., Granzin, M., Hakala, J., Hofbauer, V., Hoyle, C. R., Kim, C., Kong, W., Lamkaddam, H., Lee, C. P., Lehtipalo,
1469 K., Leiminger, M., Mai, H., Manninen, H. E., Marie, G., Marten, R., Mentler, B., Molteni, U., Nichman, L., Nie, W., Ojdanic,
1470 A., Onnela, A., Partoll, E., Petäjä, T., Pfeifer, J., Philippov, M., Quéléver, L. L. J., Ranjithkumar, A., Rissanen, M. P.,
1471 Schallhart, S., Schobesberger, S., Schuchmann, S., Shen, J., Sipilä, M., Steiner, G., Stozhkov, Y., Tauber, C., Tham, Y. J.,
1472 Tomé, A. R., Vazquez-Pufleau, M., Vogel, A. L., Wagner, R., Wang, M., Wang, D. S., Wang, Y., Weber, S. K., Wu, Y., Xiao,
1473 M., Yan, C., Ye, P., Ye, Q., Zauner-Wieczorek, M., Zhou, X., Baltensperger, U., Dommen, J., Flagan, R. C., Hansel, A.,
1474 Kulmala, M., Volkamer, R., Winkler, P. M., Worsnop, D. R., Donahue, N. M., Kirkby, J., and Curtius, J.: Molecular
1475 understanding of new-particle formation from α -pinene between -50 and $+25$ °C, *Atmos. Chem. Phys.*, 20, 9183–9207,
1476 <https://doi.org/10.5194/acp-20-9183-2020>, 2020.
- 1477
- 1478 Simpson, D. Winiwarter, W., Börjesson, G., Cinderby, S., Ferreira, A., Guenther, A., Hewitt, C. N., Janson, R., Aslam K.
1479 Khalil, M., Owen, S., Pierce, T. E., Puxbaum, H., Shearer, M., Skiba, U., Steinbrecher, R., Tarrasón, L., and Öquist, M. G.:
1480 Inventorying emissions from Nature in Europe, *J. Geophys. Res. A*, 104, 8113-8152, <https://doi.org/10.1029/98JD02747>,
1481 1999.
- 1482
- 1483 Simpson, D., Benedictow, A., Berge, H., Bergström, R., Emberson, L. D., Fagerli, H., Flechard, C. R., Hayman, G. D., Gauss,
1484 M., Jonson, J. E., Jenkin, M. E., Nyíri, A., Richter, C., Semeena, V. S., Tsyro, S., Tuovinen, J.-P., Valdebenito, Á., and Wind,
1485 P.: The EMEP MSC-W chemical transport model – technical description, *Atmos. Chem. Phys.*, 12, 7825–7865,
1486 <https://doi.org/10.5194/acp-12-7825-2012>, 2012.
- 1487
- 1488 Sinha, V., Williams, J., Lelieveld, J., Ruuskanen, T. M., Kajos, M. K., Patokoski, J., Hellén, H., Hakola, H., Mogensen, D.,
1489 Boy, M., Rinne, J., and Kulmala, M.: OH reactivity measurements within a boreal forest: evidence for unknown reactive
1490 emissions, *Environ. Sci. Technol.*, 44, 6614–6620, 2010.
- 1491
- 1492 Smiatek, G. and Steinbrecher, R.: Temporal and spatial variation of forest VOC emissions in Germany in the decade 1994–
1493 2003, *Atmos. Environ.*, 40, S166, 166-177, <https://doi.org/10.1016/j.atmosenv.2005.11.071>, 2006.
- 1494
- 1495 Spear, R. J. *The Great Gypsy Moth War: A history of the first campaign in Massachusetts to eradicate the gypsy moth, 1890-*
1496 *1901*, University of Massachusetts Press, 2005.
- 1497
- 1498 Spracklen, D. V., Carslaw, K. S., Kulmala, M., Kerminen, V.-M., Sihto, S.-L., Riipinen, I., Merikanto, J., Mann, G. W.,
1499 Chipperfield, M. P., Wiedensohler, A., Birmili, W., and Lihavainen, H.: Contribution of particle formation to global cloud
1500 condensation nuclei concentrations, *Geophys. Res. Lett.*, 35, doi: 10.1029/2007GL033038, 2008.
- 1501
- 1502 Stolzenburg, D., Fischer, L., Vogel, A. L., Heinritzi, M., Schervish, M., Simon, M., Wagner, A. C., Dada, L., Ahonen, L. R.,
1503 Amorim, A., Baccarini, A., Bauer, P. S., Baumgartner, B., Bergen, A., Bianchi, F., Breitenlechner, M., Brilke, S., Mazon, S.
1504 B., Chen, D., Dias, A., Draper, D. C., Duplissy, J., El Haddad, I., Finkenzeller, H., Frege, C., Fuchs, C., Garmash, O., Gordon,



- 1505 H., He, X., Helm, J., Hofbauer, V., Hoyle, C. R., Kim, C., Kirkby, J., Kontkanen, J., Kürten, A., Lampilahti, J., Lawler, M.,
1506 Lehtipalo, K., Leiminger, M., Mai, H., Mathot, S., Mentler, B., Molteni, U., Nie, W., Nieminen, T., Nowak, J. B., Ojdanic, A.,
1507 Onnela, A., Passananti, M., Petäjä, T., Quéléver, L. L. J., Rissanen, M. P., Sarnela, N., Schallhart, S., Tauber, C., Tomé, A.,
1508 Wagner, R., Wang, M., Weitz, L., Wimmer, D., Xiao, M., Yan, C., Ye, P., Zha, Q., Baltensperger, U., Curtius, J., Dommen,
1509 J., Flagan, R. C., Kulmala, M., Smith, J. N., Worsnop, D. R., Hansel, A., Donahue, N. M., and Winkler, P. M.: Rapid growth
1510 of organic aerosol nanoparticles over a wide tropospheric temperature range, *P. Natl. Acad. Sci. USA*, 115, 9122-9127,
1511 <https://doi.org/10.1073/pnas.1807604115>, 2018.
- 1512
- 1513 Stoyenoff, J. L., Witter, J. A., and Montgomery, M. E.: Nutritional indices in the gypsy moth (*Lymantria dispar* (L.)) under
1514 field conditions and host switching situations, *Oecologia*, 97, 158-170, <https://doi.org/10.1007/BF00323145>, 1994.
- 1515
- 1516 Sun, Z., Copolovici, L., and Niinemets, Ü.: Can the capacity for isoprene emission acclimate to environmental modifications
1517 during autumn senescence in temperate deciduous tree species *Populus tremula*?, *J. Plant Res.*, 125, 263-274,
1518 <https://doi.org/10.1007/s10265-011-0429-7>, 2012.
- 1519
- 1520 Surratt, J. D., Chan, A. W. H., Eddingsaas, N. C., Chan, M., Loza, C. L., Kwan, A. J., Hersey, S. P., Flagan, R. C., Wennberg,
1521 P. O., and Seinfeld, J. H.: Reactive intermediates revealed in secondary organic aerosol formation from isoprene, *Proc. Natl.*
1522 *Acad. Sci. U. S. A.*, 107, 6640-6645, <https://doi.org/10.1073/pnas.0911114107>, 2010.
- 1523
- 1524 Tammaru, T., Kaitaniemi, P., and Ruohomäki, K.: Realized fecundity in *Epirrita autumnata* (Lepidoptera: Geometridae):
1525 relation to body size and consequences to population dynamics, *Oikos*, 77, 407-16, doi: 10.2307/3545931, 1996.
- 1526
- 1527 Taipale, D., Aalto, J., Schiestl-Aalto, P., Kulmala, M., and Bäck, J.: The importance of accounting for enhanced emissions of
1528 monoterpenes from new Scots pine foliage in models - A Finnish case study, *Atmos. Environ. X.*, 8, 100097,
1529 <https://doi.org/10.1016/j.aeaoa.2020.100097>, 2020.
- 1530
- 1531 Taraborrelli, D., Lawrence, M., G., Crowley, J. N., Dillon, T. J., Gromov, S., Groß, C. B. M., Vereecken, L., and Lelieveld,
1532 J.: Hydroxyl radical buffered by isoprene oxidation over tropical forests, *Nat. Geosci.*, 5, 190-193,
1533 <https://doi.org/10.1038/ngeo1405>, 2012.
- 1534
- 1535 Tripathi, A. M., Fischer, M., Orság, M., Marek, M. V., Žalud, Z., and Trnka, M.: Evaluation of indirect measurement method
1536 of seasonal patterns of leaf area index in a high-density short rotation coppice culture of poplar, *Acta Univ. Agric. Silvic.*
1537 *Mendelianae Brun.*, 64, 549-556, <https://doi.org/10.11118/actaun201664020549>, 2016.
- 1538
- 1539 Tröstl, J., Chuang, W. K., Gordon, H., Heinritzi, M., Yan, C., Molteni, U., Ahlm, L., Frege, C., Bianchi, F., Wagner, R., Simon,
1540 M., Lehtipalo, K., Williamson, C., Craven, J. S., Duplissy, J., Adamov, A., Almeida, J., Bernhammer, A.-K., Breitenlechner,
1541 M., Brilke, S., Dias, A., Ehrhart, S., Flagan, R. C., Franchin, A., Fuchs, C., Guida, R., Gysel, M., Hansel, A., Hoyle, C. R.,
1542 Jokinen, T., Junninen, H., Kangasluoma, J., Keskinen, H., Kim, J., Krapf, M., Kürten, A., Laaksonen, A., Lawler, M.,
1543 Leiminger, M., Mathot, S., Möhler, O., Nieminen, T., Onnela, A., Petäjä, T., Piel, F. M., Miettinen, P., Rissanen, M. P., Rondo,
1544 L., Sarnela, N., Schobesberger, S., Sengupta, K., Sipilä, M., Smith, J. N., Steiner, G., Tomé, A., Virtanen, A., Wagner, A. C.,
1545 Weingartner, E., Wimmer, D., Winkler, P. M., Ye, P., Carslaw, K. S., Curtius, J., Dommen, J., Kirkby, J., Kulmala, M.,
1546 Riipinen, I., Worsnop, D. R., Donahue, N. M., and Baltensperger, U.: The role of low-volatility organic compounds in initial
1547 particle growth in the atmosphere, *Nature*, 533, 527-531, <https://doi.org/10.1038/nature18271>, 2016.



- 1548
- 1549 Twomey, S.: The influence of pollution on the shortwave albedo of clouds, *J., Atmos. Sci.*, 34, 1149–1152,
1550 [https://doi.org/10.1175/1520-0469\(1977\)034<1149:TIOPOP>2.0.CO;2](https://doi.org/10.1175/1520-0469(1977)034<1149:TIOPOP>2.0.CO;2), 1977.
- 1551
- 1552 Vana, M., Komsaare, K., Hörrak, U., Mirme, S., Nieminen, T., Kontkanen, J., Manninen, H. E., Petäjä, T., Noe, S. M., and
1553 Kulmala, M.: Characteristics of new-particle formation at three SMEAR stations, *Boreal Environ. Res.*, 21, 345-362, 2016.
- 1554
- 1555 van Meeningen, Y., Schurgers, G., Rinnan, R., and Holst, T.: BVOC emissions from English oak (*Quercus robur*) and European
1556 beech (*Fagus sylvatica*) along a latitudinal gradient, *Biogeosciences*, 13, 6067–6080, [https://doi.org/10.5194/bg-13-6067-](https://doi.org/10.5194/bg-13-6067-2016)
1557 2016, 2016.
- 1558
- 1559 Vapaavuori, E., Holopainen, J. K., Holopainen, T., Julkunen-Tiitto, R., Kaakinen, S., Kasurinen, A., Kontunen-Soppela, S.,
1560 Kostiaainen, K., Oksanen, E., Peltonen, P., Riikonen, J., and Tulva, I.: Rising atmospheric CO₂ concentration partially masks
1561 the negative effects of elevated O₃ in silver birch (*Betula pendula* Roth), *Ambio*, 38, 418-424, [10.1579/0044-7447-38.8.418](https://doi.org/10.1579/0044-7447-38.8.418),
1562 2009.
- 1563
- 1564 Verlinden, M. S., Broeckx, L. S., Van den Bulcke, J., Van Acker, J., and Ceulemans, R.: Comparative study of biomass
1565 determinants of 12 poplar (*Populus*) genotypes in a high-density short-rotation culture, *Forest Ecol. Manag.*, 307, 101-111,
1566 <https://doi.org/10.1016/j.foreco.2013.06.062>, 2013.
- 1567
- 1568 Vialle, A., Frey, P., Hambleton, S., Bernier, L., and Hamelin, R. C.: Poplar rust systematics and refinement of *Melampsora*
1569 species delineation, *Fungal Divers.*, 50, 227-248, <https://doi.org/10.1007/s13225-011-0129-6>, 2011.
- 1570
- 1571 Voegelé, R. T. and Mendgen, K.: Rust haustoria: nutrient uptake and beyond, *New Phytol.*, 159, 93-100,
1572 <https://doi.org/10.1046/j.1469-8137.2003.00761.x>, 2003.
- 1573
- 1574 Waring, P. and Townsend, M.: *Field Guide to the Moths of Great Britain and Ireland*, British Wildlife Publishing, 2009.
- 1575
- 1576 Wells, K. C., Millet, D. B., Payne, V. H., Deventer, M. J., Bates, K. H., de Gouw, J., Graus, M., Warneke, C., Wisthaler, A.,
1577 and Fuentes, J. D.: Satellite isoprene retrievals constrain emissions and atmospheric oxidation, *Nature*, 585, 225-233,
1578 <https://doi.org/10.1038/s41586-020-2664-3>, 2020.
- 1579
- 1580 Williamson, C. J., Kupc, A., Axisa, D., Bilsback, K. R., Bui, T., Campuzano-Jost, P., Dollner, M., Froyd, K. D., Hodshire, A.,
1581 L., Jimenez, J. L., Kodros, J. K., Luo, G., Murphy, D. M., Nault, B. A., Ray, E. A., Weinzierl, B., Wilson, J. C., Yu, F., Yu,
1582 P., Pierce, J. R., and Brock, C. A.: A large source of cloud condensation nuclei from new particle formation in the tropics,
1583 *Nature*, 574, 399-403, <https://doi.org/10.1038/s41586-019-1638-9>, 2019.
- 1584
- 1585 Winterhalter, R., Herrmann, F., Kanawati, B., Nguyen, T. L., Peeters, J., Vereecken, L., and Moortgat, G. K.: The gas-phase
1586 ozonolysis of β -caryophyllene (C₁₅H₂₄), Part I: an experimental study, *Phys. Chem. Chem. Phys.*, 11, 4152-4172,
1587 <https://doi.org/10.1039/B817824K>, 2009.
- 1588
- 1589 Yan, C., Nie, W., Vogel, A. L., Dada, L., Lehtipalo, K., Stolzenburg, D., Wagner, R., Rissanen, M. P., Xiao, M., Ahonen, L.,
1590 Fischer, L., Rose, C., Bianchi, F., Gordon, H., Simon, M., Heinritzi, M., Garmash, O., Roldin, P., Dias, A., Ye, P., Hofbauer,



- 1591 V., Amorim, A., Bauer, P. S., Bergen, A., Bernhammer, A.-K., Breitenlechner, M., Brilke, S., Buchholz, A., Buenostro
1592 Mazon, S., Canagaratna, M. R., Chen, X., Ding, A., Dommen, J., Draper, D. C., Duplissy, J., Frege, C., Heyn, C., Guida, R.,
1593 Hakala, J., Heikkinen, L., Hoyle, C. R., Jokinen, T., Kangasluoma, J., Kirkby, J., Kontkanen, J., Kürten, A., Lawler, M. J.,
1594 Mai, H., Mathot, S., Maulding III, R. L., Molteni, U., Nichman, L., Nieminen, T., Nowak, J., Ojdanic, A., Onnela, A., Pajunoja,
1595 A., Petäjä, T., Piel, F., Quéléver, L. L. J., Sarnela, N., Schallhart, S., Sengupta, K., Sipilä, M., Tomé, A., Tröstl, J., Väisänen,
1596 O., Wagner, A. C., Ylisirmö, A., Zha, Q., Baltensperger, U., Carslaw, K. S., Curtius, J., Flagan, R. C., Hansel, A., Riipinen,
1597 I., Smith, J. N., Virtanen, A., Winkler, P. M., Donahue, N. M., Kerminen, V.-M., Kulmala, M., Ehn, M., and Worsnop, D. R.:
1598 Size-dependent influence of NO_x on the growth rates of organic aerosol particles, *Sci. Adv.*, 6, eaay4945, doi:
1599 10.1126/sciadv.aay4945, 2020.
1600
- 1601 Ye, J., Jiang, Y., Veromann-Jürgenson, L.-L., Niinemets, Ü.: Petiole gall aphid (*Pemphigus spyrothecae*) infestation of *Populus*
1602 × *petrowskiana* leaves alters foliage photosynthetic characteristics and leads to enhanced emissions of both constitutive and
1603 stress-induced volatiles, *Trees*, 33, 37–51, 10.1007/s00468-018-1756-2, 2019.
1604
- 1605 Yli-Juuti, T., Riipinen, I., Aalto, P. P., Nieminen, T., Maenhaut, W., Janssens, I. A., Claeys, M., Salma, I., Ocskay, R., Hoffer,
1606 A., Imre, K., and Kulmala, M.: Characteristics of new particle formation events and cluster ions at K-puszta, Hungary, *Boreal*
1607 *Environ. Res.*, 14, 683–698, 2009.
1608
- 1609 Yli-Juuti, T., Nieminen, T., Hirsikko, A., Aalto, P. P., Asmi, E., Hörrak, U., Manninen, H. E., Patokoski, J., Dal Maso, M.,
1610 Petäjä, T., Rinne, J., Kulmala, M., and Riipinen, I.: Growth rates of nucleation mode particles in Hyytiälä during 2003–2009:
1611 variation with particle size, season, data analysis method and ambient conditions, *Atmos. Chem. Phys.*, 11, 12865–12886,
1612 <https://doi.org/10.5194/acp-11-12865-2011>, 2011.
1613
- 1614 Yli-Pirilä, P., Copolovici, L., Kännaste, A., Noe, S., Blande, J. D., Mikkonen, S., Klemola, T., Pulkkinen, J., Virtanen, A.,
1615 Laaksonen, A., Joutsensaari, J., Niinemets, Ü., Holopainen, J. K.: Herbivory by an outbreaking moth increases emissions of
1616 biogenic volatiles and leads to enhanced secondary organic aerosol formation capacity, *Environ. Sci. Technol.*, 50, 11501-
1617 11510, doi: 10.1021/acs.est.6b02800, 2016.
1618
- 1619 Ylisirmö, A., Buchholz, A., Mohr, C., Li, Z., Barreira, L., Lambe, A., Faiola, C., Kari, E., Yli-Juuti, T., Nizkorodov, S. A.,
1620 Worsnop, D. R., Virtanen, A., and Schobesberger, S.: Composition and volatility of secondary organic aerosol (SOA) formed
1621 from oxidation of real tree emissions compared to simplified volatile organic compound (VOC) systems, *Atmos. Chem. Phys.*,
1622 20, 5629–5644, <https://doi.org/10.5194/acp-20-5629-2020>, 2020.
1623
- 1624 Ylivinkka, I., Itämies, J., Klemola, T., Ruohomäki, K., Kulmala, M., and Taipale, D.: Investigating evidence of enhanced
1625 aerosol formation and growth due to autumnal moth larvae feeding on mountain birch at SMEAR I in northern Finland, *Boreal*
1626 *Environ. Res.*, 25, 121–143, 2020.
1627
- 1628 Yu, H., Ortega, J., Smith, J. N., Guenther, A. B., Kanawade, V. P., You, Yi., Liu, Y., Hosman, K., Karl, T., Seco, R., Geron,
1629 C., Pallardy, S. G., Gu, L., Mikkilä, J., and Lee, S.-H.: New particle formation and growth in an isoprene-dominated Ozark
1630 forest: from sub-5 nm to CCN-active sizes, *Aerosol Sci. Technol.*, 48, 1285–1298, DOI: 10.1080/02786826.2014.984801,
1631 2014.
1632



- 1633 Zannoni, N., Gros, V., Lanza, M., Sarda, R., Bonsang, B., Kalogridis, C., Preunkert, S., Legrand, M., Jambert, C., Boissard,
1634 C., and Lathiere, J.: OH reactivity and concentrations of biogenic volatile organic compounds in a Mediterranean forest of
1635 downy oak trees, *Atmos. Chem. Phys.*, 16, 1619–1636, <https://doi.org/10.5194/acp-16-1619-2016>, 2016.
1636
1637 Zhao, D., Pullinen, I., Fuchs, H., Schrade, S., Wu, R., Acir, I.-H., Tillmann, R., Rohrer, F., Wildt, J., Guo, Y., Kiendler-Scharr,
1638 A., Wahner, A., Kang, S., Vereecken, L., and Mentel, T. F.: Highly oxygenated organic molecules (HOM) formation in the
1639 isoprene oxidation by NO₃ radical, *Atmos. Chem. Phys. Discuss.*, <https://doi.org/10.5194/acp-2020-1178>, in review, 2020.
1640
1641 Zúbrik, M., Novotný, J., and Kozánek, M.: The effect of gamma radiation on the host preferences of the gypsy moth larvae
1642 (*Lymantria dispar* L., Lep.: Lymantriidae), *Lesn. Čas. For. J.*, 53, 15-23, 2007.
1643

1644 **Appendix A: Leaf age effect**

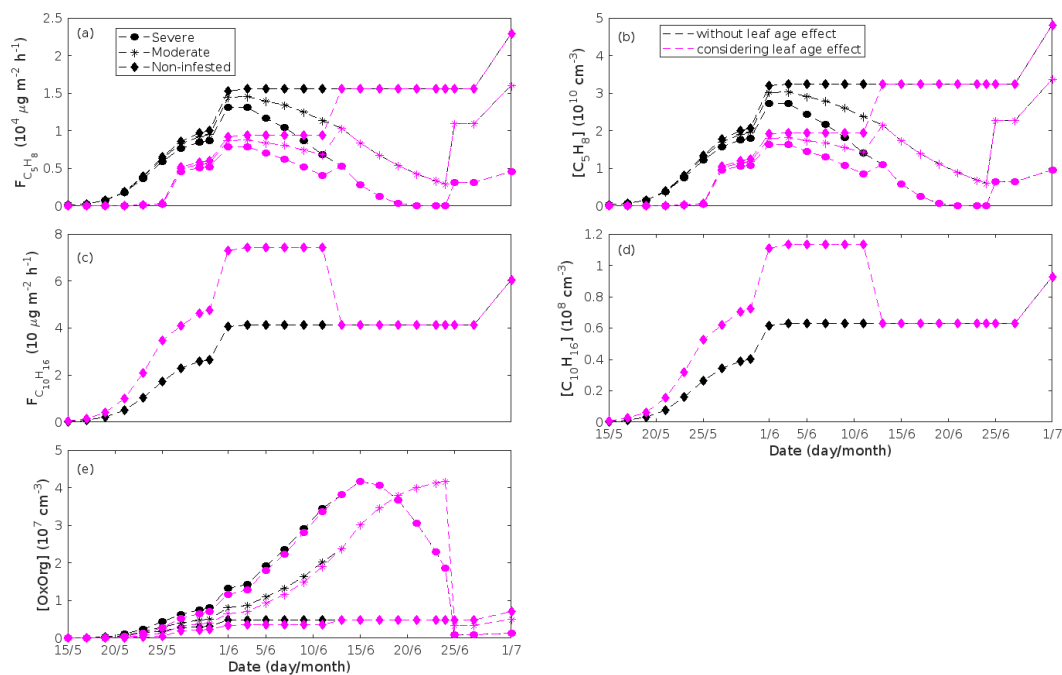
1645 **Simulations of pedunculate oak infested with European gypsy moth larvae**

1646 It seems likely that Copolovici et al. (2017) conducted their measurements on leaves that emit isoprene at peak rate, since their
1647 reported emission rate of isoprene from non-infested leaves is comparable to the rates reported from mature leaves in previous
1648 studies (e.g. Smiatek and Steinbrecher, 2006; Perez-Rial et al., 2009; van Meeningen et al., 2016). The impact of leaf age was
1649 tested during the period with stress utilising the moderations shown in Table A1. The first period covers the number of days
1650 between budbreak and the induction of isoprene emission, while the second period ends when initiation of peak isoprene
1651 emission rates has been reached. The duration of these two periods were calculated using Eq. 18a and Eq. 19 in Guenther et
1652 al. (2006) and our assumptions about the ambient temperature conditions (Fig. 4b). Since isoprene does not show an induced
1653 response in emission upon gypsy moth herbivory, the emission rate of isoprene was reduced in simulations of both non-infested
1654 and infested oak forest. The applied factors used for reductions are from Guenther et al. (2012). The emission rate of
1655 monoterpenes was increased in the beginning of the growing season for simulations of a non-infested oak stand utilising the
1656 coefficients from Guenther et al. (2012). Stress-induced emissions were not altered, since we do not know the effect of leaf
1657 age on these types of emissions and Guenther et al. (2012) e.g. also assumed the same. The results are shown in Fig. A1-2.
1658

1659 **Table A1.** Moderations made in order to consider the effect of leaf age. $\epsilon_{\text{isoprene}}$ and $\epsilon_{\text{monoterpenes}}$ are the emission factors of
1660 isoprene and monoterpenes, respectively, used in the simulations when the leaf age effect has been considered, while $\epsilon_{\text{iso,mature}}$
1661 and $\epsilon_{\text{mono,mature}}$ are the emission factors of isoprene and monoterpenes, respectively, used in the default simulations (i.e.
1662 resulting in Fig. 5-6). The moderations have been applied to the simulations of either only non-infested oak or also stressed
1663 oak as indicated under “simulations”.

Period (day/month)	$\epsilon_{\text{isoprene}}$	Simulations	$\epsilon_{\text{monoterpenes}}$	Simulations
15-26/5	$0.05 \times \epsilon_{\text{iso,mature}}$	Non-infested, moderate stress, severe stress	$2 \times \epsilon_{\text{mono,mature}}$	Non-infested
27/5-11/6	$0.6 \times \epsilon_{\text{iso,mature}}$	Non-infested, moderate stress, severe stress	$1.8 \times \epsilon_{\text{mono,mature}}$	Non-infested
12/6-	$\epsilon_{\text{iso,mature}}$	Non-infested, moderate stress, severe stress	$\epsilon_{\text{mono,mature}}$	Non-infested, moderate stress, severe stress

1664

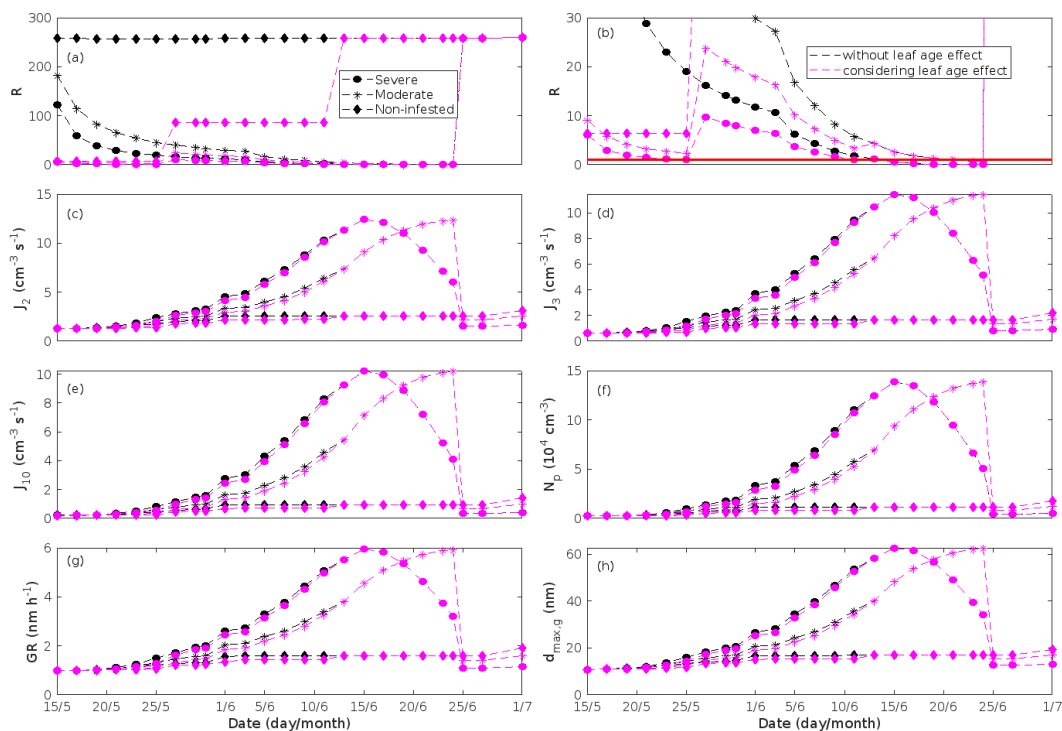


1665

1666

Figure A1. An oak stand infested with European gypsy moth larvae in comparison to a non-infested oak stand simulated with and without considering the impact of leaf age on the rates of emissions. Canopy emissions of (a) isoprene and (c) monoterpenes, atmospheric concentrations of (b) isoprene, (d) monoterpenes and (e) OxOrg. “Moderately” and “severely” refer to 30 % and 80 %, respectively, of the leaf area that has been consumed by the end of the feeding period. Black markers are for simulations where the effect of leaf age was not considered, while magenta markers are for simulations where the effect of leaf age was considered. Simulation results (independently of whether the effect of leaf age was considered or not) for “severe” is always indicated by circles, for “moderate” by asterisks, and for “non-infested” by diamonds.

1673



1674

1675 **Figure A2.** An oak stand infested with European gypsy moth larvae in comparison to a non-infested oak stand simulated with
 1676 and without considering the impact of leaf age on the rates of emissions. (a) the ratios of isoprene-to-monoterpene carbon
 1677 concentrations provided as a zoom in (b), where the red line indicates $R = 1$. Formation rates of (c) 2, (d) 3 and (e) 10 nm
 1678 particles. (f) number concentrations of formed particles, (g) growth rates of newly formed particles, and (h) the daily maxima
 1679 diameter of the growing particle mode. Symbols mean the same as in Fig. A1.

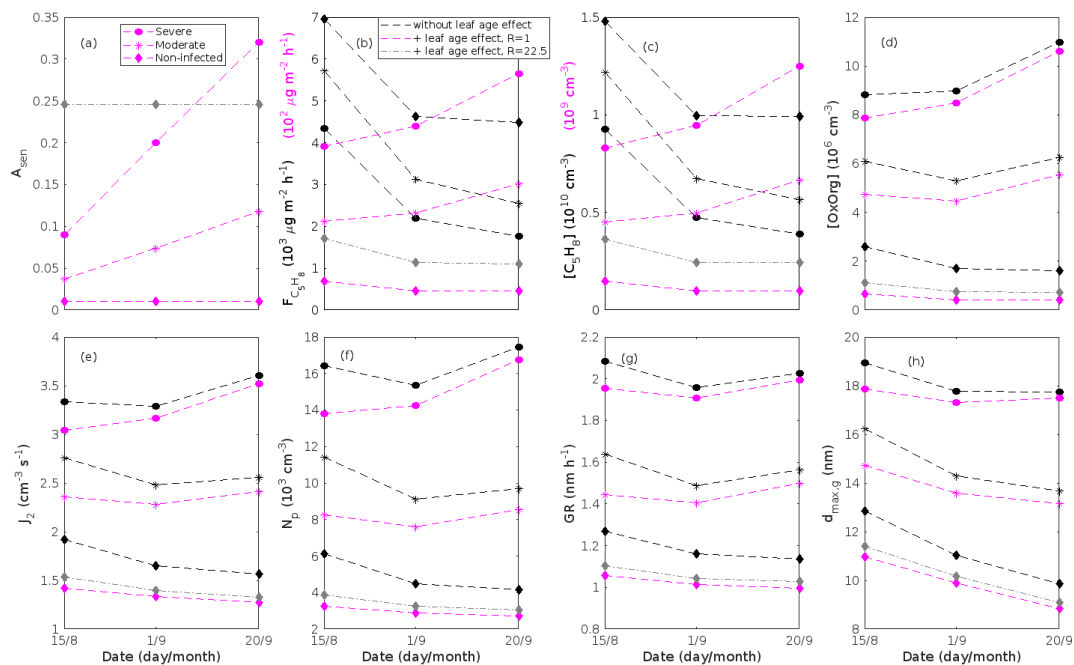
1680

1681 **Simulations of pedunculate oak infected by oak powdery mildew and balsam poplar infected by rust fungi**

1682 The emission rates used for simulations of oak and poplar, with and without pathogenic infection, were measured in the middle
 1683 and beginning of September, respectively, in Estonia (Copolovici et al., 2014; Jiang et al. 2016). Representative photographs
 1684 of control leaves indicate that the measured leaves were mature and without any visible signs of senescence (Copolovici et al.,
 1685 2014; Jiang et al. 2016).

1686 When leaves grow old, they eventually lose their ability to photosynthesise and produce isoprene (Monson et al.,
 1687 1994; Schnitzler et al., 1997; Sun et al., 2012) and Guenther et al. (2012) e.g. assumed a reduction of 10 % in the emissions of
 1688 isoprene from senescing leaves (compared to that of mature leaves). However, a reduction on such a scale (i.e. 10 %) is not
 1689 sufficient to decrease the ratio of isoprene to monoterpene carbon concentration to less than one in our simulations of oak and
 1690 poplar infected by fungi. The impact of leaf age was therefore tested during the period with stress by decreasing the emission
 1691 rate of isoprene to such a degree that R was either just under 22.5 or just under 1. Since isoprene does not show an induced
 1692 response in emission upon oak powdery mildew or rust infection, the emission rate of isoprene was reduced in simulations of
 1693 both non-infested and stressed oak and poplar forest. The results are shown in Fig. A3-4.

1694



1695

1696

1697

1698

1699

1700

1701

1702

1703

1704

1705

1706

1707

1708

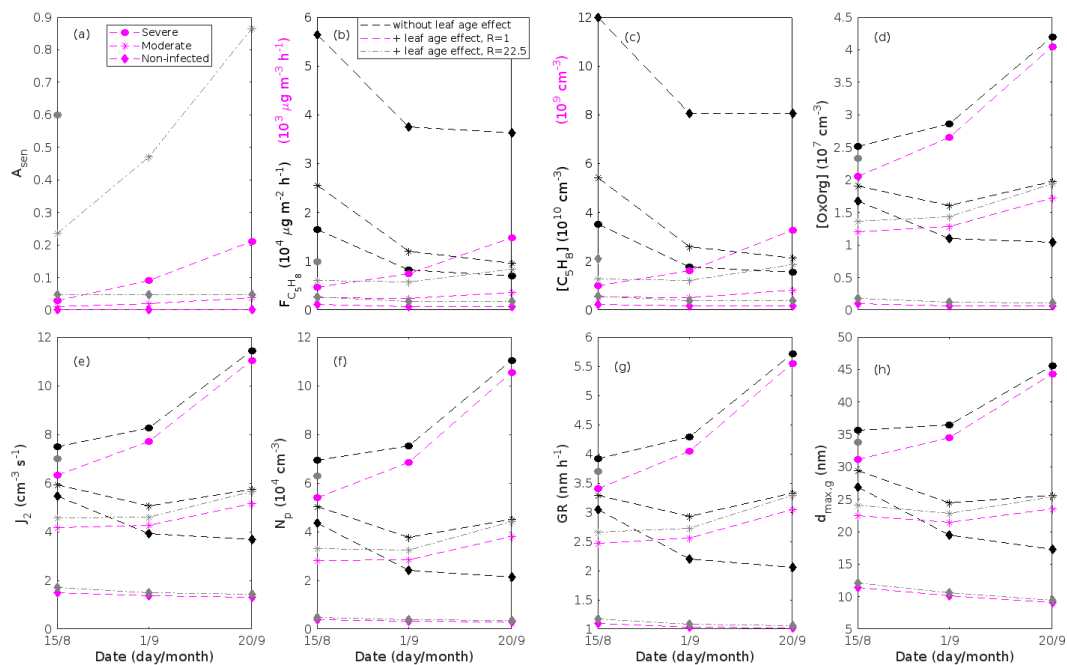
1709

1710

1711

1712

Figure A3. An oak stand infected by oak powdery mildew in comparison to a non-infected oak stand simulated with and without considering the impact of leaf age on the rates of isoprene emissions. **(a)** the fraction of isoprene emitted in comparison to simulations where the leaf age effect was not considered. For example, in order to reach $R = 1$ in simulations of a non-infected stand (magenta diamonds), the leaves are assumed to only emit 1% of isoprene compared to our default simulations of a non-infected stand (black diamonds in Fig. 7a). The syntax is equivalent to that of Guenther et al. (2012, p. 1476). **(b)** canopy emissions of isoprene and atmospheric concentrations of **(c)** isoprene and **(d)** OxOrg. The units provided in black in **(b-c)** are connected to black and grey data points, while the units in magenta in **(b-c)** are connected to magenta data points. **(e)** formation rate of 2 nm particles, **(f)** number concentrations of formed particles, **(g)** growth rates of newly formed particles, and **(h)** the daily maxima diameter of the growing particle mode. The values of other parameters during these simulations are the same as in Fig. 7. “Moderately” and “severely” refer to 30 % and 80 %, respectively, of the leaf area being infected by fungi by the 20th of September. Black markers are for simulations where the effect of leaf age was not considered (see Fig. 7 for what R is then), while magenta markers are for simulations where the emission of isoprene was reduced sufficiently for R to be just under 1. Grey diamonds are used to illustrate simulation results of a non-infected oak stand, where the emission of isoprene has been reduced sufficiently for R to be just under 22.5. Simulation results (independently of whether the effect of leaf age was considered or not) for “severe” are always indicated by circles, for “moderate” by asterisks, and for “non-infected” by diamonds.

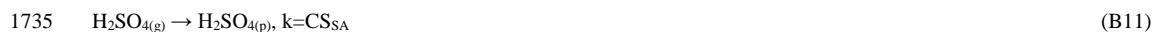
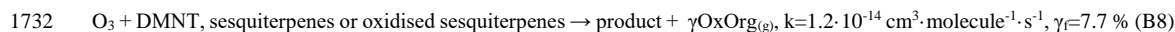
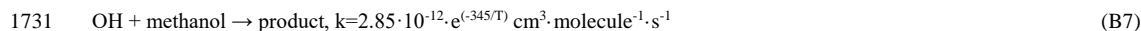
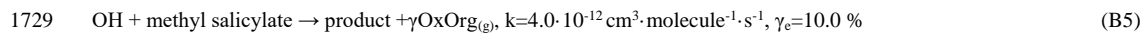
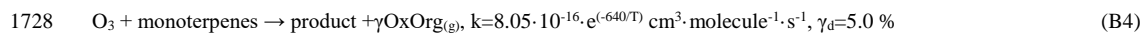
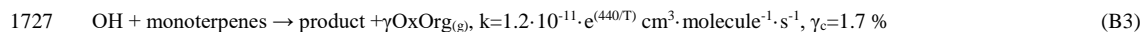
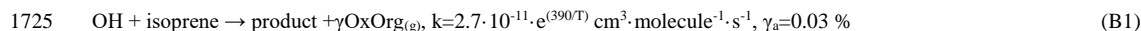


1713

1714 **Figure A4.** A poplar stand infected by rust in comparison to a non-infected poplar stand simulated with and without
 1715 considering the impact of leaf age on the rates of isoprene emissions. (a) the fraction of isoprene emitted in comparison to
 1716 simulations where the leaf age effect was not considered. (b) canopy emissions of isoprene and atmospheric concentrations of
 1717 (c) isoprene and (d) OxOrg. The units provided in black in (b-c) are connected to black and grey data points, while the units
 1718 in magenta in (b-c) are connected to magenta data points. (e) formation rate of 2 nm particles, (f) number concentrations of
 1719 formed particles, (g) growth rates of newly formed particles, and (h) the daily maxima diameter of the growing particle mode.
 1720 The values of other parameters during these simulations are the same as in Fig. 8. Grey markers are for simulations where the
 1721 emission of isoprene was reduced sufficiently for R to be just under 22.5. Symbols are the same as in Fig. A3.
 1722

1723 Appendix B: Chemical reactions in the model

1724 We considered the following chemical reactions in our model:





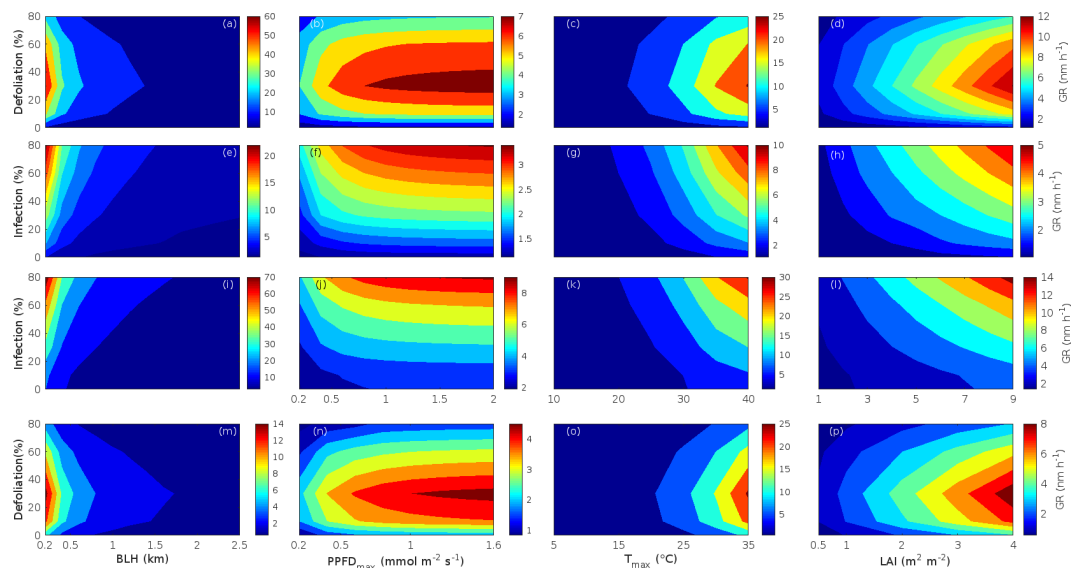
1736 T is temperature (K), p indicates “particle phase”, CS_{SA} is the condensation sink determined for sulfuric acid, while γ_i are the
 1737 fractions of organic products which can partition to the particle phase (OxOrg). In practice, γ_i are either reported HOM yields,
 1738 as defined in Ehn et al. (2014), or reported SOA yields / 2.2. SOA yields are decreased by a factor of 2.2 in order to account
 1739 for the fact that SOA yields represent mass yields, and not molar yields as it is the case of HOM yields. We utilised HOM
 1740 yields based on Jokinen et al. (2015) (γ_a , γ_b , γ_c , γ_d), Berndt et al. (2016) (γ_e), and Ehn et al. (2014) (γ_d). We used SOA yields
 1741 from Mentel et al. (2013) (γ_e , γ_f).

1742 Appendix C: Sensitivity tests

1743 **Table C1.** Constrained parameters for sensitivity tests and their range of values. Nine different sensitivity tests (ST1-9) were
 1744 conducted for all plant species and infections, where only one parameter was changed at a time. BHL is the planetary boundary
 1745 layer height, $PPFD_{max}$ is the daily maximum photosynthetic photon flux density, T_{max} is the maximum daily temperature, LAI
 1746 is the leaf area index of non-infested leaves, CS_{SA} is the condensation sink determined for sulfuric acid and γ_{OxOrg} is the yield
 1747 of OxOrg. “HPB” and “SMEAR I” refer to simulations conducted in Hohenpeissenberg (i.e. oak and poplar) and SMEAR I
 1748 (i.e. birch) conditions, respectively.

Sensitivity test no.	Parameter that changes	HPB	SMEAR I	Notes and references
ST1	BLH (m)	200 - 2500		Classical textbook example.
ST2	$PPFD_{max}$ ($\mu\text{mol m}^{-2} \text{s}^{-1}$)	200 – 2000	200 - 1600	The lower limit is based on observations at the SMEAR I station, the upper on the theoretical clear sky maxima.
ST3	T_{max} ($^{\circ}\text{C}$)	10 - 40	5 - 35	Based on observations and the IPCC 2014 predictions of the regional temperature increase.
ST4	LAI ($\text{m}^2 \text{m}^{-2}$)	1 - 9	0.5 – 4	The upper limit is based on Tripathi et al. (2016).
ST5	$[\text{O}_3]$ (ppb)	35 - 100	20 - 70	Naja et al. (2003), Ruuskanen et al. (2003). The upper end for HPB simulations is similar to the highest values which are observed in the Amazon where concentrations of isoprene can be very high (e.g. Pacifico et al., 2015)
ST6	$[\text{OH}]_{max}$ (molec cm^{-3})	$0.1 \cdot 10 \cdot 10^6$	$1 \cdot 25 \cdot 10^5$	Petäjä et al. (2009), Berresheim et al. (2000), Rohrer and Berresheim (2006). The lower limit has not been observed in HPB, but is included in order to test the impact of potential OH depletion on our results.
ST7	$[\text{H}_2\text{SO}_4]_{max}$ (molec cm^{-3})	$5 \cdot 25 \cdot 10^6$	$1 \cdot 6.5 \cdot 10^6$	Birmili et al. (2003), Kyrö et al. (2014).
ST8	CS_{SA} (s^{-1})	$2 \cdot 8 \cdot 10^{-3}$	$0.2 \cdot 3.5 \cdot 10^{-3}$	Birmili et al. (2003), Vana et al. (2016), Kyrö et al. (2014).
ST9	γ_{OxOrg}	$0.1 - 2 \cdot \gamma_{OxOrg, default}$		Ehn et al. (2014), Jokinen et al. (2015), Bianchi et al. (2019), McFiggans et al. (2019).

1749



1750

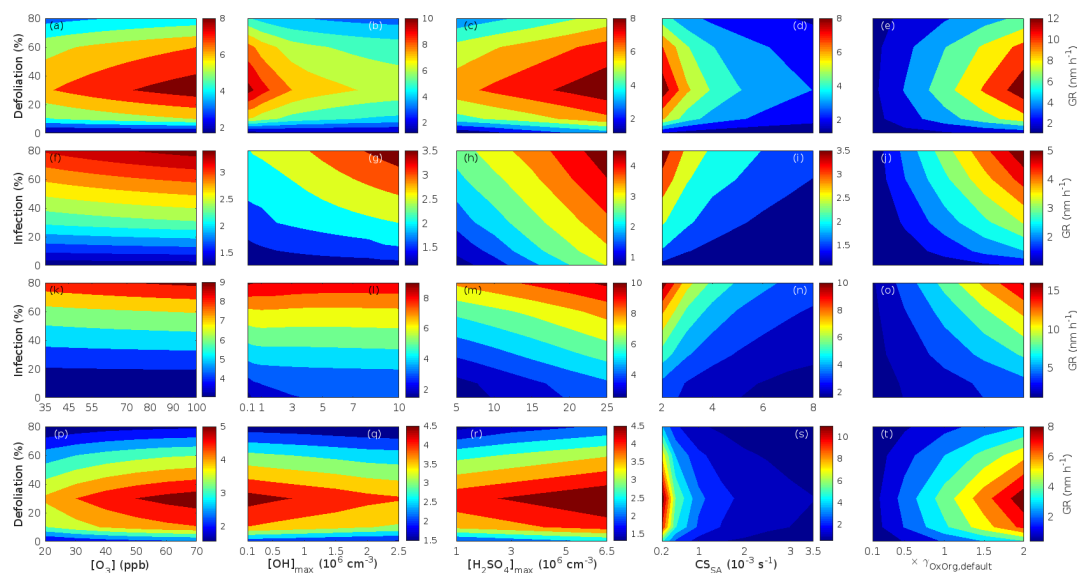
1751

Figure C1. Impact of changed boundary conditions on the growth rate of small particles in non-infected and biotically stressed forest stands. The subplots correspond to those in Fig. 10, except the subplots here display growth rate, and not number of particles. Thus we refer to Fig. 10 for further explanations.

1752

1753

1754



1755

1756

Figure C2. Impact of changed boundary conditions on the growth rate of small particles in non-infected and biotically stressed forest stands. The subplots correspond to those in Fig. 11, except the subplots here display growth rate, and not number of particles. Thus we refer to Fig. 11 for further explanations.

1757

1758